UNIVERSITY OF CALIFORNIA, SAN DIEGO

Ets2 regulates colonic stem cells and sensitivity to tumorigenesis

A dissertation submitted in partial satisfaction of the

requirements for the degree of Doctor of Philosophy

in

Molecular Pathology

by

Jorge O. Múnera

Committee in charge:

Professor Robert G. Oshima, Chair
Professor Mark Kamps, Co-Chair
Professor Sara Courtneidge
Professor Lars Eckmann
Professor Eyal Raz

2010

The dissertation of Jorge O. Munera is approved, and it is acceptable in quality and form for publication on microfilm:

_____

_____

_____

_____
Co-Chair

_____
Chair

University of California, San Diego

2010

Table of Contents

Abbreviations

AOM	Azoxymethane
bFGF	basic fibroblast growth factor
BMM	bone marrow derived macrophage
BRCA	breast cancer
Caco2	colon cancer cell line
CDC2L2	cdc2 like kinase 2
Cdx2	caudal-type 2 homoebox gene
ChIP	chromatin immunoprecipitatoin
c-Myc	v-Myc avian myelocytomatosis viral oncogene
Cox-2	cyclooxygenase 2
CSF-1	colony stimulating factor 1
DAB	3, 3'-diaminobenzidine
DSS	dextran sulfate sodium salt
E	embryonic day
EGF	epidermal growth factor
Ets	e26 specific
FN-A72	flag tagged nuclear localized Ets2 T72A
FN-DBD	flag tagged nuclear localized Ets2 DNA binding domain
FNEts2	flag tagged nuclear localized Ets2
GPR49	G-protein coupled receptor 49
HEK293	human epithelial kidney cell line
IFN	interferon
IL12p40	interleukin 12 p40 subunit

IL1beta	interleukin 1 beta
K-ras	v-Ki-Ras Kirsten Rat Sarcoma Viral oncogene homolog
Lgr5	leucine-rich-repeat-containing G-protein-coupled receptor 5
LPS	lipopolysaccharide
Lux	luciferase
MEF	mouse embryonic fibroblast
MG132	proteasome inhibitor
MMP	matrix metalloprotease
MMTV	mouse mammary tumor virus
PBS	phosphate buffered saline
PCR	polymerase chain reaction
PMA	phorbol myristate acetate
PTEN	Phosphatase and tensin homolog
PTHrP	parathyroid hormone related protein
PyMT	polyoma virus middle T antigene
qRT-PCR	quatitative reverse transcriptase polymerase chain reaction
TCF4	T-cell transcription factor 4
VEGF	vascular endothelial growth factor
Wnt	Wingless integration

List of Figures

List of Tables

Acknowledgements

I owe a great deal of thanks to the many people in my life who have helped me through this journey. It has at times been difficult but it has also been joyous and rewarding.

First of I would like to thank my family. I would like to thank my mother Maria and my father Carlos for their care and understanding and for always making education a priority. I would also like to thank my older brother Juan Carlos and my sister Laura for their encouragement and for their love throughout this ordeal. I would also like to thank my late younger brother Rafael for his friendship, his sometimes 'tough' love and his wise words.

I would also like to thank my friends for helping me throughout these last years. I first would like to thank Rachel for all with help in my application to graduate school. I could not have started this journey without her. I would also like to thank all the friends that I have made during my time at UCSD. You have enriched my life with joy, love and compassion.

During my time in the lab I have had the pleasure of working with a diverse group of colleagues who have helped me in every aspect imaginable. First and foremost I would like to thank Marie Jaksch for her friendship, her willingness to help and for always cheering me up when I felt down. I would also like to thank John Tynan, Fang Wen, Grace Cecena and Jacqueline Lesperance for helping me adjust to the lab, for their assistance with experiments and for teaching me the skills necessary to complete my thesis work. I would also like to thank Miriam Wankwell for her assistance in the tumors studies and Paul Jedlicka for his interpretation of intestinal

histology. I would also like to thank Jochen Maurer and David Castro for their scientific advice and for the good times.

Many thanks for the members of the various core facilities at the Sanford-Burnham Medical Research Institute. I would especially like to thank Katina Candee, Michael Florio and Adriana Charbono of the animal facility for their help with animal experiments. I would also like to thank Robbin Newlin and the staff of the histology facility for their assistance.

To my committee members, thanks for taking interest in my research, thank you for your constructive criticism and for your advice. Thanks to all the support staff of the Molecular Pathology Graduate program for all their hard work and especially Kathy Kazules. Thanks to Dr. Mark Kamps for his guidance and advice as the program coordinator.

Finally, I would like to thank my advisor Robert Oshima for his patience, his motivation and his support throughout the years. I am forever indebted to him for helping me learn the importance of hard work, persistence and humility. These lessons have not only helped me grow as a scientist but also as person.

Vita

EDUCATION

2004-2010 Ph.D. Molecular Pathology
University of California, San Diego
Department of Pathology, School of Medicine

1999-2002 M.S. Biological Sciences
Illinois State University

1994-1998 B.S. Biology
University of Illinois, Urbana-Champaign

PUBLICATIONS

1. Wen F, Tynan JA, Cecena G, Williams R, **Múnera J**, Mavrothalassitis G, Oshima RG. Ets2 is required for trophoblast stem cell self-renewal. Dev Biol. 2007 Dec 1; 312(1):284-99.

2. Jaksch M, **Múnera J**, Bajpai R, Terskikh A, Oshima RG. Cell cycle-dependent variation of a CD133 epitope in human embryonic stem cell, colon cancer, and melanoma cell lines. Cancer Res. 2008 Oct 1;68(19):7882-6.

3. **Múnera J** et al. Epithelial Ets2 represses monoclonal conversion, niche succession and tumorigenesis is the mouse distal colon. In preparation.

SUPPORT

2007-2009 Research supplement to promote diversity in health-related research from National Cancer Institute grant PO1 CA102583.

ABSTRACT OF THE DISSERTATION

Ets2 regulates colonic stem cells and sensitivity to tumorigenesis

by

Jorge O. Múnera

Doctor of Philosophy in Molecular Pathology

University of California, San Diego 2010

Professor Robert G. Oshima, Chair
Professor Mark Kamps, Co-Chair

Colorectal cancer is one of the leading causes of cancer related death in the U.S. Approximately 150,000 cases and 50,000 deaths due to the disease occurred last year. Alterations in the Wnt signaling pathway (Wnt, APC, β-catentin) are common in colorectal cancer. As the disease progresses mutations in K-ras, p53 and TGF-β also arise. Given the role of Wnt signaling in the maintenance of the intestinal epithelium, colorectal cancer is likely due to a misregulation of normal developmental pathways. Ets2, a member of the Ets family of transcription factors, has been identified as a Wnt target in colorectal cancer cells and in intestinal stem cells. Ets2 has also been identified as a tumor repressor of APC^{Min} intestinal tumorigenesis in the mouse equivalent of trisomy 21. In contrast to a tumor repressive effect, previous studies in this lab have shown that Ets2 has a tumor supportive function through the tumor

microenvironment in transgenic mouse mammary tumor models. This apparent paradox can be resolved if Ets2 regulates an intestinal specific tumor suppressive mechanism.

Ets2 has been previously shown to activate transcription of the caudal-type homeobox 2 gene (Cdx2) by through a conserved distal region of its promoter in both trophoblast stem cells and in colon cancer cells. Since Cdx2 functions as a tumor suppressor in the distal colon, the cell autonomous role of Ets2 was examined in postnatal colon development and in suppression of tumorigenesis. Using a conditional allele of Ets2 ($Ets2^{flox}$), and Cre-mediated deletion within the intestinal epithelium, the cell autonomous role of Ets2 was examined. Ets2 deficient cells had a selective advantage in populating distal colon crypts. Furthermore, Ets2 deficient crypts increased in number during the developmental period in which crypt fission rates peak. Consistent with this observation, Ets2 deficient crypts underwent fission more frequently than crypts retaining Ets2. This data suggest that Ets2 deficient stem cells have a selective advantage due to an increase in stem cell proliferation.

An increase in stem cell number or proliferation may lead to an increase in tumorigenesis since stem cells are the cell of origin of intestinal tumors in mouse. To test this hypothesis, the colitis associated cancer (CAC) model was used. Tumor multiplicity was increased significantly is $Ets2^{flox/flox}$ $VillinCre^{+}$ versus $Ets2^{flox/+}$ $VillinCre^{+}$ or $Ets2^{flox/flox}$ $V\text{-}Cre^{-}$ mice. Tumor size did not differ significantly between the three genotypes. These data support the conclusion that Ets2 acts as a cell autonomous tumor suppressor of intestinal tumorigenesis by inhibiting tumor initiation.

To determine if Ras/MAPK activation of Ets2 is required for its tumor suppressive activity, mice carrying a hypomorphic allele defective in Ras/MAPK activation ($Ets2^{A72}$) were subjected to the colitis associated cancer model. $Ets2^{A72/A72}$ mice developed twice

as many tumors as wild-type animals. Furthermore, induction of acute colitis revealed no significant differences in clinical or histological scoring. In addition, $Ets2^{A72}$ mice subjected to multiple AOM injections in the absence of colitis had an increase in tumor incidence and multiplicity. These data indicate that activation of Ets2 by phoshorylation of Thr-72 is important for inhibiting tumor development and this affect is not likely mediated by inflammation.

To gain insight into how Ets2 is regulated in human colon cancer cells, studies were conducted using the Caco2 human colon cancer cell line. Caco2 cells recapitulate many aspects of differentiation of intestinal epithelial cells. Increased Ets2 protein expression was found to be associated with a more differentiated state of these cells. The increase in protein levels was not due to an increase in Ets2 mRNA, suggesting that Ets2 protein levels are regulated post-transcriptionally in the Caco2 differentiation model. This observation was confirmed by treatment of proliferating cells with the proteasome inhibitor MG132.

I. INTRODUCTION

1. The Ets transcription factor family.

Ets2 is a member of the Ets family of 25 transcription factors that share a characteristic Ets domain which mediates binding to DNA sequences containing a central GGAA/T core (Wasylyk et al., 1993). Ets factors were indentified based on their homology to the oncogenic v-ets protein carried by the avian erythroblastosis virus E26 (Leprince et al., 1983). Ets family transcription factors are involved in a wide variety of biological functions including growth, apoptosis, development, differentiation and tumor progression (Oikawa and Yamada, 2003). A subgroup within the Ets family, which includes Ets2, also contains a pointed domain that mediates interaction with Erk and is named after the Drosophila gene *pointed*. A threonine residue at amino acid 72 adjacent to this domain is phosphorylated by MAP kinase and regulates the function of Ets2 (Brunner et al., 1994; Wasylyk et al., 1997). Ets2 is a downstream mediator of the Ras-Raf-MAPK pathway in *C. elegans* and *Drosophila* and has similar activity in mammalian cells.

2. Ets2 in placenta development.

Ets2 is expressed in all cell types and tissues examined but has tissue specific functions. The Ets2 transcription factor has been inactivated in mice via targeted deletion of the DNA binding domain and nuclear localization signal ($Ets2^{db1}$) (Figure1). Ets2 deficient embryos die at E8.5 due to a failure in proliferation of the ectoplacental cone and trophoblast stem cells (Yamamoto et al., 1998). However, these mice could be rescued by aggregation with tetraploid embryos that are able to

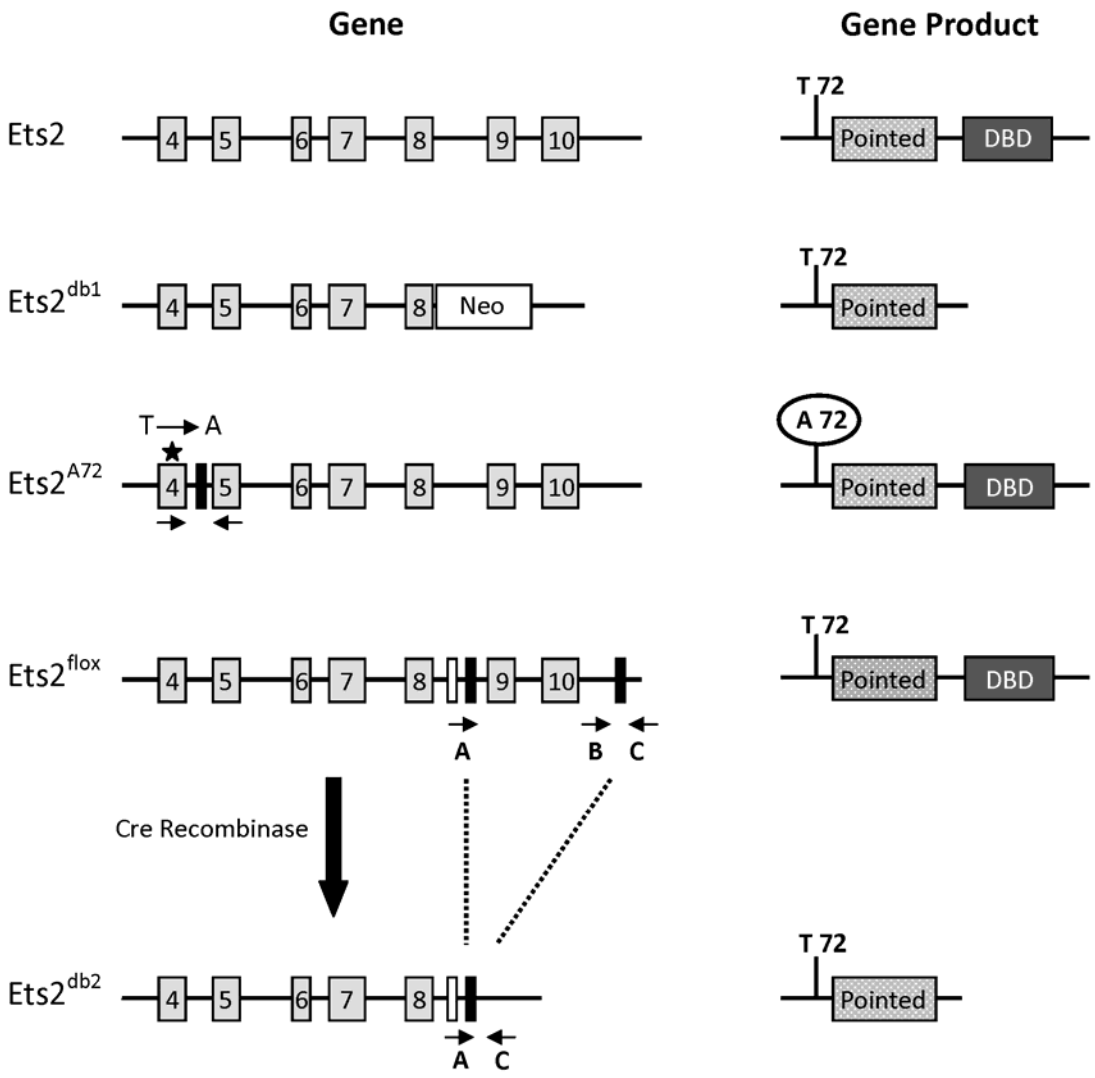

Figure 1. Schematic of Ets2 targeted alleles in mice. The 'Gene' column illustrates the targeted Ets2 alleles in mice. The grey boxes represent exons of the Ets2 gene with exon number represented within the box. '*' in the $Ets2^{A72}$ allele indicates the mutation in exon four giving rise to the T72A mutation. Solid black bars in $Ets2^{A72}$, $Ets2^{flox}$, and $Ets2^{db2}$ alleles indicate loxP sequences. Arrows below the $Ets2^{A72}$ allele represent primers used to distinguish this allele. Arrows below the $Ets2^{flox}$ and $Ets2^{db2}$ allele indicate PCR primer sites used to distinguish these alleles (see Table 1). The 'Gene Product' column represents the resulting protein of the indicated Ets2 allele.

form only extra-embryonic tissue. This indicates that lethality in Ets2 deficient embryos is due to extra-embryonic defects. The use of conditionally targeted alleles and Cre recombinase has allowed targeted Ets2 inactivation exclusively in embryonic tissues. Rescued Ets2 deficient embryos were viable and fertile. In addition they had curly hair and whiskers resembling the phenotype of TGFα knockout mice and Egfr hypomorphic mutants. Examination of skin from these animals showed the presence of misaligned hair follicles. From these rescue experiments it is apparent that adult functions of Ets2 may be complemented by other Ets members or may only be revealed when appropriately challenged (Wen et al., 2007).

In contrast to $Ets2^{db1/db1}$, $Ets2^{A72/A72}$ mice are viable and fertile (Man et al., 2003a). These mice are homozygous for a single codon mutation which changes the threonine 72 residue to an alanine residue. Consequently $Ets2^{A72}$ is unable to be phosphorylated by MAP kinase. However, when these mice are combined with $Ets2^{db1}$ or $Ets2^{db2}$ the resulting $Ets2^{db1/A72}$ or $Ets2^{db2/A72}$ embryos die at about E12 with placental defects. Because of the viability and fertility $Ets2^{A72/A72}$ and the delayed embryonic lethality of $Ets2^{db1/A72}$ and $Ets2^{db2/A72}$ the allele is designated as a hypomorphic allele.

The $Ets2^{Flox}$ mice were developed by Fang Wen (Wen et al., 2007). In these mice, exons 9 and 10 are flanked by loxP sites. The DNA binding domain can be excised by cre recombinase mediated excision resulting in $Ets2^{db2}$ which is similar to $Ets2^{db1}$. The $Ets2^{Flox}$ allele allows tissue specific deletion of Ets2 via the use of a tissue specific cre recombinase.

3. Ets2 and Cancer

There is convincing evidence that Ets2 is involved in the support of mammary tumors. Reporter assays show that Ets2 is able to regulate the promoters of urokinase plasminogen activator (uPA) and metalloproteinase-9 (MMP-9), genes associated with tumor cell invasion, after stimulation with epidermal growth factor (EGF). Furthermore, Ets2 protein levels from human breast cancer biopsies correlate with decreased disease free survival in patients. The development of tumors induced by MMTV driven polyomavirus middle T antigen (PyMT) or activated Neu/ErbB2 are restricted by decreased levels or activity of Ets2 (Neznanov et al., 1999). In these oncogene driven models, with little or only modest involvement of inflammation, the Ets2 restriction was shown to be exclusively due to a stromal function which may involve fibroblasts, immune cells and endothelial cells (Tynan et al., 2005).

Recently, the stromal effect of Ets2 on mammary tumors was shown to occur in the fibroblasts. Conditional deletion of Phosphatase and Tensin homolog (PTEN) within fibroblasts using fsp-cre (fibroblast specific cre) leads to decreased tumor take, tumor size and decreased tumor load of transplanted Erb2 tumors (Trimboli et al., 2009). In addition, deletion of PTEN leads to an increase in Ets2 mRNA levels and also an increase in phosphorylated Ets2^{T72}. Consequently, several Ets2 targets were upregulated including MMP9 and Ccl3. Furthermore binding of Ets2 to the promoters of these genes was shown by chromatin immunoprecipitation (ChIP). When Ets2 was deleted in tandem with PTEN, the effect of PTEN deletion alone was reversed suggesting that Ets2 was essential for the effects of PTEN deletion.

4. Cdx2 and Colorectal cancer

The Cdx2 gene is involved in colon organogenesis and has been implicated as tumor suppressor in colorectal cancer. Colorectal cancer is the third most common type of cancer in the world and is second only to lung cancer as the leading cause of cancer death. Cdx2 expression is decreased in human colorectal cancers and is down regulated by oncogenic Ras(Lorentz et al., 1999). In addition, knockout mice heterozygous for Cdx2 developed villiform structures in their cecum and proximal colon. When Cdx2 heterozygosity is combined with an APC mutation, colonic polyposis closely resembling the human disease occurs (Aoki et al., 2003). Cdx2 mice were found to be hypersensitive to chemical mutagen induced colonic tumors. Interestingly, Cdx2 expression was decreased as the tumors advanced from adenoma to adenocarcinoma, a similar expression pattern as seen for Ets2 in microarray data. Of note, the decrease in Cdx2 expression was not due to deletion of the remaining wild-type allele suggesting transcriptional control of Cdx2 expression. We suggest that Ets2 regulates Cdx2 in the colon as it does in the trophoblast. Cdx2 is necessary for the development of trophoblast stem cells and is turned off when trophoblast stem cells differentiate. The role of Ets2 regulation of Cdx2 in colon differentiation may also influence the progenitor state of the differentiating colon.

5. Inflammation and colorectal cancer

One of the high-risk conditions for colorectal cancer is inflammatory bowel disease which includes Crohn's disease and ulcerative colitis. Chronic inflammation is a key factor in the progression of colorectal cancer (CRC) in colitis associated cancer patients. First, the risk of CRC development is directly correlated with the duration of

colitis. After seven years of colitis, the risk of developing CRC increases as much as 1% per year. Second, the extent of the colitis lesions is also correlated with increased risk of developing CRC. Third, risk of developing colorectal dysplasia and cancer is reduced in patients who receive anti-inflammatory medications such as 5-aminosalicylates (van Staa et al., 2005).

More direct evidence for the role of inflammation on CRC has been obtained with the use of the colitis associated cancer model (CAC)(Okayasu et al., 1996). In this model, colorectal cancer is induced by pretreating mice with azoxymethane (AOM) and then subjecting them to three administrations of 3% dextran sodium sulfate. The chronic inflammation induced by this treatment promotes the development of adenomas and adenocarcinomas. Mice pretreated with AOM and subjected to DSS develop an average of 10.5 tumors/mouse while mice treated with AOM or DSS alone do not develop any tumors during the same time span (Okayasu et al., 1996). The CAC model has been used to study the effect of NF-κB signaling on the development of colorectal tumors. Mice which harbor a conditional deletion of IKK-β in their intestinal epithelial cells show a decrease in tumor incidence while mice with a conditional deletion in myeloid cells show a decrease in tumor size (Greten et al., 2004). Taken together, these data suggest that the CAC model is appropriate for studying the effect of inflammation on colorectal cancer.

6. Ets2 is involved in inflammation

In vivo evidence of the role of Ets2 in inflammation has been obtained by the use of the motheaten viable model (me-v) of chronic inflammation. me-v mice harbor a mutation in the hematopoietic cell phosphatase, Hcph/Shp1, which leads to

constitutive phosphorylation of Ets2. These mice show a severe inflammatory phenotype which is characterized by massive macrophage and neutrophil infiltration of the skin, spleen and lungs. As a result, most of these mice die at around 3 months of age due to interstitial pneumonia. Furthermore these mice show a severe arthritis-like condition in their limbs and joints. When me-v mice were crossed with $Ets2^{A72/A72}$ mice, the resulting double homozygotes had a dramatic increase of survival at 100 days as compared to me-v mice (75% vs 12%). In addition, there was a significant decrease in macrophage and neutrophil infiltration in the skin, and lungs in double homozygous mice (Wei et al., 2004).

Bone marrow macrophages derived from $Ets2^{A72/A72}$ have decreased expression of several pro-inflammatory genes (Man et al., 2003a; Tynan, 2005; Wei et al., 2004) such as IL-1B, cox-2 and IL12p40 in response to macrophage colony stimulating factor (CSF-1). Interestingly, CSF-1 and CSF-1 receptor expression in human breast carcinomas is correlated with poor prognosis. Furthermore when mice homozygous for a recessive null mutation in CSF-1 were crossed MMTV-PyMT mice, the CSF-1 null progeny displayed a reduction in progression to malignancy although growth and incidence of primary tumors was not affected (Lin et al., 2001). A similar phenotype was noted in mice in which Ets2 was deleted in tumor associated macrophages (Zabuawala et al.). These data suggest that Ets2 promotes progression and metastasis of mammary tumors by activating extracellular matrix modifying genes in tumor associated macrophages.

Recently Ets2 has been implicated in human chronic inflammatory diseases (van der Pouw Kraan et al., 2009). Expression profiles of ulcerative colitis in humans and TNBS induced colitis mice were compiled to generate a list of genes which were

unregulated in both conditions compared to healthy host tissue (UC) or control mice (TNBS colitis). They then examined the 500bp upstream regions of unregulated genes for transcription factor binding sites and found and enrichment for Ets2 binding sites. It should be noted that TNBS colitis in the SJL/J strain is most useful for studying T-helper cell-dependent mucosal immune responses rather than innate-immune responses as in the DSS colitis model. Analysis of bacterial-induced colitis in mice failed to find and enrichment or Ets2 binding sites suggesting that Ets2 may not be involved in this type of colitis.

Several studies have identified Ets2 as a target of TCF4, a transcription factor involved in activation of Wnt target genes following stimulation of the pathway. Despite being a target of TCF4, Ets2 has tumor repressive effect in the intestine. Activation of the Wnt pathway occurs in 80% of colorectal cancers (Bienz and Clevers, 2000; Sparks et al., 1998). This suggests that Ets2 acts downstream of Wnt signaling in a process other than proliferation.

7. Wnt pathway

The Wnt pathway is a highly conserved pathway which is present all metazoans and controls many events during embryonic development and in self-renewing tissues in adults. The name Wnt is derived from the homology of the pathway to Wingless in drosophila and its discovery as an integration site for the mouse mammary tumor virus (MMTV) (Wg+Int1=Wnt)(Nusse and Varmus, 1982) (Rijsewijk et al., 1987). The main effector of the Wnt pathway is β-catenin (Figure 2). β-catenin protein stability is tightly regulated by a destruction complex composed of the

Figure 2. Schematic of Wnt pathway. In the absence of a Wnt ligand, β-catenin levels are minimized by a destruction complex made up of casein kinase I alpha (CKIα), glycogen synthase kinase 3 β (GSK3β), Adenomatous polyposis coli (APC) and Axin. Formation of the destruction complex results in the phosphorylation β-catenin and its subsequent ubiquitination and destruction by the proteasome. In the nucleus, TCF factors bind the transcriptional repressor Groucho and represses transcription of target genes. In the presence of Wnt ligand, the destruction complex is destablilized and β-catenin levels increase. β-catenin is then able to translocate into the nucleus and displaces Groucho and acts as a transactivation domain for TCF.

Absence of Wnt ligand

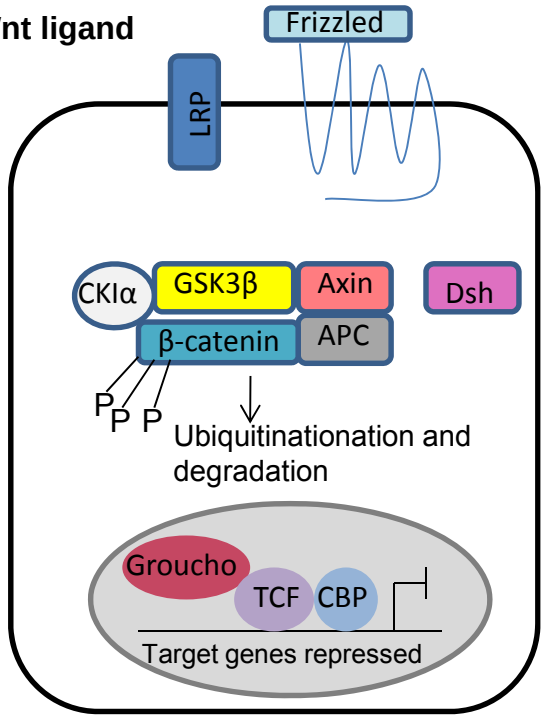

Presence of Wnt ligand

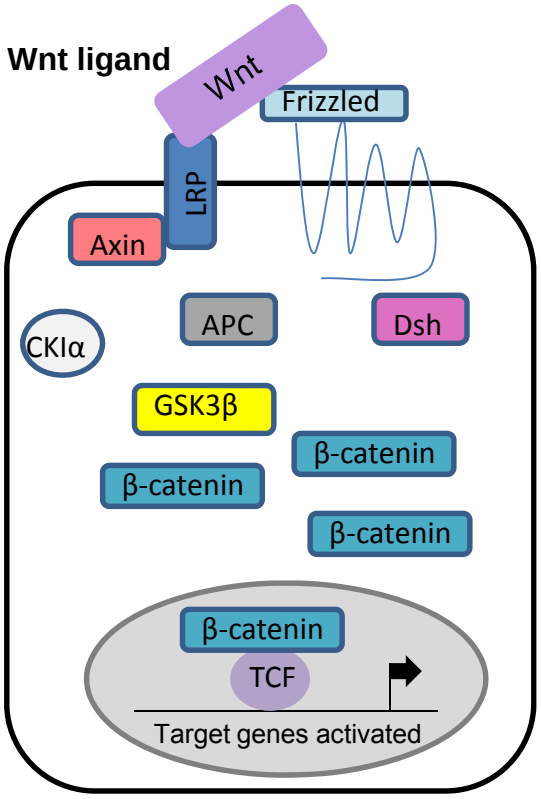

Adenomatous Polyposis Coli (APC) tumor suppressor, Axin/Axin2 and the serine/threonine kinases casein kinase I (CK1) and glycogen synthase kinase 3 β (GSK3β) (Gregorieff and Clevers, 2005). In the absence of a Wnt signal CK1 and GSK3B phosphorylate β-catenin on a series of residues found on the N-terminus of the protein. These phosphorylation events target β-catenin for ubiquitination and subsequent degradation through the proteasome. In the nucleus, the TCF/Lef family of transcription factors bind DNA and recruit the co-repressor Groucho creating a repressor complex which prevents transcription of Wnt target genes.

In the presence of a Wnt signal, the destruction complex is compromised and β-catenin is stablilzed. Stabilized β-catenin is able to translocate into the nucleus and is able to displace Groucho. The newly formed β-catenin /Tcf complex is then able to act as a transcriptional activator of Wnt target genes including c-Myc, Cyclin-D1, Dickkopf-related protein 1 (DKK1) and Axin2. Of note Wnt target genes do not only include genes involved in proliferation such as C-Myc and Cyclin-D1, but also include genes which are involved in negative feedback regulation of the pathway.

8. Intestinal development

The intestinal tract is derived from the definitive endoderm following gastrulation. Wnt signaling is required in the development of the definitive endoderm. Inactivation of β-catenin within this region results in its conversion to precardiac mesoderm (Lickert et al., 2002). Development of the gastrointestinal tract begins at mid-gestation during the development of the gut tube from the endoderm at embryonic day 8.5 (E8.5) in the mouse. Following formation of the gut tube, the intestinal tract undergoes patterning from anterior to posterior from E9.5 to E14.5. During this

patterning period the gut tube gives rise to 3 subdivisions: the foregut, the midgut and the hindgut. The foregut gives rise to the stomach. The midgut gives rise to the small intestine and the hindgut gives rise to the large intestine. At E14.5 the intestinal tract undergoes cytodifferentiation and villus formation. In the small intestine villi are formed and are separated by intervillus regions which contain proliferative cells. The colon forms as a flat epithelium with immature crypts which contain proliferative cells at their base. The differentiated cells of the small intestine and colon also become evident during this period (Gordon and Hermiston, 1994; Ponder et al., 1985).

At birth the intervillus regions begin to form crypts. In the colon, crypts are present but not fully formed. Proliferative stem cells are found at the base of these immature crypts. TCF4 is required for maintenance of the stem cell population, consequently TCF4 deficient mice are born but die in the first day of life (Korinek et al., 1998). Perforation of the intestinal epithelium was observed suggesting a possible cause of neonatal death. Examination of the small intestine revealed the absence of proliferative cells in the crypt. This observation suggests that Wnt signaling is required for maintenance of the stem cell population in newborn mice.

During the first 2 weeks after birth there is extensive remodeling of the intestinal tract (Menard et al., 1994). In the small intestine, the intervillus regions begin to invade the submucosa and form crypts. Within these crypts the stem cell niche is formed and maintained throughout the lifetime of the animal. In the colon a similar stem cell niche is formed at the base of the crypts. Within the stem cell niche, competition between stem cells exists. Stem cells which have a selective advantage replace their competitors during the first weeks of life (Schmidt et al., 1988). Also within the first 2 weeks, crypts begin to divide longitudinally by crypt fission. Crypt

fission in the colon peaks within this period with 30% of crypts being in fission (Cheng and Bjerknes, 1985). By 4 weeks of age crypt fission rates drop to 1-2% as the crypts reach homeostasis. From this point forward, growth of the crypt occurs through an increase in depth rather than by crypt fission. Crypt fission rates remain low but present throughout the lifetime of the animals. Replacement of crypts occurs very rarely as the mean crypt cycle time in mice is 187 weeks (Li et al., 1994).

The adult intestine is a rapidly renewing organ with a turnover time of 4-5 days (van der Flier and Clevers, 2009). The stem cells are located in the small intestinal crypts in the small intestine, and at the base of colon crypts (Figure 3). Stem cells give rise to rapidly dividing transient-amplifying cells (or transit-amplifying cells). These TA cells then undergo differentiation into one of four lineages. Enterocytes (or colonocytes) function in absorption of nutrients or water. The goblet cells secrete mucus into the intestinal lumen and aid in passage of luminal contents. The enteroendocrine cell secretes hormones. Paneth cells reside strictly in the small intestine and secrete lysozyme and antibacterial peptides.

9. Crypt Fission

Crypt fission was first described in irradiated mice. Following irradiation there was an extensive loss of crypts with 77% of crypts being lost. Within 3 weeks the crypts were almost completely replaced by crypts which had expanded by bifurcation and then fission (Cairnie and Millen, 1975). Crypt fission also occurs following bowel resection suggesting that the process is active during regeneration and repair following injury. Although 35 years have passed since these seminal studies, crypt fission process is still poorly understood. The rate limiting factor in crypt fission is

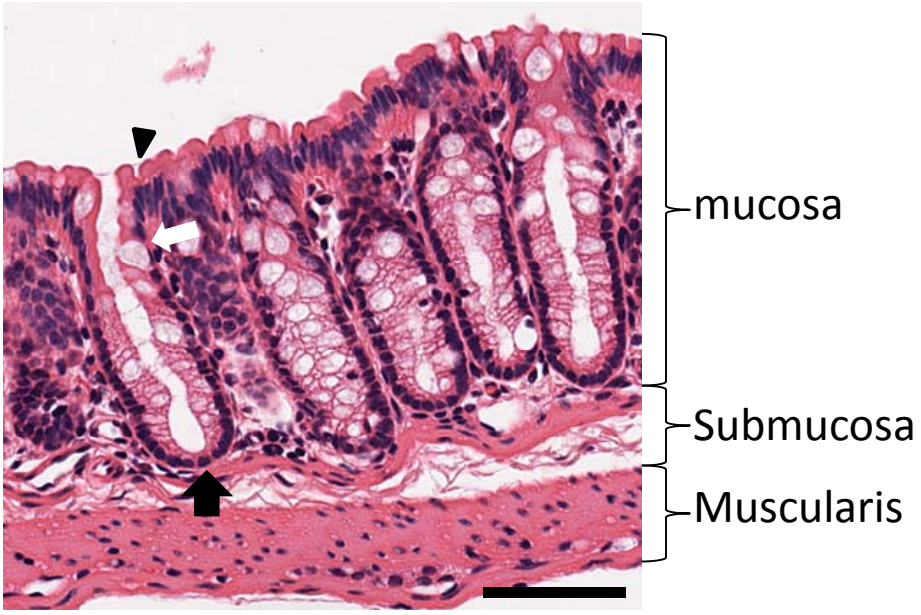

Figure 3. Histology of mouse distal colon. A longitudinal section of mouse colon is shown above. The lumen of the colon is at the top of the figure. The black arrowhead points to the surface epithelium also referred as the “cuff”. The white arrowhead depicts a goblet cell. The black arrow denotes the crypt base which is the site of the stem cell niche. Scale bar=50 microns.

believed to be number of stem cells (Loeffler et al., 1997). Indirect evidence of this has been observed in APC^{min}/+ (Multiple intestinal neoplasia) mice (Bjerknes et al., 1997). These mice display increased crypt fission rates likely due to the increase number of cells in the stem cell compartment. More direct evidence of this was shown in PTEN deficient mice (He et al., 2007). PTEN deficient mice have an increase in the number of putative stem cells expressing the RNA binding protein Musashi and phospho β-catenin . Moreover, these intestinal stem cells (ISC) were found within the branched areas of crypts in fission. The authors concluded that these stem cells are responsible for the induction of crypt fission. However, Musashi has been shown to be a more general marker of progenitor cells rather than a stem cell specific marker (Barker et al., 2007).

Although crypt fission is important for early postnatal development of the intestine and mice and humans, crypt fission is rarely seen in healthy mouse or human adults. Cheng and co-workers quantitated the number of crypts undergoing fission in normal human colonic epithelium and compared it to the epithelium from patients from ulcerative colitis, Crohn's disease and multiple polyposis (Cheng et al., 1986). Epithelium from normal patients displayed only a small but definitive percentage of branching crypts of 0.44±0.16. In contrast patients with Ulcerative colitis, Crohn's disease and multiple polyposis, the percentage of branching crypts was significantly increased to 30.4, 15.1 and 13.2 respectively. These data suggest that in conditions in which large stretches of epithelium are lost, crypt fission acts a mechanism for replacement of damaged crypts. Although crypt damage is not present in multiple polyposis patients, mutation of the APC tumor suppressor results in increased crypt fission rates (Bjerknes et al., 1997).

10. Ets factors in intestinal development

Although nearly two-thirds of the 28 Ets factors present in mice have been genetically inactivated, only Elf3 (E74-like factor-3) and Spdef display an intestinal phenotype. Elf3 was originally indentified as one of 5 Ets factors expressed within the epithelium (Tymms et al., 1997). Inactivation of Elf3 led to embryonic lethality in 30% of mice by embryonic day 11.5 (Domon-Dell et al., 2002). By weaning, two-thirds Elf3 mice died due to a wasting phenotype. In addition Elf3-deficient mice had decreased body weight from P1 to P21. In contrast, $Elf3^{+/-}$ were nearly identical in weight compared to $Elf3^{+/+}$ mice during this same period. Examination of the small intestine of Elf3 deficient mice revealed that altered enterocyte morphogenesis and differentiation correlated with decreased expression of transforming growth factor ß receptor II (TGF-ß RII). This observation was later confirmed by rescue of Elf3 deficiency by overexpression of TGF-ß RII within intestinal epithelial cells (Flentjar et al., 2007). These studies provided the first evidence that an ets factor could influence intestinal morphogenesis in a cell autonomous and haplosufficient manner.

Recently the Clevers lab reported the phenotype of Spdef knockout mice (Gregorieff et al., 2009). Spdef was previously identified as a Tcf4 target gene and was therefore hypothesized to be involved in intestinal development. Spdef deficient mice had decreased numbers of PAS-positive goblet cells in the proximal small intestine, the proximal colon and the distal colon compared to wild-type mice. Interestingly, there was no difference in goblet cell numbers in the distal small intestine suggesting that gene function may have regional specificity throughout the intestinal tract. In addition to affecting goblet cells Spdef deficiency led to decreased

numbers of paneth cells in the distal and proximal small intestine along with increased expression of the paneth cell genes Mmp7 and Ang4 in the colon.

11. Lgr5 marks intestinal stem cells

Lgr5 (leucine-rich-repeat-containin G-protein coupled receptor 5) also known as Gpr49 was first indentitfied as a Wnt target in a screen of genes whose expression decreased upon expression of a dominant negative TCF4 in colon cancer cells (van de Wetering et al., 2002). Lgr5 was further characterized within the small intestine and it mRNA expression was restricted to the small intestinal crypts (Barker et al., 2007). Furthermore, Lgr5 was upregulated in adenomas from ApcMin mice. In an elegant series of experiment Barker and colleagues demonstrated that Lgr5 marked the intestinal stem cells of both the small intestine and colon. The Lgr5-eGFP-IRES-creERT2 knockin mouse was crossed with the Rosa26-LacZ reporter mouse. Upon treatment with tamoxifen, these mice activated LacZ within intestinal stem cells. β-galactosidase expressing cells conformed to several defining characteristics of stem cells including the ability to repopulate entire crypts, undergo self-renewal and ability to differentiate into the different cell lineages. It was noted however that stem cells within the colon seem to have different kinetics. Unlike in the small intestine, Lgr5 positive stem cells in the colon rarely gave rise to wholly-uniformly blue crypts at 5 days post injection with tamoxifen. This suggests that colon stem cells are more quiescent than the stem cells in the small intestine and therefore the colon undergoes less frequent renewal.

In addition to tracing experiments, Sato and co-workers established an in vitro culture system that recapitulates crypt-villus physiology (Sato et al., 2009). In the

presence of EGF, R-spondin, Noggin and matrigel, both isolated small intestinal crypts and sorted Lgr5-GFP+ cells were able to form organoid structures which maintained the crypt-villus organization. Organoid structures derived from Lgr5-GFP+ cells were able to give rise to all differentiated cell types found in the small intestine. In addition, organoids were able to expand the crypt –like structures by fission and also maintained the stem cells niche. These results further strengthen the identification of Lrg5-GFP+ cells as the intestinal stem cells.

12. Ets2 is a TCF4 Target

Ets2 was first implicated as a TCF4 target in 2002. Expression of dominant negative TCF4 leads to a block in proliferation and decreased levels of several genes including c-myc, cyclin-D1 and Ets2 in two different colorectal cell lines (van de Wetering et al., 2002). However Ets2 expression does not rescue the proliferative defect caused by interrupting the Wnt signaling pathway, in contrast to Myc. These data suggest that Ets2 may act downstream of TCF4 in a process other than proliferation. Our data and others' suggest that Ets2 could act as a negative regulator of proliferation induced by the Wnt pathway by inducing growth arrest and consequent differentiation in enterocytes.

More recent experiments have confirmed the initial observation that Ets2 is a TCF4 target. In 2007 Van der Flier and colleagues reported that Ets2 is upregulated in Wnt activated primary colon adenoma and colon adenocarcinoma samples compared to normal colon (Van der Flier et al., 2007). Recently Hatzis and colleagues used a chromatin immunoprecipitation (ChIP)-coupled DNA microarray analysis (ChIP-on-chip) analysis to investigate the genome wide pattern of TCF

occupancy. Ets2 was one of the genes identified using this procedure (Hatzis et al., 2008). Further analysis revealed that TCF4 binds an intronic site and a 3' enhancer site within the ETS2 gene. When these sites were cloned in to a luciferase reporter vector, the resulting construct displayed transcriptional activity when cells were transfected with TCF4 but not a dominant negative TCF4.

13. Ets2 is expressed in intestinal stem cells

Using the Lgr5-eGFP-IRES-creERT2 knockin mouse van der Flier and colleagues determined the transcriptional signature of Lgr5+ cells by using FACS to sort cells into GFP-high and GFP-low populations (van der Flier et al., 2009b). Microarray analysis was used to compare the two cell populations and to generate a list of genes which were upregulated in intestinal stem cells. Among the genes that were differentially expressed were CD44, SOX9 and Ets2 all of which had been previously identified as TCF4 targets. In addition, in situ hybridization experiments confirmed the presence of Ets2 transcript with small intestinal crypts. This data suggests that Ets2 is expressed in the intestinal stem cells. However, Ets2 transcript is also present in the GFP-low cells suggesting that Ets2 may also be expressed in the transient amplifying cell compartment. In accordance with this, Ets2 was found to be expressed in the bottom third of colon crypts in human sections (Segditsas et al., 2008). Taken together these observations confirm the initial report that Ets2 is a TCF4 target within stem cells.

14. Intestinal stem cells are the origins of intestinal cancer

The idea that stem cells are the origin of colorectal cancer has been based on the long latency for development of colorectal carcinoma and the observation that the intestine undergoes renewal every 4-7 days. Based on these observation it was hypothesized that stem cells are the likely culprit since they are the only cells within the intestine that persist long enough to acquire the genetic insults needed to progress to a colorectal adenocarcinoma. In recent years, enrichment of colon cancer initiating cells has been achieved using the CD133/Prominin marker (O'Brien et al., 2007; Ricci-Vitiani et al., 2007). Traditionally these studies examine the ability of these cells to initiate tumors in immunocompromised mice. It should be noted however that the CD133 epitope has been shown to vary depending on cell cycle suggesting that it is a marker of proliferative cells rather than actual stem cells (Jaksch et al., 2008).

In the mouse, prominin 1 is expressed in the stem cells and early progenitors in the mouse small intestine but not in the colon (Snippert et al., 2009). Furthermore, prominin 1 expressing cells are expanded upon activation of stabilized form of β-catenin. When Prominin 1 positive cells were isolated and grown in a colony forming assay, prominin 1 positive cells isolated from mice expressing the stabilized form of β-catenin formed 4 times as many colonies as prominin 1 positive cells isolated from mice expressing wild-type β-catenin (Zhu et al., 2009). This suggests that activated β-catenin can expand the intestinal stem cell pool. However, prominin 1 expression is not confined to the Lgr5+ stem cells region but rather encompasses the entire proliferative region (stem cell and transit amplifying) of the small intestine (Snippert et

al., 2009). Taken together these data indicate that prominin 1 may mark proliferative cells within a tumor but not necessarily the tumor initiating cell.

Definitive proof of crypt stem cells as the source of intestinal tumors came from a study by Barker and colleagues (Barker et al., 2009). In this study the cytochrome P-450 promoter Ah-cre mouse was used. In this mouse cre recombinase can be induced by injection of β-naphthoflavone (β-NF). The authors found a concentration of β-NF which could target the entire intestinal epithelium except the stem cells. This mouse was crossed with $Apc^{flox/flox}$ to demonstrate that deletion of Apc in non-stem cells only induced intestinal adenomas after 284 days. Using the Lgr5-eGFP-IRES-creERT2 knockin mouse crossed with $Apc^{flox/flox}$, they demonstrated that targeting the stem cell led to formation of macroscopic adenomas within 36 days. Furthermore, these adenomas retained only a small percentage of Lgr5 positive cells. These data demonstrate that the intestinal stem cell is the origin of intestinal cancer.

15. Ets2 suppresses APC^{Min} tumorigenesis

Ets2 deficiency results in a significantly increased number of adenomas cause by a combination of chemical carcinogenesis and induced colitis (see Results). This model preferentially results in activation of the Wnt pathway, commonly through activating mutations of β-catenin (Greten et al., 2004). This increase in intestinal tumor formation associated with limited Ets2 activity was independently demonstrated in a study of the mouse equivalent of human trisomy 21 (Sussan et al., 2008). The smallest interval of trisomy that resulted in decreased intestinal tumors arising in $Apc^{min/+}$ mice included Ets2 among the 30 candidate genes. Combining an undescribed targeted Ets2 allele with the additional chromosomal intervals revealed

an Ets2 copy number dependent suppression of intestinal tumors. The authors suggested that the Ets2 tumor repressive activity might be active against multiple types of tumors and thus support the hypothesis that trisomy 21 may confer broad resistance to cancer. In contrast to a tumor repressive effect, we have previously shown that Ets2 has a stromal, supportive function on multiple transgenic mouse mammary tumor models (Man et al., 2003a; Neznanov et al., 1999; Tynan et al., 2005). This apparent paradox (Threadgill, 2008) suggests that the Ets2 role as a tumor repressor activity is specific for the organ system (intestine vs mammary gland).

16. Ets2 regulates p16INK^{4a}.

Transformation of human diploid fibroblasts (HDFs) with activated Ras oncogene (or downstream effectors Raf and MEK) induces the cells to arrest in the G1 phase of the cell cycle (Ohtani et al., 2001). This induced arrest is due to increased expression of p16INK4a which inhibits Cyclin dependent kinases (Cdks) 4 and 6. Analysis of the p16INK^{4a} promoter revealed that it contains 2 conserved Ets binding sites located at approximately 120 base pairs upstream of the translational start site. Promoter analysis using luciferase reporter revealed that Ets2 was able to activate the promoter and that activation occurred through binding to the conserved Ets sites. Furthermore the authors demonstrated that Ets2 binds the p16INK^{4a} using ChIP assay. However, p16INK^{4a} expression is not downregulated in Ets2$^{db1/db1}$ rescued mice suggesting that other Ets factors may compensate for Ets2 deficiency.

In addition to its role in inducing cell cycle arrest in HDFs, p16INK^{4a} had also been implicated in cell cycle arrest of human colorectal cancer cells. Examination of

sporadic carcinomas, adenomas and aberrant crypt foci (ACF) revealed that p16INK^{4a} was expressed early in the earliest neoplastic lesions (Dai et al., 2000). In addition, p16INK^{4a} expression was inversely correlated with expression of several proliferation markers including Ki67, Cyclin A and retinoblastoma protein. Staining of colon specimens from ulcerative colitis (UC) patients revealed that although p16INK4a was only expressed in 1% normal colon crypts, it was expressed in 33% of colon crypts from UC patients (Furth et al., 2006). Furthermore, p16INK4a expression correlated with the degree of crypt distortion and was inversely correlated with Ki67 expression. These data suggest that p16INK^{4a} may be important in constraining tumor growth.

17. Ets2 is a potential substrate for APC-Cdh1 (Anaphase promoting complex)

Cdh1 (*fizzy related 1*) deficient mice die during embryogenesis due to an inability to form giant cells through endoduplication (Li et al., 2008). In addition, MEFs from these mice grow slower than WT or heterozygous mice during early passage. Analysis of Cdh1 deficient MEFs revealed that Ets2 protein levels were significantly increased as were the protein levels of the Ets2 target gene p16INK^{4a}(Esteller et al., 2001). As a result of overexpression of these proteins, MEFs from Cdh1 mice entered replicative senescence prematurely. The authors identified Ets2 as a potential substrate for APC-Cdh1 and identified a putative destruction box at the N-terminus that when mutated stabilized exogenous Ets2 protein levels. These data suggests that degradation of Ets2 and consequent downregulation of p16INK^{4a} may be a mechanism for colorectal tumor progression.

18. Goals of the dissertation.

The goals of this thesis were to determine the cell autonomous function of Ets2 within the intestinal epithelium. The role of Ets2 in the intestinal epithelium was first determined in vivo using the conditionally targeted $Ets2^{flox}$ allele in conjunction with intestinal epithelial cell specific Cre expression and a Rosa26 LacZ reporter. This allowed targeting Ets2 within the intestinal epithelium and allowed tracking of the descendants of Ets2 deficient cells. Ets2flox Villin-Cre mice were then subjected to a colitis associated cancer regimen in order to determine if Ets2 has a cell autonomous tumor suppressive effect. To test whether Erk phosphorylation of Ets2 is required for tumor suppression wild-type and $Ets2^{A72/A72}$ mice were subjected to the colitis associated cancer regimen. To test if the tumor suppressive effect might be due to differences in inflammation, wild-type and $Ets2^{A72/A72}$ mice were subjected to acute colitis and tumors were induced in the absence of colitis. Finally, since Ets2 has been identified as a TCF4 target and has been shown to regulate Cdx2, Ets2 mRNA and protein expression was analyzed using a cell based model of intestinal epithelial cell differentiation.

II. **MATERIALS AND METHODS**

1. Mice.

Generation of the $Ets2^{A72}$ and $Ets2^{flox}$ alleles has been described previously (Man et al., 2003a; Wen et al., 2007)). The $Ets2^{A72}$ allele was backcrossed at least 6 generations into the FVB/n strain for tumor studies. $Ets2^{flox}$ was backcrossed into the FVB/n genetic background 6 generations prior to generating trigenic animals expressing Villin-Cre. Villin-cre mice, bred into FVB/N background were obtained from Frank Gonzales, NIH. The R26R mice in 129S3/SvImJ background (stock No. 003310) was purchased from the Jackson laboratory and was maintained by backcrossing heterozygous to the FVB/N inbred strain.

2. Genotyping of mice and tissues.

PCR was performed using tail biopsy or organ DNA. Genetically engineered mice were genotyped by PCR using the primers listed in Table 1. To determine the degree of recombination of the $Ets2^{flox}$ allele in tissues or tumors, PCR simultaneously using the primers A, B, and C (see Table 1) was performed. The percent $Ets2^{db2}$ allele was estimated from standard curves containing DNA mixtures of $Ets2^{flox}$ or $Ets2^{db2}$ alleles (Wen et al., 2007).

3. Generation of trigenic mice.

Trigenic mice were generated as by breeding $Ets2^{flox/flox}$ Villin-$Cre^{+/-}$ mice with $Ets2^{+/+}$ $R26R^{+/-}$. Mice were then backcrossed to $Ets2^{flox/flox}$ to generate $Ets2^{flox/flox}$ Villin-$Cre^{+/-}$ $R26R^{+/-}$ and $Ets2^{flox/+}$ $R26R^{+/-}$ Villin-$Cre^{+/-}$ mice. Villin-Cre were on the second generation of FVB/N but were backcrossed to FVB/N for 4 additional generations

generating mice with less than 2% B6 background. $Ets2^{flox/flox}$ and R26R mice were on FVB/N for more than 10 generations.

Table 1. Genotyping primers for mice used in study.

Gene	Sense primer	Antisense primer	Product Size (bp)
Villin-Cre	CTGGCATTTCTGGGGATTGC	ACGGAAATCCATCGCTCGAC	199
R26R	GCTGACAAAGAAAGGCTGC	ATCCAGGTCCAGCCAGTCTA	~250
Ets2	TGGGCCTGTCTTTGAAATGCTC	GTGGCCCTCAACAATTCACCAA	201(Ets2) 300($Ets2^{A72}$)
Ets2	(Primer B) GACCCACTTGCTCCAAAGAC	(Primer C) GCTTCCCAGAGACTCTTCCC	176 (Ets2) 217 ($Ets2^{flox}$) no prod. ($Ets2^{db2}$)
Ets2	(Primer A) GCCACAGCAAACCTCTTTCT	(Primer C) GCTTCCCAGAGACTCTTCCC	~2170 (Ets2, $Ets2^{flox}$) 280 ($Ets2^{db2}$)

4. Tumor induction.

An azoxymethane (AOM) stock solution of 10 mg/ml in water was made and used immediately or aliquoted and stored a -20ºC as done previously (Neufert et al., 2007). For injection into animals, the AOM stock was diluted to 0.62 mg/ml in PBS for the colitis associated cancer regimen and 0.5 mg/ml for multiple AOM injection regimen . At these concentrations a 25 gram mouse would receive a 0.5 ml injection in order to inject at a final dose of 12.5 mg/kg or 10 mg/kg respectively. All regimens used are shown in Figure 4. For the colitis associated cancer regimen (figure 4A), 8 week old mice were injected with 12.5 mg/kg of AOM. A week later animals were subjected to 2.5% DSS for 5 days followed by a 16 day recovery. The DSS cycle was repeated once more and then a final cycle of 2% DSS for 4 days with a recovery period of 10 days was done. Animals were sacrificed at the end of the regimen. As controls for the colitis associated cancer regimen, one group of animals was injected with AOM

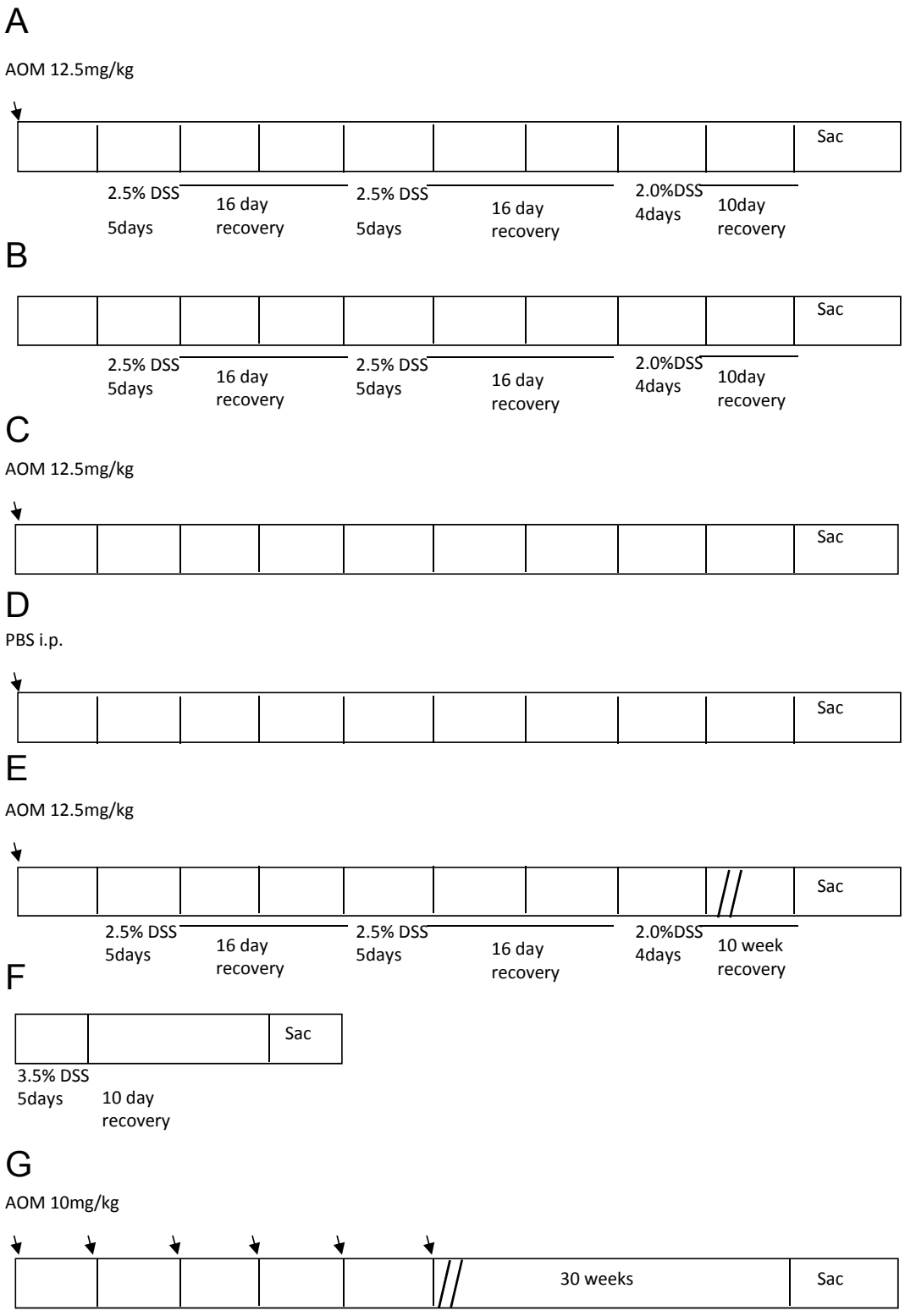

Figure 4. AOM DSS treatments used in this study.

but no DSS was administered (Figure 4C). Another control group received DSS but PBS alone was injected (Figure 4B). The final control group was did not receive AOM or DSS (Figure 4D). For the 19 week AOM DSS treatment mice were subjected the colitis associated cancer treatment but were sacrificed 10 weeks later (Figure 4 E). For acute colitis, mice were given 3.5% DSS for 5 days followed by 10 day recovery after which the animals were sacrificed (Figure 4F). For the multiple AOM injection experiment, 8 week old mice were injected weekly for 6 weeks with 10 mg/kg of AOM. After 4 months, animals were sacrificed and colons were examined (Figure 4G). Macroscopic tumors were observed under a dissection microscope while microadenomas were counted from histological sections.

5. Isolation of colons

Mice were euthanized and then their colons were removed using a scalped and scissors. Colons were placed in a petri dish filled with ice cold PBS. Colons were then flushed using a syringe with a 21 gauge needle in order to remove feces. For microarray analysis, colons were snap frozen in liquid nitrogen and stored at -80ºC in RNA Later (Qiagen, 76106). For histological analysis, after flushing colons were flushed with 4% paraformaldhyde in PBS or 2% paraformaldehyde and 0.2% glutaraldehyde in PBS in order to fix the colon epithelium. Colons were then placed on sharkskin analytical paper and cut longitudinally to expose the epithelial layer. The colons were then flattened out (with the epithelial layer facing up) and placed in fixative overnight. The next day, colons were placed in 70% ethanol for embedding or in LacZ solution.

6. LacZ staining

Colons were fixed in 2% paraformaldehyde and 0.2% glutaraldehyde in PBS overnight, washed one in PBS and twice in *lacZ* wash buffer (2mM $MgCl_2$, 0.01% sodium deoxycholate, 0.02% NP-40 in PBS) for 5 minutes. Staining was carried out in 1 mg/ml X-gal, 10 mM potassium ferrocyanide, and 10 mM potassium ferricyanide in lacZ wash buffer at 37ºC overnight. Colons were then placed in PBS to stop the staining reaction. Colons were then embedded in paraffin and 5 micron sections were cut. Nuclear Fast Red stain was used to visualize lacZ-negative cells.

7. Scanning of Slides

Slides were scanned at 20X using an Aperio Scanscope XT slide scanner. Digital images of slides were saved on the Burnham scanscope server and examined using Aperio Imagescope software. Measurements of length were made using the pen tool. Measurements of crypt depth were made using the ruler tool. Slide annotations were saved and data was exported to excel using the export function under the annotations. For quantitation of PCNA, F480 and TUNEL in tumors, tumor areas were circled using the ellipse tool and DAB staining was quantiated using a macro for this stain. Quantitation is presented as positive pixels per unit area.

8. Quantitation of the percentage of uniformly blue crypts

Colon slides were stained with nuclear read and scanned. Digital images were examined at 20X. At least 100 well oriented distal colon crypts were examined per slide. Blue crypts were defined as those crypts in which no β-galactosidase negative cells were evident. The percentage of uniformly blue crypts was calculated as the

number of blue crypts divided by the total number of crypts counted multiplied by 100. To validate this method 4 slides were scored by an independent observer blinded to the genotype of the slide. The results from the independent observer for each individual slide were within 6% (on average) of the original quantitation.

9. Quantitation of crypt fission

Crypt fission was determined by examining at least 100 well oriented crypts per mouse. A crypt in fission was defined as a bifurcated crypt with bisecting fissure and a single luminal opening. A similar method has been used recently (Wang et al., 2006). To document crypts which were scored as bifurcated crypts, arrows were used to annotate the digital slide. Crypt fission results were plotted using Graphpad Prism software.

10. Quantitation of patch size

A patch was defined as at least 2 uniformly blue crypts adjacent to each other. At least 100 well oriented crypts were scored per slide. The number crypts in a patch was determined for each slide examined.

11. Crypt depth

To determine crypt depth, the Imagescope ruler tool was used to measure the distance from the submucosa to the luminal surface. The measurements were made perpendicular to the submucosa in all slides in order to standardize the measurement. The crypt depth was measured along the length of the distal colon at least 6 different points. The crypt depths were then exported as an excel list from

each digital slide examined. To ensure there was no positional bias in sampling, crypt depths were plotted versus the distance from the anus. The distance from the anus was measured using the pen tool in the Imagescope program.

12. Crypt density

For crypt density measurements, the lengths of at least 3 stretches with 10 or more well oriented crypts were measured using the pen tool in Imagescope. The measurements of the lengths were then exported as an excel spreadsheet and compiled for each digital slide examined. The number of well oriented crypts was then measured and then divided by the length determined.

13. Number of cells per crypt

To determine the number of cells per crypt, 30-50 well oriented crypts were examined as done previously (Ramsay et al., 2004). Imagescope images were examined at 200X adjusted for contrast in order to visualize nuclei. Numbers are presented as cells per crypt.

14. Percentage of goblet cells

The percentage of goblet cells was measured as done previously (Gregorieff et al., 2009). Briefly, 5 randomly selected fields of distal colon from each PAS stained section were photographed. Images were then adjusted in brightness and contrast in Windows Photo Gallery in order to see PAS positive cells and nuclei. The total number of goblet cells per crypt was divided by the total number of nuclei per crypt and multiplied by 100. Four mice per genotype at 30 days of age were examined.

15. Laser capture microdissection

For laser capture, 5 micron sections were placed on membrane slides (Molecular Machines and Industries, 50102) and stained for neutral red. Individual crypts were dissected from distal colon tissue using MMICellCut tools and a CellCut Plus laser capture microdissection microscope (Molecular Machines and Industries). Dissected crypts were collected in isolation caps (Molecular Machines and Industries, 50202).

16. PCR of microdissected tissue

Microdissected tissue was resuspended in PBND lysis (50mM KCL, 10mM Tris-HCL, 2.5mM MgCl2, 0.1 mg/ml gelatin, 0.45% NP-40, and 0.45% Tween20, pH 8.3) with proteinase K freshly added at 1:100 from a 10 mg/ml solution. Samples were then digested overnight at 55ºC and samples were then boiled for 12 minutes to inactivate the proteinase K. Samples were then briefly centrifuged at full speed to pellet debris. For a 20 μl reaction the PCR mix consisted 2μl of sample, 2μl of primer and 16μl of Platinum supermix (Invitrogen). For PCR of the db2 allele the primers used were db2fwd1 (CCGTGTAGCAGAGAGACAGG) and db2rev2 (GGGGGTCTCATACAGGACAG) at a concentration of 1μm. For PCR of the flox allele the primers used were PshA1.a (GCCACAGCAAACCTCTTTCT) and PshA1.b (ACTTGTTGCATGGGACACAC) at a concentration of 5μm. The PCR parameters include an initial denaturation step at 95ºC for 5 minutes, followed by 35 amplification cycles of 95ºC for 1 minute, 63ºC for 1 minute and 72ºC for 40 sec and a final extension at 72ºC for 10 minutes.

17. Colitis Scoring

Colitis scoring was done according to the colitis scoring system used previously (Williams et al., 2001). The distal colons of mice from each genotype were examined and scored. Briefly the colitis score was based on 4 parameters: inflammation severity, inflammation extent, crypt damage and percent involvement. Inflammation severity was scores as follows: 0-none, 1-mild, 2-moderate, 3-severe. Inflammation extent was scored as follows: 0-none, 1-mucosa, 2-mucosa and submucosa, 3-transmural. Inflammation extent was scored as follows: 0-none, 1-mucosa, 2-mucosa and submucosa, 3-transmural. Crypt damage was scored as follows: 0-none, 1-basal 1/3 damaged, 2-basal 2/3 damaged, 3-crypts lost; surface epithelium present, 4-crypts lost surface epithelium lost. Percent involvement was scored as follows: 0-0%, 1-1-25%, 2-26-50%, 3-51-75%, 4-76-100%. The colitis score is presented as the total of the 4 parameters mentioned above.

18. Cell culture.

293T cells were cultured in Dulbecco's modified Eagle's medium (DMEM) containing 10% fetal bovine serum (FBS), 4.5 g/L glucose and 32 ug/ml gentamycin (Sigma, G1397). Caco2 cells were grown in DMEM containing 20% fetal bovine serum (FBS), 4.5 g/L glucose and 32 ug/ml gentamycin.

19. Caco2 cell differentiation

Caco2 cells at around 80% confluence were trypsinized and plated at a density of $3x10^5$ cells per plate in a 6cm plate. At this density cells reached confluence at day 3 after seeding. At day 2 RNA and protein are collected from the cells. These samples

correspond to day 2 sub-confluent cells. At day 9 RNA and protein were collected. These samples correspond to day 9 (6 day post-confluent) non-proliferative differentiating cells. Caco2 cells were maintained in culture up to 21 days (terminally differentiated).

20. RNA extraction from Caco2 cells

Caco2 cells were washed once in PBS and then 0.5-1.0 ml of TRI reagent is added to the tissue culture plate on ice. Cells are then resuspended in TRI reagent and frozen at -80°C until the RNA is extracted using the manufacturer's protocol.

21. Protein extraction from Caco2 cells

Caco2 cells are washed once with ice cold PBS and then lysed in 300ul of RIPA lysis buffer (25 mM Tris•HCl pH 7.6, 150 mM NaCl, 1% NP-40, 1% sodium deoxycholate, 0.1% SDS) + protease inhibitor cocktail (Sigma). Alternatively cells were lysed in urea lysis buffer (9.5 M urea, 2% CHAPS, 0.8% Pharmalyte pH 3-10, 1% (w/v) dithiothreitol). Cells are scraped off the plate using a tissue culture scraper and are incubated on ice for 20 minutes. Cells are then placed at -80°C until used for Western blotting.

22. Western blotting.

Caco2 cells were lysates were thawed on ice. Protein concentrations were determined with the Bio-Rad DC protein assay (Bio-Rad, 500-0006). Samples were boiled in 4X LDS Sample Buffer (Invitrogen, NP0007) with β-mercaptoethanol for 10 minutes. Samples were then centrifuged to remove debris and ~20μg was loaded on

4-12% Bis-Tris gel (Invitrogen, NP0322). The gel wa then transferred to a PVDF membrane and the membrane was blocked overnight blocking in 5% non-fat milk in PBS tween 0.05%. Endogenous Ets2, Cdx2 and tubulin were detected by immunoblotting using the rabbit polyclonal anti-Ets2 (Santa Cruz, SC-351) at a 1:1,000 dilution, monoclonal anti-Cdx2 (BioGenex, MU392-UC) at a 1:1,000 dilution and anti-α-tubulin (Sigma, T6199) antibodiy at 1:5,000 dilution in blocking buffer. Blots were then washed and then incubate in 1:2,000 HRP conjugated secondary antibody or 1:12,000 of Licor IRDye® labeled secondary antibody for 30 minutes at 4°C. This incubation was followed by 3 more washes of 5 minutes each in PBS-tween 0.05% and a final wash in DI water for 1 minute. Blots were the developed using ECL plus reagent from (Amersham, RPN2132) or using the Licor Odyssey system.

23. Microarray analysis.

Total RNA from whole colons of Ets2A$^{72/A72}$ and WT mice was extracted using the TRI Reagent (Molecular Research Center, Inc. TR118) according to the manufacturer's protocol. Four samples (2 males, and 2 females) of each of two mouse genotypes was analyzed as biological quadruplicates. For Caco2 cells, 4 samples from Caco2 cells grown for 2 days and 4 samples from Caco2 grown for 9 days were used. Labeled cRNA was prepared from 500 ng RNA using the Illumina RNA Amplification kit from Ambion. The biotin-labeled cRNA (750ng) was hybridized 18 h at 58ºC to the MouseRef-8 or HumanRef-8 Expression BeadChip (Illumina) according to the manufacturer's instructions. BeadChips were scanned with an Illumina BeadArray Reader,and hybridization efficiency was monitored using BeadStudio software (Illumina). BeadStudio software was used for the normalization

and quality control of the data. To identify statistically significant changes, the data were evaluated by GeneSpring software. A volcano plot was used to identify genes with changed at least 1.5-fold and had reproducibility P values of 0.05 or less. The list of genes passing these thresholds was compared with
publicly available data using the Nextbio search engine.

24. Immunohistochemical staining.

Colon blocks were deparaffinized with xylene and then rehydrated by washing in sequential dilutions of ethanol followed by rehydration in PBS. Antigen retrieval was done by heating samples in Dako Target Retrieval Solution (Dako, S1699). Samples were then washed 3X with PBS containing 0.1% Triton X-100 (PBS-T). Samples were then blocked with DAKO protein block serum free ready to use (Dako, X0909) for 1hr. Samples were then incubated with diluted primary antibodies for PCNA (Sigma, P8825), TUNEL and F4/80. Samples were then washed with PBS-T followed by addition of a 1:200 dilution of secondary biotinylated rabbit anti-rat IgG (Vector Laboratories) in PBS-T for 30 minutes at room temperature. Samples were rinsed and washed 5 minutes with PBS-T followed by addition of Vectorstain ABC Regeant in PBS-T for 30 minutes at room temperature. Following a final wash with PBS-T, staining was detected with DAB precipitate (Sigma, D4293).

25. Plasmids and cloning of CDX2 promoter constructs.

The flanking regions of the mouse Cdx2 gene (nt -3031 to +73) was amplified by PCR using Expand High Fidelity PCR kit (Roche) from BglII/NotI digested pcS170 genomic clone containing the Cdx2 locus (Tamai et al., 1999) and cloned into

MluI/XhoI sites of pGL3B (Promega). Fragments of Cdx2 promoter were cloned by PCR Supermix High Fidelity(Invitrogen) amplification of pcS170. Primers CGTCTCGAGTTACTAATAGAGTCTTGTAACGT and AGATCTTTCCTTCTTTCCTCCCACC spanned nt -56 to +73 of the Cdx2 promoter and generated XhoI and BglII restriction sites at the 5′ and 3′ ends, respectively, of the amplified product. Overlap PCR using two primer pairs (ACGCGTGGGACAATTAGCCAGCGG and CGAGTGTTTACAAGACTCTATTTAGGACTATCTCCCTCCC, GGGAGGGAGATAGTCCTAAATAGAGTCTTGTAAACACTCG and AGATCTTTCCTTCTTTCCTCCCACC) generated a fusion product of nucleotide -2233 to -1991 and nucleotide -51 to +73 of the Cdx2 promoter. PCR fragments were cloned into the pCR2.1TOPO vector and sequenced. The minimal Cdx2 promoter fragment was cloned into XhoI/BglII sites of pGL3B to generate Cdx2_56. The Cdx2_56DE1 fusion product was cloned into SacI/XhoI sites of pGL3B. The E18 Ets2 reporter gene and the FN-Ets2 expression have been described (Galang et al., 1994). The plasmids encoding Ets2 (FNEts2) has been previously described (Galang et al., 1996). FN-Ets2 DBM (Destruction box mutant) was kindly provided by Dr. Pumin Zhang and has been described previously (Li et al., 2008). Mutations in Cdx2_56DE1 were made using the Quickchange® II Site-Directed Mutagenesis Kit (Stratagene, 200523) using the manufacture's protocol.

26. Transfection and luciferase assays.

100,000 Caco-2 cells were plated to each well of 24-well plates in DMEM with 20% fetal calf serum and 32 ug/ml gentamycin (Sigma, G1397). The next day the

media was changed to media without antibiotics. Following the media change 0.5 ug of reporter vector, 250 ng of expression vector and 50 ng of pRLnull vector were transfected using Lipofectamine 2000 (Invitrogen, 11668019). Media was changed to DMEM containing 0.5% serum one day after transfection and cells were incubated overnight before lysis. Luciferase was detected using the Dual Luciferase Assay System kit (Promega, E1910) on a Veritas luminometer (Turner Biosystems).

III. ETS2 DELETION CONFERS A SELECTIVE ADVANTAGE TO STEM CELLS IN THE DISTAL COLON

1. Intestinal epithelial cell specific deletion of Ets2.

Since Ets2 has been shown to be a TCF4 target and suppresses ApcMin tumorigenesis in a gene dose dependent manner, Ets2 was specifically deleted in intestinal epithelial cells. To accomplish this, the Villin-Cre (V-Cre) transgene was used. In this mouse Cre recombinase is under the control of a 12.4kb regulatory region of the Villin promoter which is expressed specifically in epithelial cells of both the small and large intestine (el Marjou et al., 2004; Madison et al., 2002). This transgene contains an additional 3.4kb of 5' upstream flanking sequence and more closely recapitulates endogenous villin expression compared to a previously reported Villi-cre transgene (Pinto et al., 1999). The transgene is expressed within the stem cell compartment as is evident by monoclonal conversion R2RLacZ-reporter crypts. Figure 5 shows a schematic of the gene structure of the Villin-Cre and Rosa26LacZ reporter.

Villin-Cre transgenic animals were first crossed to Rosa26-reporter mice to determine the specificity of the transgene. As seen in figure 6, the small intestinal epithelium shows nearly completely uniform β-galactosidase staining. In contrast the colon shows a high degree of mosaicism with only 1/3 of the crypts being uniformly beta-galactosidase positive at 60 days of age consistent with previous studies which have used this transgene (Madison et al., 2002).The high degree of mosaicism presented both a problem and a benefit. The problem being that only a fraction of the cells in the colon could be targeted for both Ets2 deficiency and tumorigenesis. The

benefit being that the dynamics of Ets2 deficient cells could be traced throughout development within the context of neighboring crypts and cells with Ets2.

2. Ets2 deficient distal colons have decreased mosaicism throughout postnatal development.

To determine if Ets2 could influence the mosaicism of LacZ positive crypts within the colon, $Ets2^{Flox/Flox}$ mice were crossed to Villin-Cre and GTROSA26R to generate trigenic mice. Examination of whole mounts at 90 days revealed that there was an obvious decrease in mosaicism in the distal colon (Figure 7). This suggested that Ets2 deficient crypts might have a selective advantage in the colon. To determine when this selective advantage occurred, an aged related study was performed.

Mice were examined at 15, 30, 60 and 90 days after birth. By 15 days of age large patches of β-galactosidase crypts could be seen in whole mounts. Furthermore an enzymatic assay confirmed an increase in β-galactosidase activity at 18 days of age (Figure 8). Histological sections were then examined at all time points (Figure 9). During normal intestinal development in mice at two weeks of age crypts have formed and become uniformly blue and can be scored based on this criterion. Uniformly blue crypts were defined as crypts in which the entire crypt was populated from base to cuff with β-galactosidase positive crypts. Surprisingly, crypts from $Ets2^{F/F}$ $VillinCre^{+}Rosa26R^{+}$ had an increased percentage of uniformly blue crypts throughout the entire span of time tested compared to $Ets2^{F/+}$ $VillinCre^{+}Rosa26R^{+}$ and $Ets2^{+/+}$ $VillinCre^{+}Rosa26R^{+}$ mice (Figure 10). These data suggest that Ets2 deficiency confers a selective advantage to colon stem cells and thus facilitates the monoclonal conversion of these crypts. In addition the selective advantage due to Ets2 deficiency

is recessive since the presence of one functional allele prevents this selective advantage.

To ensure that blue crypts represented crypts which were indeed db2/db2 a PCR assay was optimized which allowed the detection of db2 or the flox allele down to one cell (5pg). Blue and white crypts were laser capture microdissected from $Ets2^{F/F}$ $VillinCre^{+}Rosa26R^{+}$mice. Microdissected crypts were then subjected to PCR analysis. As seen in figure 11, blue crypts from $Ets2^{F/F}$ $VillinCre^{+}Rosa26R^{+}$ mice contained the db2 allele and had undetectable levels of the flox allele. In contrast, white crypts had undetectable levels of the db2 allele and contained the flox allele. These data suggests that blue crypts in Ets2 have deleted Ets2. Furthermore, the absence of the flox allele supports the interpretation that blue crypts are uniformly Ets2 deficient.

3. Ets2 deficient crypts spread by crypt fission.

The most significant increase in blue crypts is seen at the time period between 15 and 30 days. This is the time period in which crypt fission peaks (Cheng and Bjerknes, 1985). In order to determine if crypt fission might account for the significant increase in blue crypts, the colons of 15 day old mice were examined for crypt bifurcation which is an indicator of crypt fission. As seen in figure 12, Ets2 deficient mice had a 2-fold increase in the percentage of crypts in fission. In addition when the bifurcated crypts were divided into blue and white crypts a dramatic difference in the percentage of blue crypts undergoing fission was seen. In $Ets2^{F/F}$ $VillinCre^{+}Rosa26R^{+}$ mice ~34% of uniformly β-galactosidase positive crypts were bifurcated compared to only ~13% in $Ets2^{F/+}$ $VillinCre^{+}Rosa26R^{+}$ and 10% in $Ets2^{+/+}$ $VillinCre^{+}Rosa26R^{+}$ mice. These data suggest that Ets2 deficient crypts have an increased fission rate.

Consistent with this, the increase in blue crypts reaches its peak at 30 days then the percentage of blue crypts remains stable up to 90 days. This is consistent with previously published reports in which crypt fission decreases to 1-2% of crypts after postnatal day 28. Interestingly, blue crypts continue to increase in percentage up to 90 days in both the $Ets2^{F/+}$ $VillinCre^{+}Rosa26R^{+}$ and $Ets2^{+/+}$ $VillinCre^{+}Rosa26R^{+}$ mice. Crypt fission is unlikely to account for this increase since bifurcating crypts were absent in colon sections from these animals at 60 and 90 days of age. One explanation for this is that the Villin-Cre transgene continues to be activated in stem cells generating uniformly β-galactosidase positive crypts by competition with β-galactosidase negative cells within the same crypt.

4. Spread of monoclonal crypts by fission leads to an increase in patch size.

It was hypothesized that Ets2 deficient crypts spread by crypt fission. To test this hypothesis patch sizes were measured at 15, 30, 60 and 90 days. Figure 13 shows the results of these measurements. When patch sizes of $Ets2^{F/F}$ $VillinCre^{+}Rosa26R^{+}$ mice at different ages were compared, there was a significant difference in patch size relative to age. This is consistent with the spread of Ets2 deficient crypts by fission and suggests that Ets2 deficient crypts are derived from other Ets2 deficient crypts. The increase in patch size is consistent with the increase in the percentage of uniformly blue crypts.

In contrast, when the heterozygous mice were compared, there was no significant difference in patch size relative to age. This suggests that uniformly blue crypts in heterozygous mice do not spread by crypt fission and are not related. This reinforces the conclusion that the increase in uniformly blue crypts seen in heterozygous

animals throughout the period of time studied is due to stochastic expression of Villin-Cre within the stem cell population rather than crypt fission.

Comparison of patch sizes between $Ets2^{F/F}$ $VillinCre^{+}Rosa26R^{+}$ and $Ets2^{F/+}$ $VillinCre^{+}Rosa26R^{+}$ revealed that there was a significant difference in patch size at 15, 30, 60 and 90 days. This suggests that Ets2 deficient crypts have a clear selective advantage compared Ets2 heterozygous crypts. These data are consistent with increased selective advantage of Ets2 deficient crypts and increased fission of these crypts.

5. Ets2 deficient colons have increased crypt depth, increased crypt density, increased percentage of goblet cells and increased proliferation.

Ets2 deficient colons had an increase in uniform β-galatosidase positive crypts. Despite this phenotype, there was no readily observable difference in morphology of Ets2 deficient crypts. In order examine any differences between Ets2 deficient and heterozygous mice, morphometric analysis of Ets2 deficient colons was performed.

To examine if crypt depths were different between $Ets2^{F/F}$ $VillinCre^{+}Rosa26R^{+}$ versus $Ets2^{F/+}$ $VillinCre^{+}Rosa26R^{+}$ mice, crypts from animals of 15, 30, 60 and 90 days were measured along different lengths of the distal colon. Figure 14 shows the results of measurements of crypt depth. Although crypt depth was not significantly different at 15 days, there was a significant difference at both 30 and 60 days. At 90 days, there was no significant difference. Interestingly there was a fluctuation in crypt depth occurring throughout the period studied. This fluctuation in crypt depth has been reported previously (Cheng and Bjerknes, 1985).

To insure that there was no bias in sampling, crypt depth measurements were plotted versus the distance from the anus from which the crypt depth measurement was taken (data not shown). Consistent with the crypt depth data, there was no difference in crypt depth at 15 and 90 days of age regardless of where the crypt depth measurement was made. In contrast, at 30 and 60 days of age crypt depth was higher in $Ets2^{F/F}$ $VillinCre^{+}Rosa26R^{+}$ versus $Ets2^{F/+}$ $VillinCre^{+}Rosa26R^{+}$ mice regardless of where the crypt depth measurement was made.

Since there was a significant increase in crypt depth at 30 days of age it was hypothesized that there would be an increase in the number cells per crypt. To test this hypothesis, the number of nuclei per crypt was measured. Figure 15 shows an example of used for these measurements. Surprisingly, there was no difference in the number of cells per crypt between $Ets2^{F/F}$ $VillinCre^{+}Rosa26R^{+}$ and $Ets2^{F/+}$ $VillinCre^{+}Rosa26R^{+}$ mice. This suggested that there might be a increase in the cell size or composition of the crypts.

To examine if there was a difference in the composition of the crypts, the number of goblet cells was measured at 30 days. This time point was chosen because of sample size (4 mice per genotype), and the percentage of uniformly blue crypts peaked at this time period. Figure 16 shows the results of these measurements. As can be seen there is a significant increase in the percentage of goblet cells in $Ets2^{F/F}$ $VillinCre^{+}Rosa26R^{+}$ versus $Ets2^{F/+}$ $VillinCre^{+}Rosa26R^{+}$ mice. This suggests that the increase in crypt depth of $Ets2^{F/F}$ $VillinCre^{+}Rosa26R^{+}$ versus $Ets2^{F/+}$ $VillinCre^{+}$ $Rosa26R^{+}$ mice is due to an increase in the large goblet cells.

Crypt density was then measured to determine if more crypts were present in the $Ets2^{F/F}$ $VillinCre^{+}Rosa26R^{+}$ versus $Ets2^{F/+}$ $VillinCre^{+}Rosa26R^{+}$ mice. Crypt density was

measured within the same length of the distal colon in which crypt depth was measured. Crypt density was consistently higher in $Ets2^{F/F}$ $VillinCre^{+}$ $Rosa26R^{+}$ versus $Ets2^{F/+}$ $VillinCre^{+}$ $Rosa26R^{+}$ mice at all ages examined (Figure 17). This suggests that although the percentage of total crypts in fission did not differ significantly between $Ets2^{F/F}$ $VillinCre^{+}Rosa26R^{+}$ versus $Ets2^{F/+}$ $VillinCre^{+}Rosa26R^{+}$ mice, the actual number of crypts in fission is increased.

In summary, epithelial specific deletion of Ets2 in the colon provides a selective advantage to Ets2 deficient cells. As a consequence Ets2 deficient stem cells and their progeny replace cells which retain Ets2. Ets2 deficient crypts are able to spread through crypt fission giving rise to new Ets2 deficient crypts. This results in an increase in the size of patches of Ets2 deficient crypts as animals age.

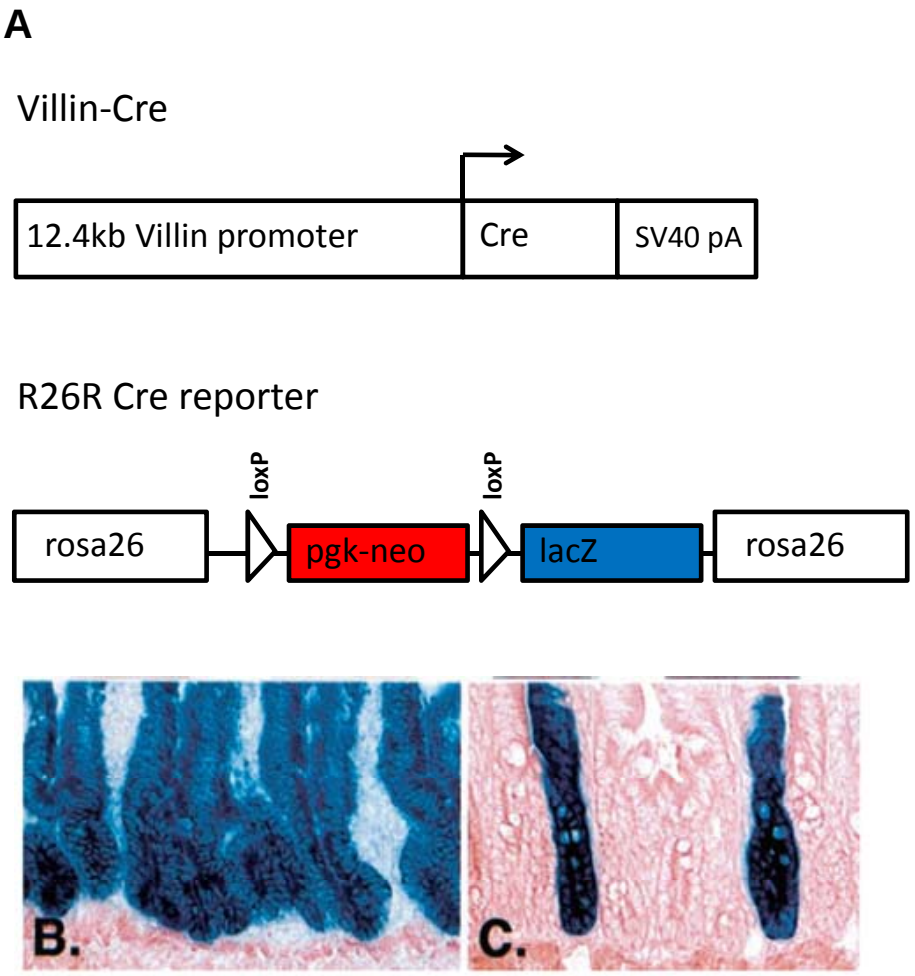

Figure 5. Villin-Cre transgenic line and Cre reporter mouse. (A) Illustration of the villin-Cre transgenic line and the R26R allele. Cre, Cre recombinase. SV40 pA, SV40 polyadenylation signal. B,C) Detection of Cre activity in villin-cre mice using R26R reporter, which was reported by el Madison *et al*. 2002. Recombination is detected throughout the entire crypt-villus axis with no recombination seen outside of the epithelium. In the small intesitine (B) nearly complete recombination occurs. C)Villin-cre recombination is mosaic in the colon.

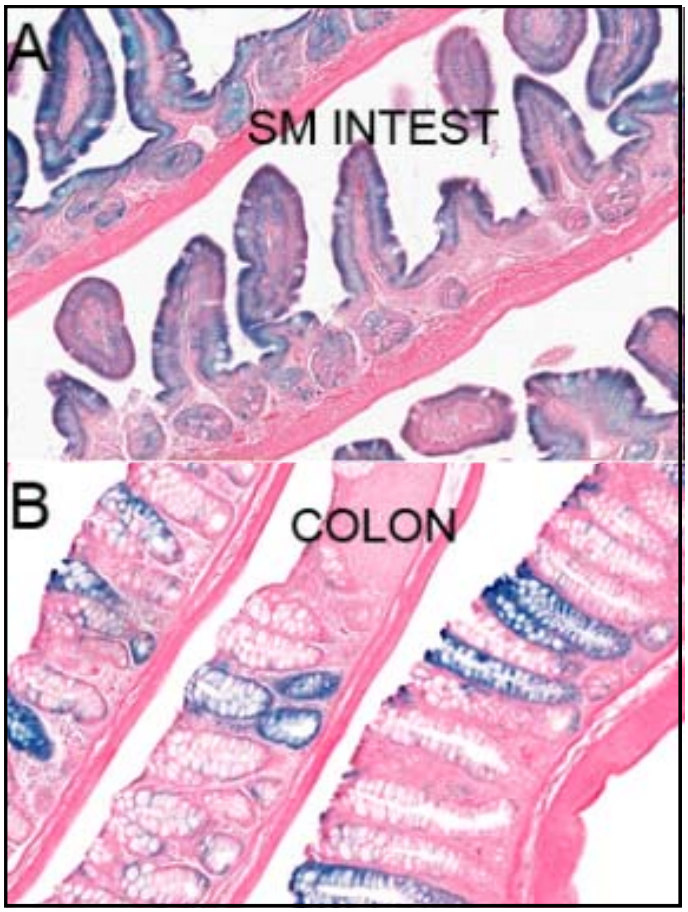

Figure 6. Cre activity is revealed by X-gal staining (blue color) in small intestine (A) and colon (B) of Villin-Cre; R26R bitransgenic mice. Nearly complete recombination can be seen in small intestinal epithelium. In the colon only ~1/3 of crypts is recombined.

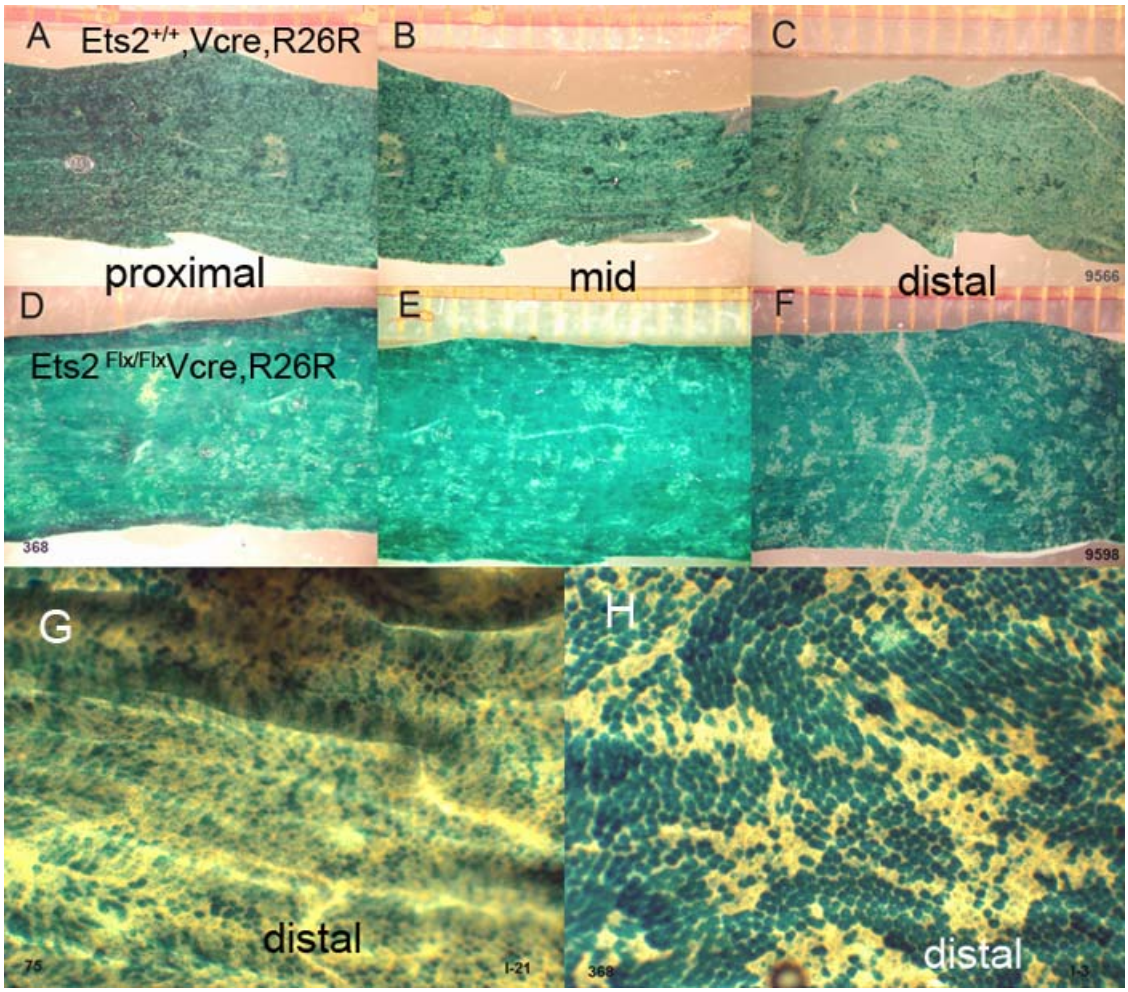

Figure 7. Villin-Cre mosaicism is decreased in $Ets2^{Flox/Flox}$ vs $Ets2^{+/+}$ mice. To examine mosacism of the Villin-Cre transgene, Villin-Cre Rosa 26 reporter mice were crossed with Ets2floxed of WT mice. Colons were removed fixed and stained for LacZ. Notice that Ets+/+ exhibit mosaicism in proximal, mid and distal regions with the distal colon (A,B,C). In contrast Ets2floxed mice exhibit decreased mosaicism (D,E,F). Random distribution of crypts is seen in the colon of WT mice (G) while patches of recombined crypts are seen Ets2Flox mice (H).

Figure 8. Decreased mosaicism of Ets2flx/flx at 15 days. Comparison of whole mounts of $Ets2^{+/+}$ (A,D), $Ets2^{flx/+}$ (B,E) and $Ets2^{flx/flx}$ (C,F) mice at 15 days. Random β-galactosidase crypts are seen in $Ets2^{+/+}$ and $Ets2^{flx/+}$ colons. In contrast, large patches of β-galactosidase are seen suggesting crypt are related. (G) Results of assay for β-galactosidase activity at 18 days. Colons were removed and divided into 4 different portions. The y-axis represents the total luciferase units. Each bar represents the results of the β-galactosidase activity assay for an individual mouse. In the x-axis proximal, mid-1, mid-2 and distal represents the region of the colon which was assays.

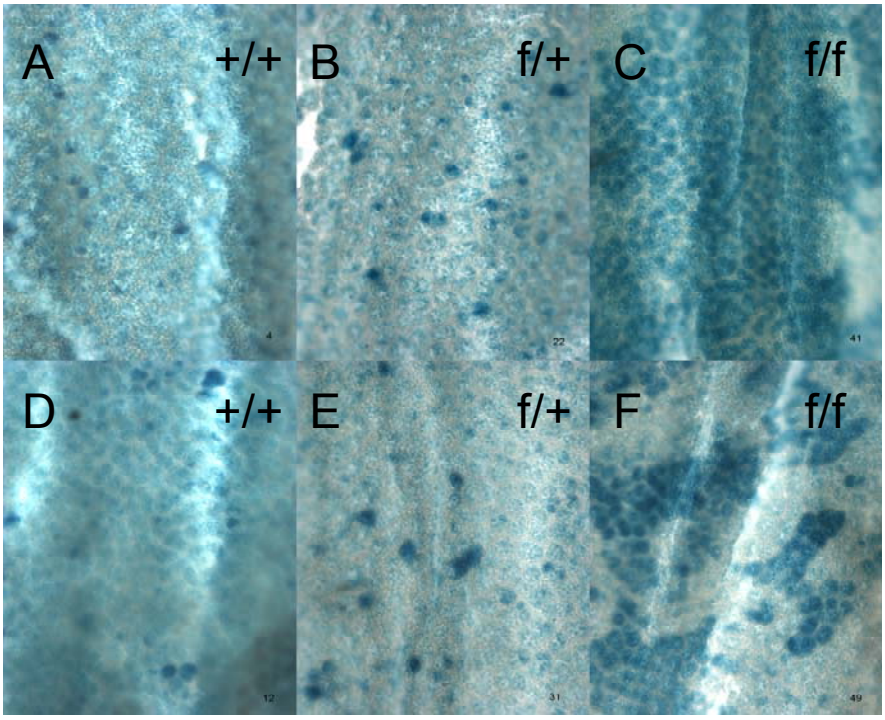
A
+/+
B
f/+
C
f/f
D
+/+
E
f/+
F
f/f

G

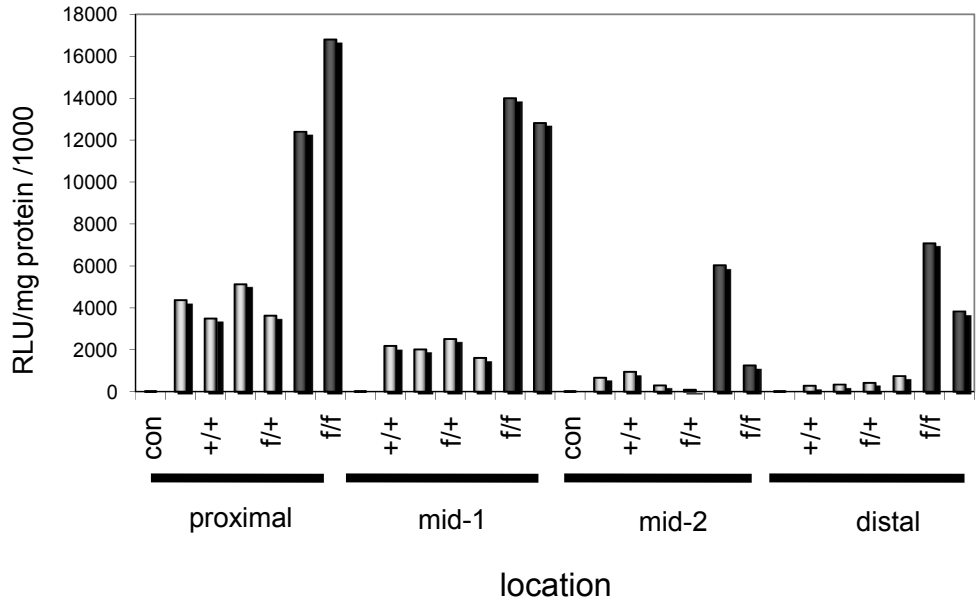
RLU/mg protein /1000
18000
16000
14000
12000
10000
8000
6000
4000
2000
0
con
+/+
f/+
f/f
+/+
f/+
f/f
con
+/+
f/+
f/f
+/+
f/+
f/f
proximal
mid-1
mid-2
distal
location

Figure 9. Comparative histology of $Ets2^{F/F}$ V-Cre^{+} $R26R^{+}$ and $Ets2^{F/+}$ V-Cre^{+} $R26R^{+}$ colons. Photographs of the distal colon of mice of 15, 30, 60 and 90 days are shown. At each time point there is a obvious difference in the number of uniform β-galactosidase positive crypts. Scale bar represents 100μm.

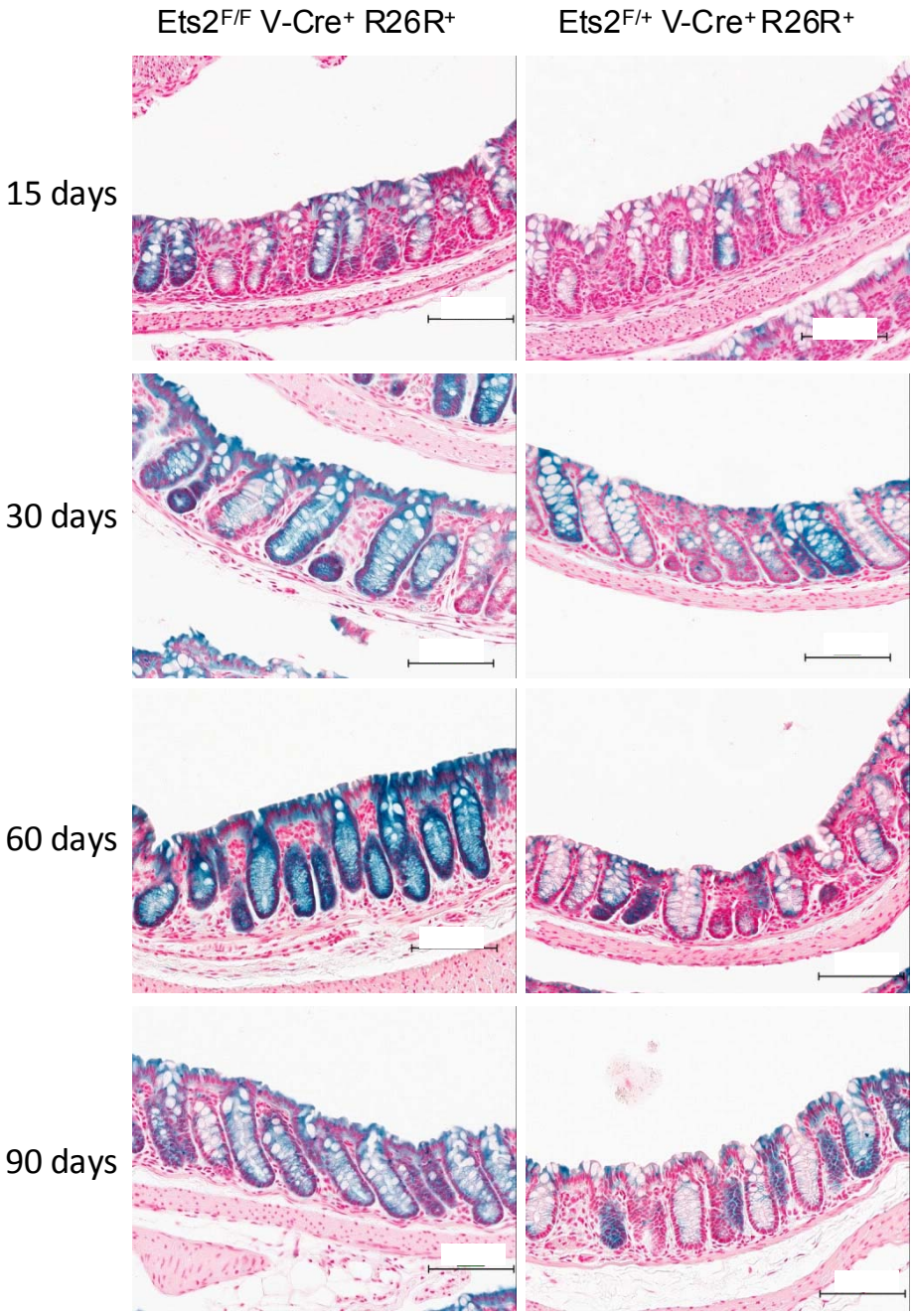
Ets2F/F V-Cre+ R26R+
Ets2F/+ V-Cre+ R26R+
15 days
30 days
60 days
90 days

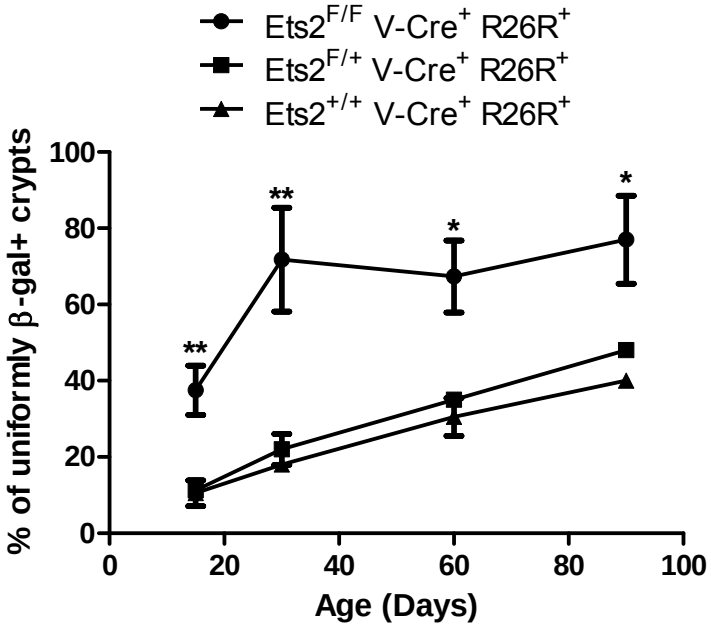

Figure 10. Percentage of uniformly blue crypts as a function of age. For 15 days the n= 2, 2 and 2 for Ets2flx/flx, Ets2flx/+ and Ets2+/+ respectively with 2 sections quantitated per mouse. For 30 days n= 4, 4, and 1. For 60 days n=3,2 and 2. For 90 days n= 3, 1 and 2. ** represents a p-value <0.01 from a two-tailed t-test. * represents a p-value <0.05 from a two-tailed t-test. At 60 and 90 days Ets2flx/+ and Ets2+/+ were group together for the t-test. Error bars represent standard deviation.

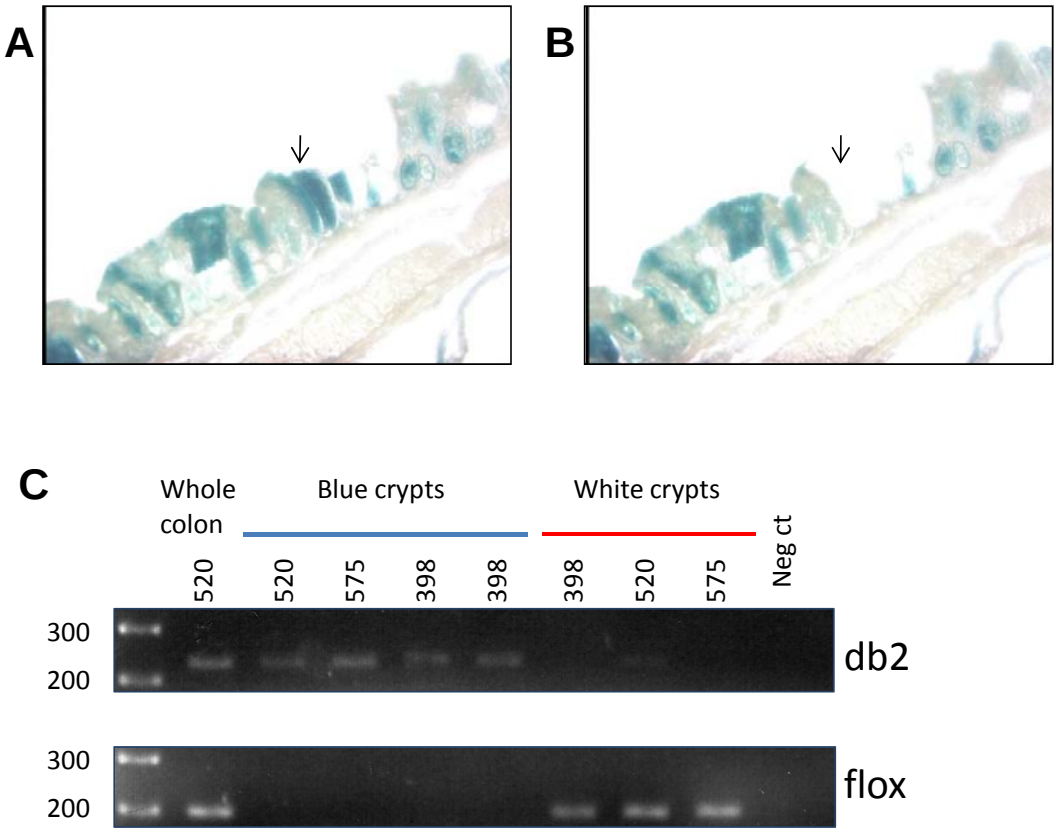

Figure 11 . Ets2 is deleted in LacZ positive but not in LacZ negative crypts. A, Example of blue crypts from Ets2Flox/Flox Villin-Cre+ R26R+ mice prior to laser capture microdissection (LCM). B, Photo post LCM. DNA was isolated and used for PCR. C, Results of PCR showing deletion of Ets2 in blue crypts but not in white crypts. The floxed allele is still present in 3 of the 3 white crypts. Numbers above lane represent individual animals.

Figure 12. Crypt fission rates as a function of time. (A) Examples of crypts in fission for each genotype at postnatal day 15 (P15). Arrows point to bifurcated crypts. (B) Crypt fission rates during time points tested. The % of bifurcating crypts is the percentage of crypts in bifurcation divided by the total number of crypts scored. For each meausurement, at least 86 well oriented crypts were scored. Error bars represent the standard deviation. For 15 days the n= 2, 2 and 2 for Ets2flx/flx, Ets2flx/+ and Ets2+/+ respectively with 2 different sections quantitated for each mouse. For 30 days n= 4, 4, and 1. For 60 days n=3,2 and 2. For 90 days n= 3, 1 and 2. (C) Percentage of blue crypts in fission was determined by scoring bifurcated crypts as blue or white. The percentage of total blue crypts that were scored as bifurcating is shown for 15 and 30 days

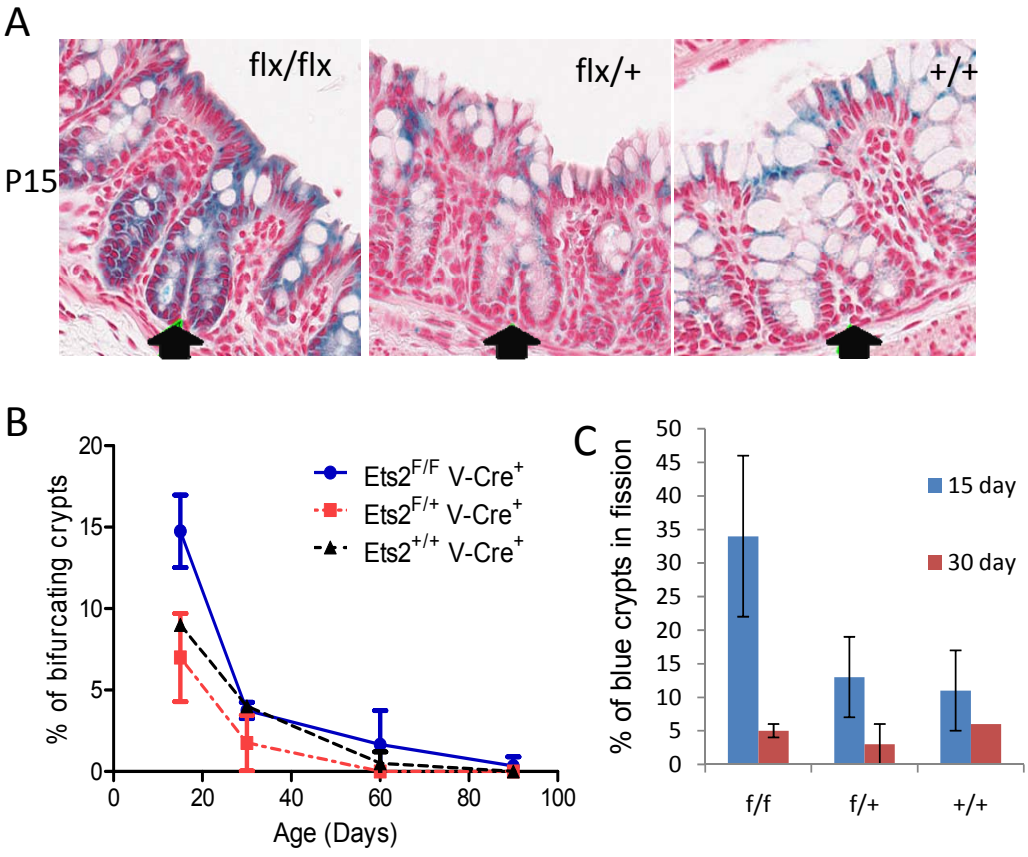
A
P15
flx/flx
flx/+
+/+
B
% of bifurcating crypts
Age (Days)
Ets2F/F V-Cre+
Ets2F/+ V-Cre+
Ets2+/+ V-Cre+
C
% of blue crypts in fission
15 day
30 day
f/f
f/+
+/+

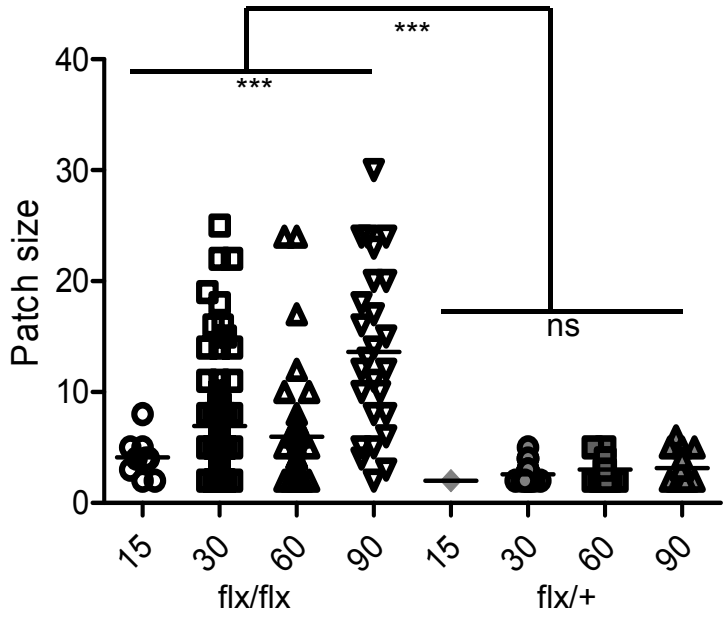

Figure 13. Patch size increases with age in Etsflx/flx but not in flx/+ mice. Patch sizes (defined as 2 or more adjacent crypts) were measured for each individual mouse at each age. In Ets2flx/flx mice, analysis of patch sizes at all different ages reveals that there is a significant difference in patch size during postnatal development. Patch sizes differences within each genotype were measured using a one-way ANOVA test. For Ets2flx/flx mice there was a significant difference in patch sizes within the group ($p<0.0001$). In contrast patch size in Ets2flx/+ mice did not change with age as revealed by a one-way ANOVA test ($p=0.25$). ns = not significant. Differences in patch size between the two genotypes was determined by Mann-Whitney test ($p<0.0001$).

Figure 14. Crypt depth during postnatal development. (A) Example of an Ets2flx/flx colon with several depths measure along the length of the distal colon. At the center of the picture is the most distal part of the colon. The “Swiss roll” represents a more proximal region as it extends from the center. (B) Graph depicting results of measurements. At least 6 crypt depth measurements were made for colon sections from each mouse (n). For 15 days the n= 2, 2 Ets2flx/flx, and Ets2flx/+ respectively. For 30 days n= 4 and 4. For 60 days n=3 and 2. For 90 days n= 3 and 1. Differences between crypt depth in Ets2flx/flx vs Ets2 flx/+ mice were examined for each timepoint. ns indicates that the difference in values of the two groups in not significant by t-test. ** indicates a p value of <0.01. *** indicates a p value <0.0001.

A

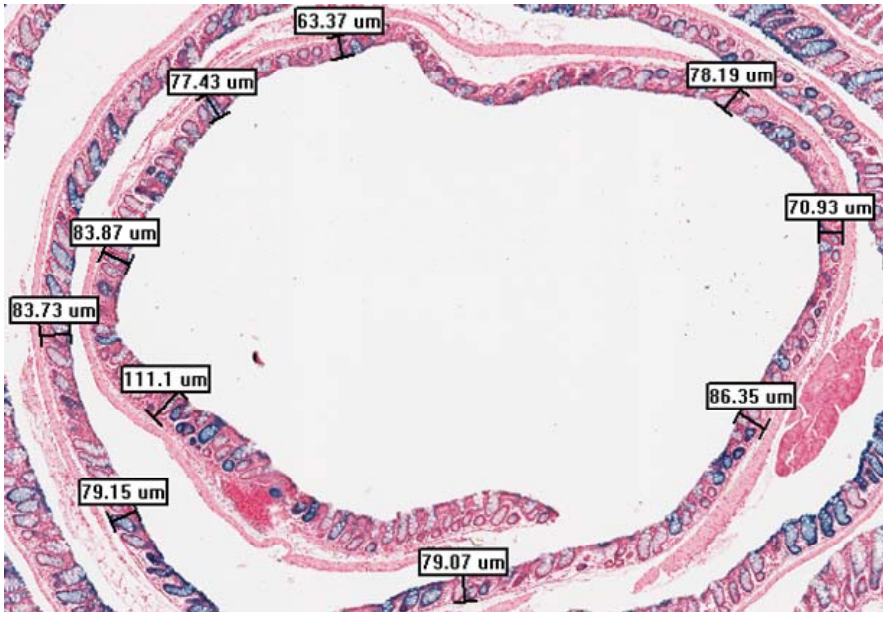
63.37 um
77.43 um
78.19 um
70.93 um
83.87 um
83.73 um
111.1 um
86.35 um
79.15 um
79.07 um

B

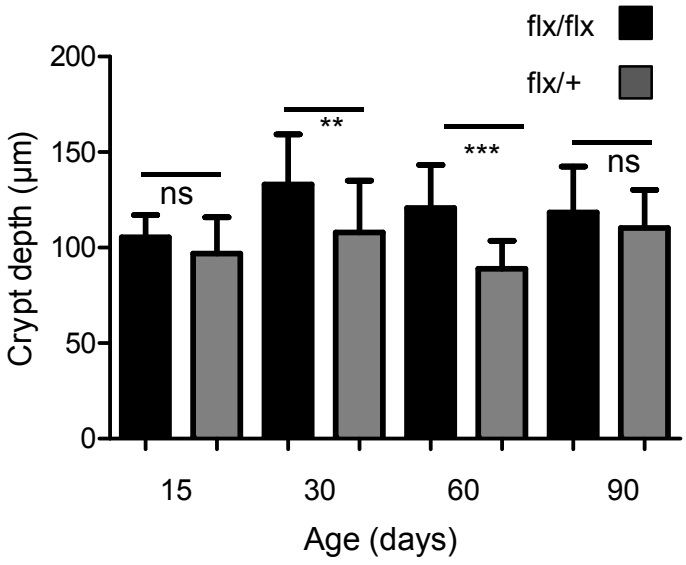
flx/flx
flx/+
200
150
100
50
0
Crypt depth (µm)
ns
**
***
ns
15
30
60
90
Age (days)

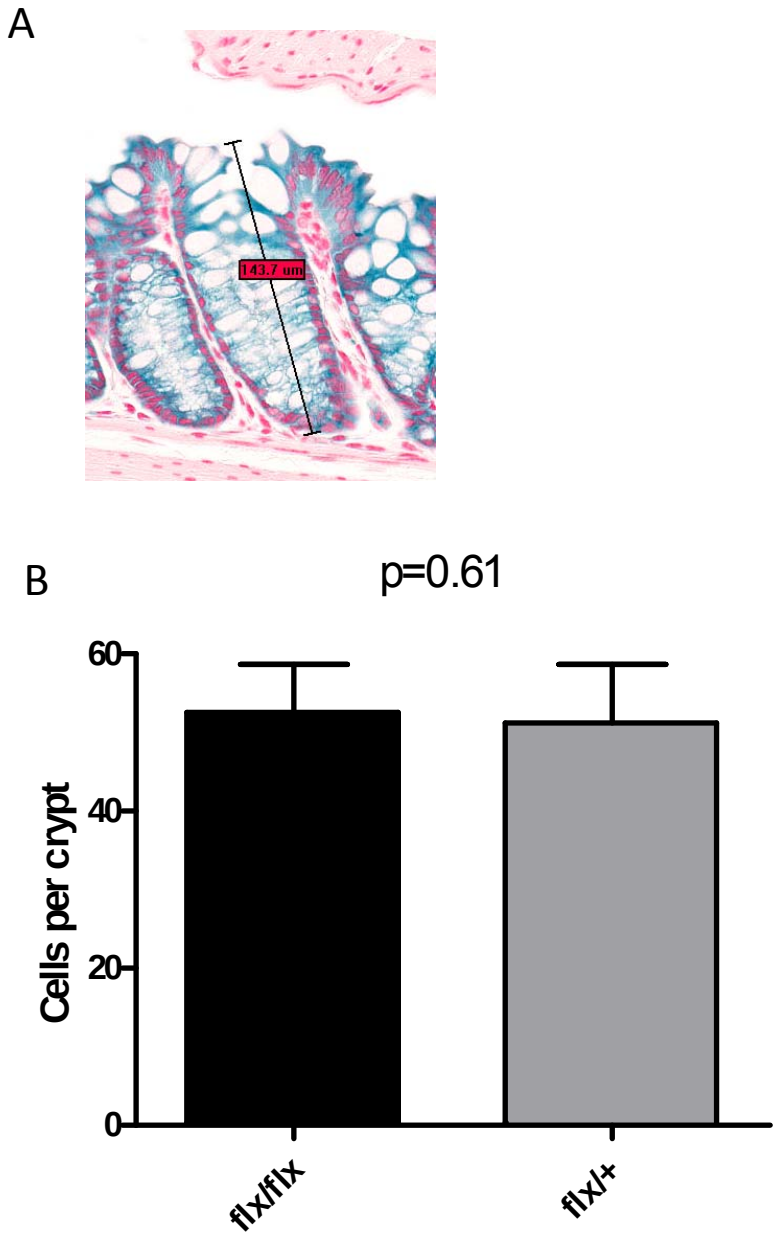

Figure 15. Cells per crypt. (A) Example of crypt used for measuring the number of cells per crypt. (B) Graph of cell numbers per crypt in Ets2 flx/flx versus flx/+. N=4 for flx/flx and n=3 for flx/+. 7-13 well oriented crypts were counted per mouse. Error bars represent standard deviation. P value is from student t-test.

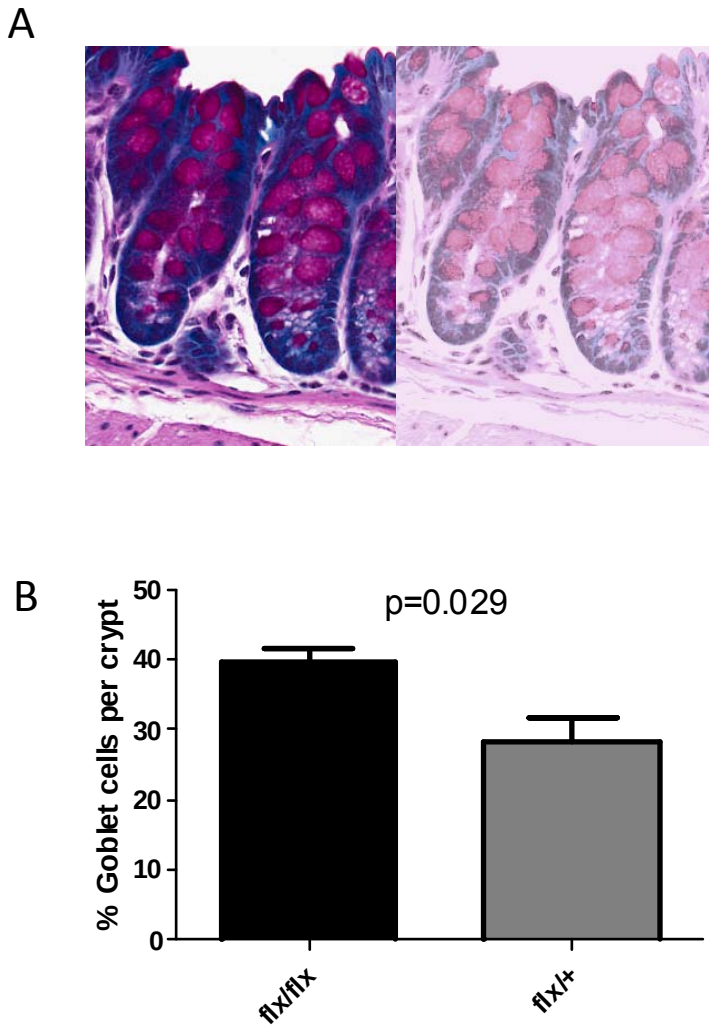

Figure 16. Goblet cell counts. (A) Five fields per mouse of PAS stained colon were photographed. The number of goblet cells and the number of nuclei were determined for each crypt within each field. Example of 2 crypts from a section of a flx/flx mouse. The picture on the right was adjusted for brightness and contrast in order to distinguish nuclei. (B) Graphs of the number of globlet cells divided by total nuclei presented as percentage. P value is from Mann-Whitney test. N=4 mice per genotype with 5 fields being scored per mouse.

Figure 17. Crypt density as a function of age. (A) Example of a section used for calculation of crypt density. The number of crypts along the purple line were counted and divided by the length in mm. (B) Graph of crypt densities at 15, 30 and 90 days. * denote grouped values which were significantly different by Mann-Whitney test. ns= not significant.

A

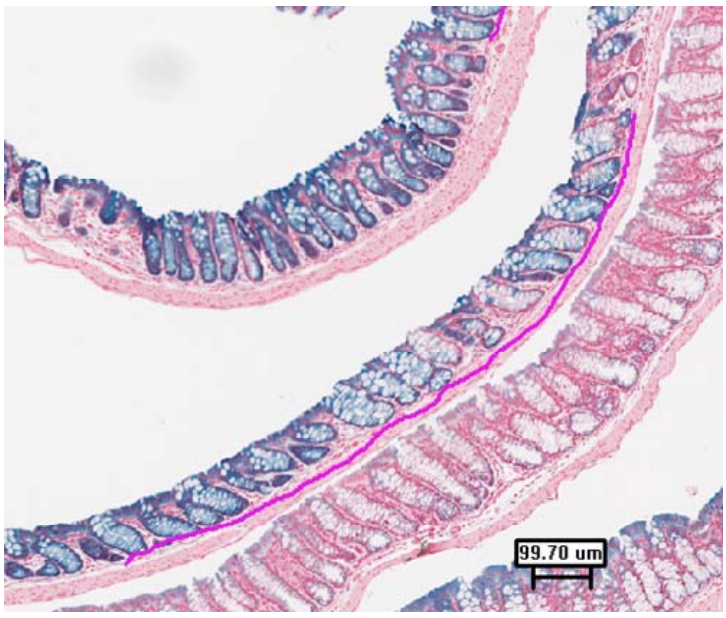

B

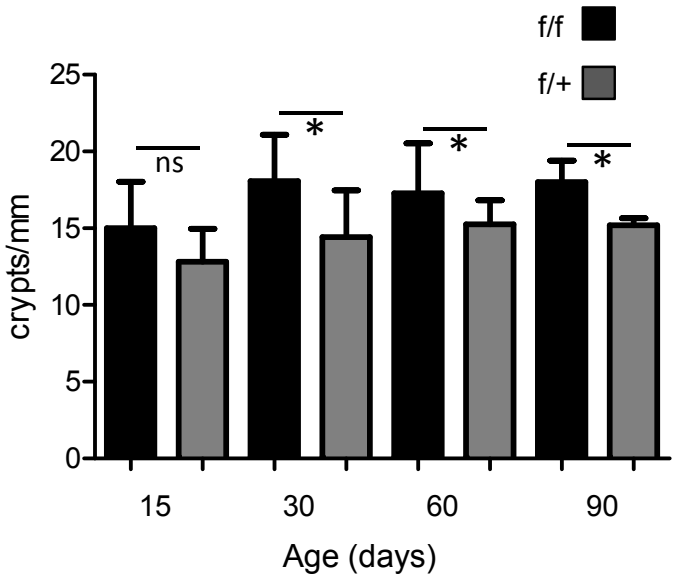

IV. ETS2 SUPPRESSES COLON TUMORIGENESIS CELL AUTONOMOUSLY.

1. Epithelium specific deletion of Ets2 leads to increased tumor multiplicity

Ets2 has been demonstrated to have to repressive activity in the ApcMin model of intestinal tumor formation. In a mouse model of trisomy 21, the number of copies of Ets2 gene inversely correlated with tumor multiplicity and tumor size (Sussan et al., 2008). However, a statistically significant difference between 2 copies and 1 copies of Ets2 was not seen likely due to accelerated mortality in mice carrying only one copy of Ets2. Furthermore, Apc^{Min} tumors appear predominantly in the small intestine and only sparsely in the colon. If Ets2 deficiency results in an increased in number or proliferative state of colonic stem cells, a cell autonomous repression of colonic tumors might be predicted. The colitis associated cancer regimen initiates tumors in the distal colon likely due to the effects of DSS on this region (Cooper et al., 1993; Okayasu et al., 1990). Another advantage of this model is the relatively short period of time needed to induce tumors (9 weeks).

$Ets2^{F/F}$ $VillinCre^{+}$, $Ets2^{F/+}$ $VillinCre^{+}$ and $Ets2^{F/F}$ $VillinCre^{-}$ mice were subjected to the colitis associated cancer regimen. Animals were then sacrificed and scored for the number of tumors and tumor size. There was a 50% increase in tumor number in $Ets2^{F/F}$ $VillinCre^{+}$ when compared to $Ets2^{F/+}$ $VillinCre^{+}$ and $Ets2^{F/F}VillinCre^{-}$ mice (Figure 18). This increase in tumor multiplicity underestimates the effect of Ets2 deficiency on tumor multiplicity since at this age only 66% crypts are uniformly Ets2 deficient at the age of AOM injection. Adjustment of the tumor number based on the actual degree of Ets2 deficiency suggests an even greater effect for uniform Ets2 deficiency. Furthermore, the $Ets2^{F/+}$ $VillinCre^{+}$ and $Ets2^{F/F}VillinCre^{-}$ mice had an

almost identical tumor number suggesting that Ets2 acts as a recessive allele. This suggests that Ets2 behaves like a classic tumor suppressor in that the loss of tumor suppressive activity requires the loss of both alleles.

2. Tumor size is not affected by Enterocyte specific deletion of Ets2

To determine if Ets2 deficiency affects tumor growth, the diameter of tumors was measured for each genotype. Tumor sizes revealed that tumors arising $Ets2^{F/F}$ $VillinCre^{+}$, $Ets2^{F/+}$ $VillinCre^{+}$ and $Ets2^{F/F}VillinCre^{-}$ mice are nearly identical in size (Figure 18). This data suggests that in the context of chronic inflammation, Ets2 is involved in the suppression of tumor initiation but not in the suppression of tumor growth.

3. Recombination in Ets2 deficient tumors.

To examine the extent of recombination of tumors in Ets2 deficient mice a PCR assay for measuring Ets2 recombination was performed. To decrease contaminant stromal cells from contributing to detection of the flox allele, laser capture microdissection was used. Laser capture microdissected samples were then subjected to PCR for the Ets2db2 and Ets2flox alleles. As seen in figure 19, all 9 tumors examined contained only the Ets2db2 allele while only 2 contained some flox allele. Predominance of the db2 allele in all 9 tumors suggests that tumors arise preferentially from Ets2 deficient cells. The presence of the flox allele in 2 of the 9 alleles may be due to contamination by stromal cells as has been reported previously (Biswas et al., 2004). At the time of tumor induction, the percentage of uniformly Ets2 deficient was 67%. This suggests that if induction of tumors was random and there

was no advantage for Ets2 deficient cells, then 35% of tumors would be expected to be completely $Ets2^{flox/flox}$.

4. Ets2 deficient crypts have increased proliferation in the stem cell compartment.

To determine if the increase in tumors in Ets2 deficient mice was due to an increase in target cells, PCNA staining was perfomed on untreated colon sections from $Ets2^{F/F}$ $VillinCre^{+}$ and $Ets2^{F/F}$ $VillinCre^{-}$ mice. Interestingly, there was a distinct difference in PCNA staining in Ets2 deficient mice. Figure 20 shows examples of 5 different crypts from 2 $Ets2^{F/F}$ $VillinCre^{+}$ mice and 4 crypts from 2 $Ets2^{F/F}$ $VillinCre^{-}$ mice. As can be seen in panel A, 4 of the 5 Ets2 deficient crypts stain positive for PCNA within the first 4 cells from the base. In contrast, only 1 of the 4 wild-type crypts stains positive for PCNA within the crypt base. This suggests that Ets2 deficient crypts are more proliferative than wild-type crypts and contain more actively cycling stem cells.

Figure 18 . Tumor multiplicity but not size is increased in $Ets2^{F/F}$ V-Cre^{+} mice compared to $Ets2^{F/+}$ V-Cre^{+} and $Ets2^{F/F}$ V-Cre^{-} mice following the 9 week AOM/DSS regimen. A, Histology of colon from an $Ets2^{F/F}$ V-Cre^{+} (Scale bar = 500 microns).B, Comparison of tumor numbers between $Ets2^{F/F}$ V-Cre^{+} (with and without adjustment for mosaicism) , $Ets2^{F/+}$ V-Cre^{+} and $Ets2^{F/F}$ V-Cre^{-} mice. F, $Ets2^{F/F}$ V-Cre^{+} , $Ets2^{F/+}$ V-Cre^{+} and $Ets2^{F/F}$ V-Cre^{-} mice. P value is from student t-test.

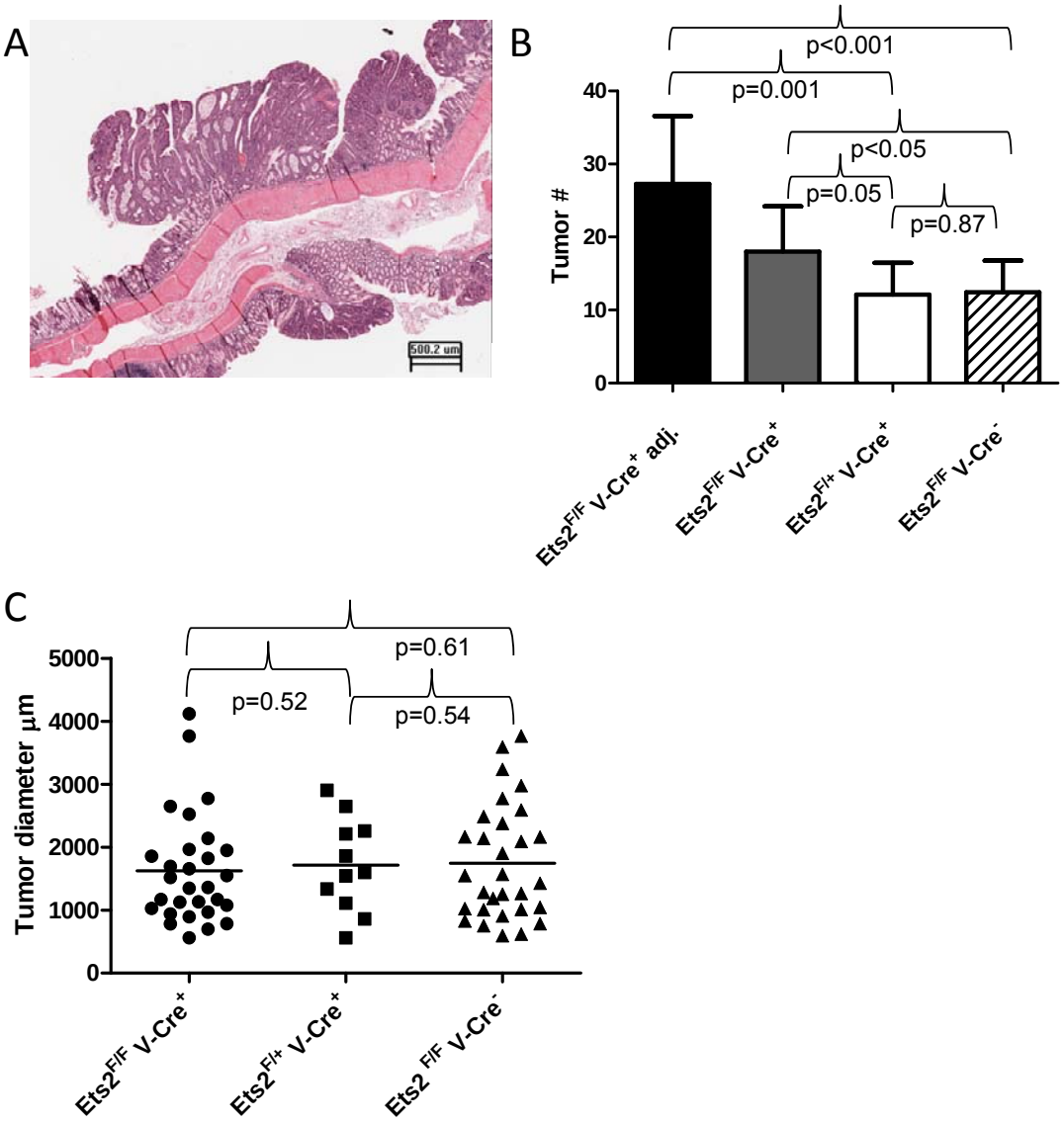
A
500.2 um
B
p<0.001
p=0.001
p<0.05
p=0.05
p=0.87
Tumor #
40
30
20
10
0
Ets2F/F V-Cre+ adj.
Ets2F/F V-Cre+
Ets2F/+ V-Cre+
Ets2F/F V-Cre-
C
p=0.61
p=0.52
p=0.54
Tumor diameter µm
5000
4000
3000
2000
1000
0
Ets2F/F V-Cre+
Ets2F/+ V-Cre+
Ets2 F/F V-Cre-

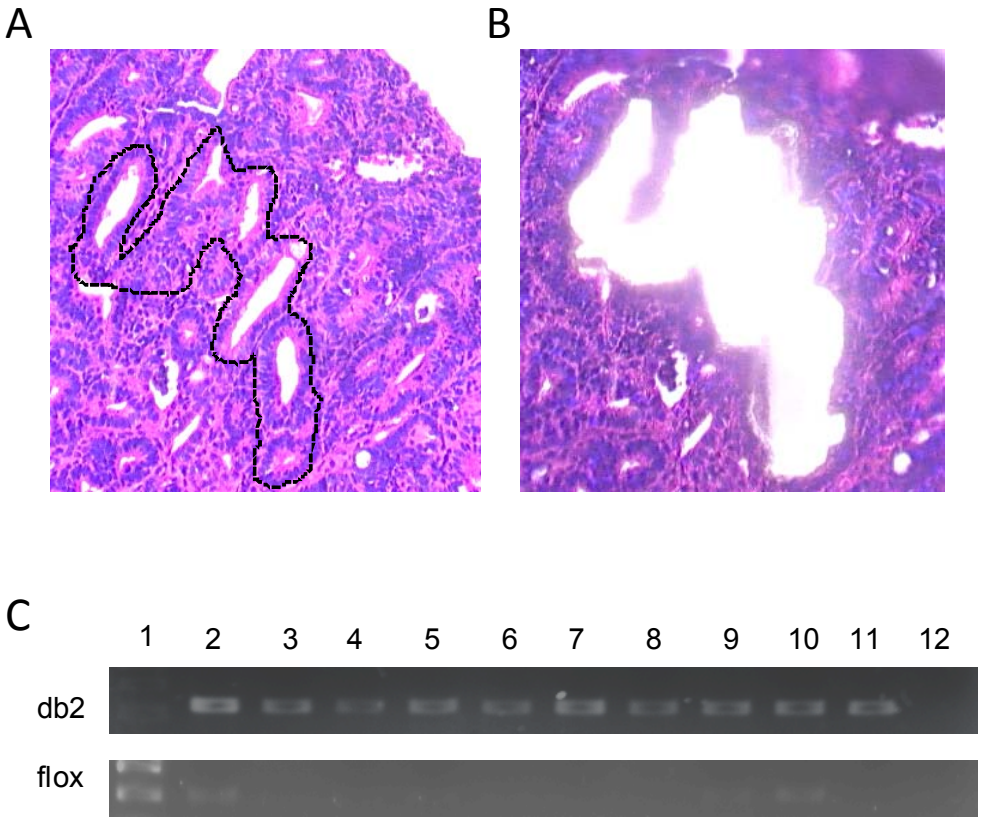

Figure 19. Ets2 is deleted within tumors from $Ets2^{F/F}$ V-Cre^{+} mice. A) Photograph of a tumor from an $Ets2^{F/F}$ V-Cre^{+} mouse prior to laser capture microdissection. The area which was microdissected is illustrated by the dotted line. B) Photograph of tumor are following microdissection. C) PCR analysis of laser capture microdissected tumors. Laser capture sections were subjected to PCR for db2 or flox alleles. Lane 1 is a 100bp ladder. Lanes 3-10 are 10 tumors from 3 different $Ets2^{F/F}$ V-Cre^{+} mice. Lane 12 is a water control.

A

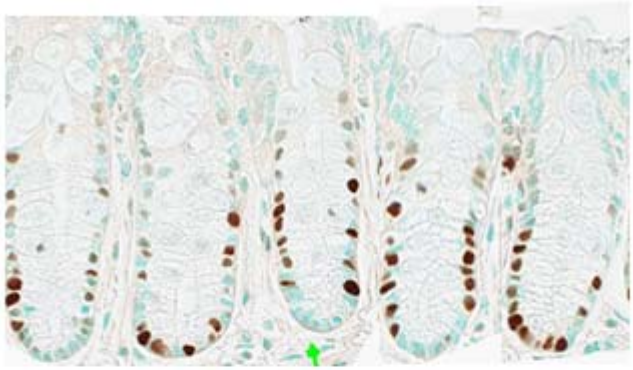

B

C.

PCNA positive cells by crypt region

Genotype	Bottom 1/3	Middle	Top 1/3	Total
Ets2Flx/Flx V-Cre+	119	42	0	161
Ets2Flx/Flx V-Cre-	35	57	0	92
ttests	<0.001	0.47	n/s	<0.05

Figure 20. The number of PCNA positive cells are increased in Ets2 deficient mice. A) Representative crypts from 2 $Ets2^{F/F}$ V-Cre^{+} mice. B) Representative crypts from 2 $Ets2^{F/F}$ V-Cre^{+} mice. C) Table summarizing results of PCNA quantitation. Two animals from each genotype were examined. 23 crypts per animal were scored.

IV. ERK PHOSPHORYLATION IS REQUIRED FOR THE TUMOR REPRESSIVE ACTIVITY OF ETS2

1. Ets2$^{A72/A72}$ mice have increased susceptibility to colitis associated cancer.

To determine if Ets2 phosphorylation by Erk is required for the tumor repressive effect of Ets2, animals in which the threonine 72 is mutated to an alanine were subjected to the CAC model as before. In addition to the colitis associated cancer treated mice, 3 control treatments were also performed. One group was injected with AOM alone, one group was subjected to the DSS cycles alone and one group remained untreated. The health of the mice was closely monitored by weighing the mice every 2 days. Treatment with DSS had a relatively little effect on the weight of the mice in the presence an absence of AOM injection suggesting the particular lot of DSS used in this experiment was relatively weak in terms of its ability to induce colitis (data not shown). Despite the relatively mild induction of colitis, Ets2$^{A72/A72}$ had a 2-fold increase in tumor number (Figure 21). However, when tumor area was measured there was no significant difference in tumor diameter between genotypes. This suggested that the increase in tumors in Ets2$^{A72/A72}$ mice was due to increase initiation rather than increased tumor progression. Neither of the control groups developed tumors recapitulating the results of previous studies (Okayasu et al., 1990; Okayasu et al., 1996).

Examination on tumors revealed that they were adenomas with high grade dysplasia. None of the tumors became invasive. Furthermore, these adenomas displayed nuclear β-catenin (Figure 21) in accordance with previous studies using this

model. This suggests that adenomas in Ets2$^{A72/A72}$ develop from stem cells which have acquired and Wnt activating mutation.

In a second trial, animals were again treated with the CAC regimen but were sacrificed 10 weeks after the last DSS treatment to permit tumors to become sufficiently large for additional analysis. As seen in figure 22, tumor numbers were very similar to those from the first group and tumor became large enough to be excised. While Ets2$^{A72/A72}$ mice developed more tumors than control animals, examination of the histopathology failed to find distinguishing characteristics of the tumors from the two genotypes of mice. Immunohistochemical staining for proliferative cells (proliferative cell nuclear antigen) confirmed that tumor cells were proliferating rapidly (Figure 23). However, quantitation of the staining over multiple tumors of each mouse did not reveal a significant genotype dependent difference (Figure 24A). Furthermore, the frequency of apoptotic cells was not significantly different (Figure 24B) although the number of slides available for the wt tumors was limited. Finally macrophages were identified by staining for the F4/80 antigen (Figure 24C). Within the tumors the number of F4/80 positive cells was not significantly different. This result was consistent with the macrophage association with mammary tumors in Ets2 deficient host (Man et al., 2003b) and macrophage number in an inflammatory disease model, *motheaten viable,* Ets2$^{A72/A72}$ (Wei et al., 2004). Macrophage development and numbers are not dependent on Ets2 activation although multiple macrophage metalloprotease, cytokines and growth factors are deficiently induced in vitro and in mammary tumors. In aggregate, these data suggest that Ets2 may act at an early stage of tumor formation.

2. Ets2A$^{72/A72}$ mice do not display decreased colitis.

Because Ets2 is involved in inflammation (Wei et al., 2004) and has been implicated in inflammatory bowel diseases (van der Pouw Kraan et al., 2009) the possible contribution of the inflammatory compartment to colitis associated tumorigenesis was determined. Acute colitis was induced using a higher dosage of DSS (3.5%). This dosage was previously used to demonstrate a difference between Villin-Cre IKKβ$^{F/\Delta}$ and IKKβ$^{F/\Delta}$ mice. Unexpectedly, Ets2$^{A72/A72}$ mice responded almost identically to this acute colitis treatment (Figure 25). Clinical signs such as stool consistency, blood in the stool and weight loss were virtually indistinguishable between the 2 genotypes. Colon length normalized to animal weight was decreased in Ets2$^{A72/A72}$ animals. In addition, animals were scored histologically for colitis. Again there was no significant difference in colitis score. Combined these data indicate that signaling through Thre-72 of Ets2 does not enhance or suppress colitis.

3. Ets2$^{A72/72}$ mice have increase susceptibility to tumorigenesis in the absence of colitis

Previous results indicated that Ets2$^{A72/A72}$ mice had increased susceptibility to colitis associated cancer but did not have increased susceptibility to colitis. This suggests that tumor suppression by Ets2^{T72} mediated by a decrease in inflammation. To test this hypothesis, a chemically induced model of colon tumorigenesis was applied. This model was chosen because it does not require the epithelial damage and colitis caused by treatment with DSS. Figure 4 in the materials and methods section shows a schematic for the multiple AOM injection regimen. At the end of treatment Ets2$^{A72/A72}$ showed a statistically significant increase in tumor multiplicity

and surprisingly in tumor size (Figure 26). Evaluation of histological sections revealed that adenomas in WT mice did not grow past the 1mm in diameter. Several of these adenomas could be classified as aberrant crypt foci (Figure 26 C and D). This is especially interesting considering that aberrant crypts foci (ACF) are believed to expand by crypt fission. It is feasible that Ets2 may prevent the expansion of ACF adenomas by inhibiting crypt fission.

Figure 21. Tumor multiplicity but not tumor size is increased in $Ets2^{A72/A72}$ following the 9 week AOM/DSS regimen. A) Example of $Ets2^{A72/A72}$ tumor from a whole mount. B) Histology of tumor $Ets2^{A72/A72}$ (Scale bar = 100 microns). Enlarged nuclei can be seen in the adenoma with normal epithelium surrounding.C) Comparison of tumor numbers between $Ets2^{A72/A72}$ and $Ets2^{+/+}$ mice. p value is from Mann-Whitney test. D) Comparison of tumor sizes (measured as area) between $Ets2^{A72/A72}$ and $Ets2^{+/+}$ tumors p value is from Mann-Whitney test. E,F) β-catenin staining of adenoma from an $Ets2^{A72/A72}$ and $Ets2^{+/+}$ animal. Nuclerar β-catenin can be seen in the adenoma.

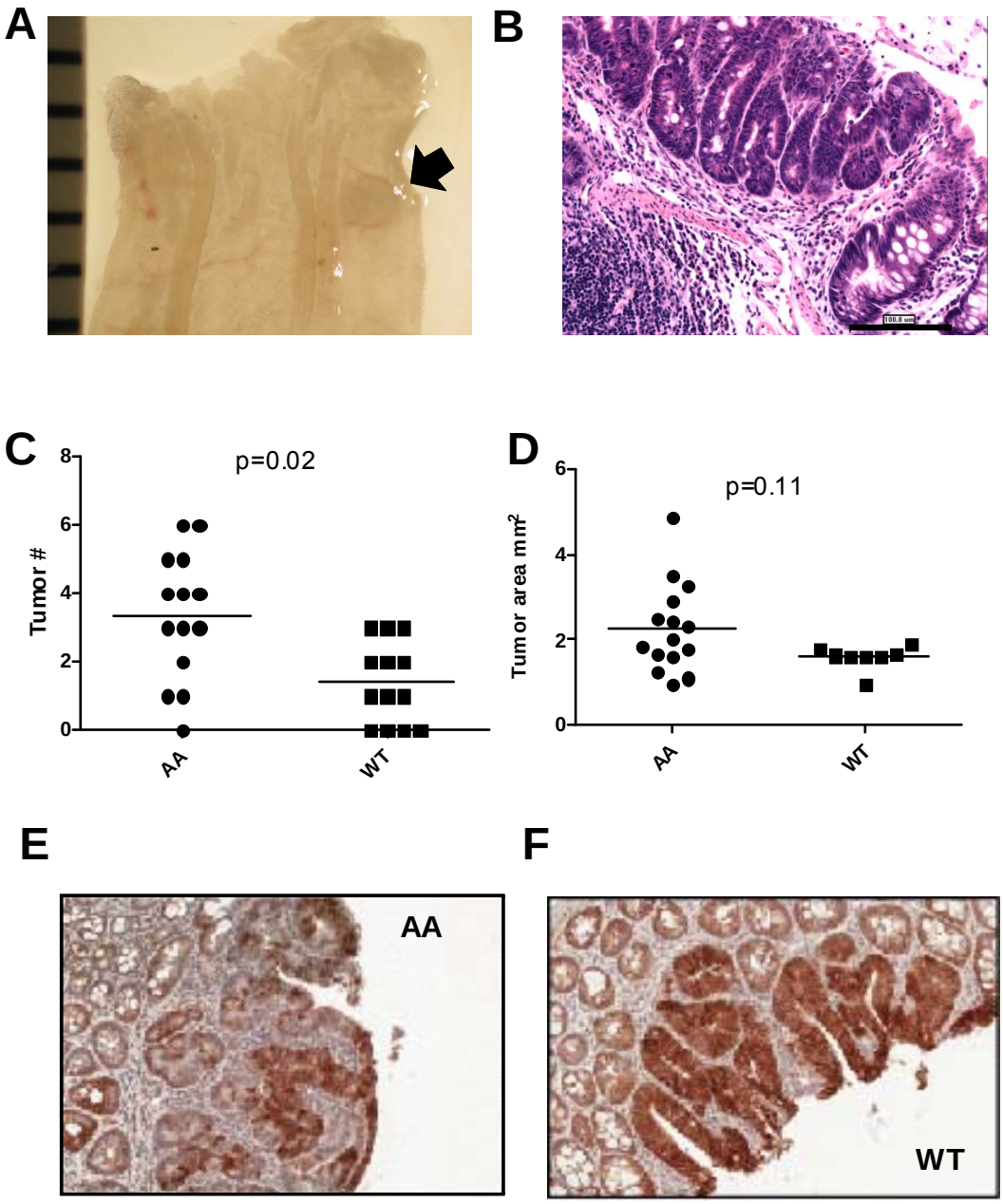
A
B
C
p=0.02
Tumor #
8
6
4
2
0
AA
WT
D
p=0.11
Tumor area mm2
6
4
2
0
AA
WT
E
AA
F
WT

Figure 22. Tumor multiplicity but not tumor size is increased in $Ets2^{A72/A72}$ following the 19 week AOM/DSS regimen. A, Example of $Ets2^{A72/A72}$ tumors viewed under a dissection scope. B) Example of an $Ets2^{+/+}$ tumor under dissection scope. C, D) Histology of $Ets2^{A72/A72}$ tumors and an $Ets2^{+/+}$ tumor. Scale bar=1mm. E) Comparison of tumor multiplicity between $Ets2^{A72/A72}$ and $Ets2^{+/+}$ tumors. P value is result of Mann-Whitney test. F) Comparison of tumor sizes (measured as tumor diameter) $Ets2^{A72/A72}$ and $Ets2^{+/+}$ tumors.

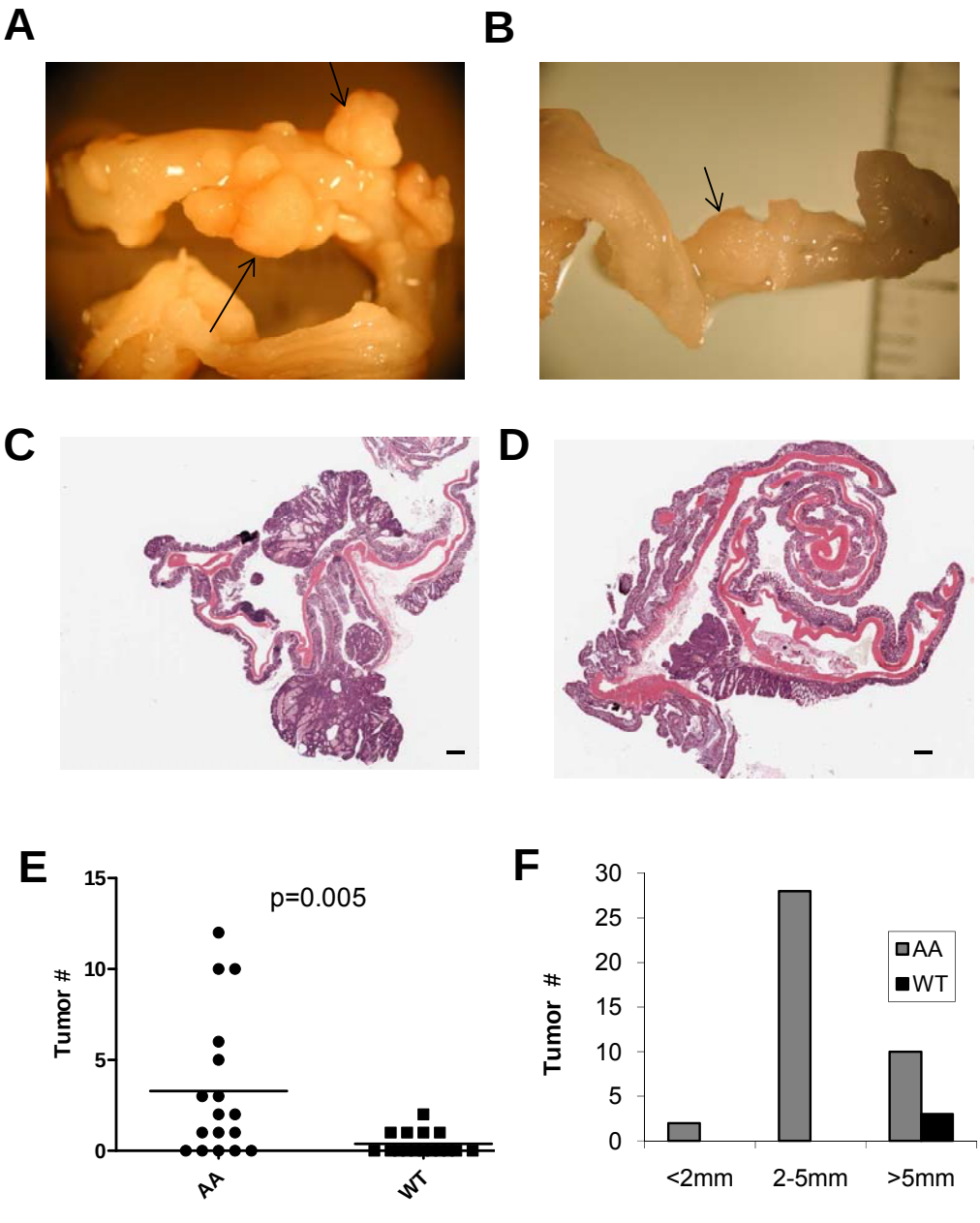
A
B
C
D
E
p=0.005
Tumor #
15
10
5
0
AA
WT
F
Tumor #
30
25
20
15
10
5
0
AA
WT
<2mm
2-5mm
>5mm

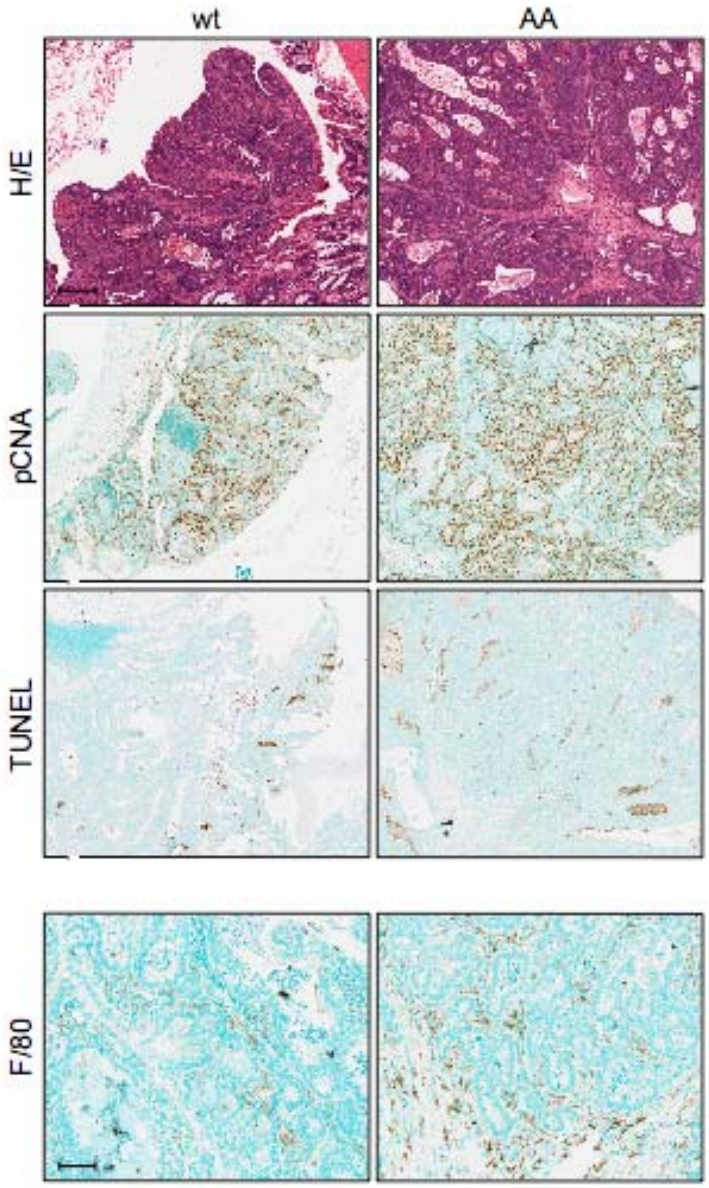

Figure 23. Comparison of late wt and AA colon tumors. Upper panel: Hematoxylin and eosin-stained sections of colon tumors of wt and AA mice, second panel: anti-pCNA staining, third panel: TUNEL staining and bottom panel: anti-F4/80 staining. Three upper panels: scale bar represents 200 microns, bottom panel: scale bar represents 50 microns.

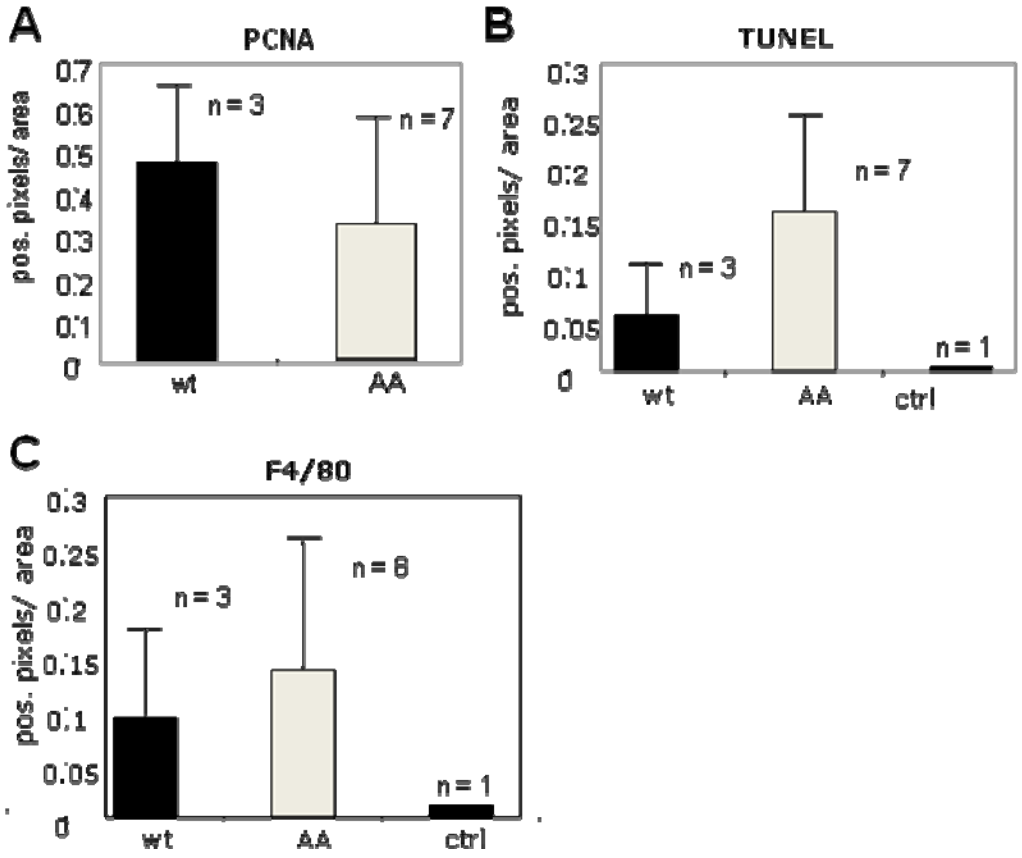

Figure 24. Quantitation of PCNA, TUNEL and F480 in tumors after 19 week treatment. A) Graph representing quantiation of PCNA staining. Numbers are given as positive pixel per are in mm^2. B) Graph representing quantiation of TUNEL staining. Numbers are given as positive pixel per are in mm^2. Ctrl represents a negative control for staining (no primary antibody). C) Graph representing quantiation of F480 staining. Numbers are given as positive pixel per are in mm^2. Ctrl represents a negative control for staining (no primary antibody).

Figure 25. Scoring of colitis in $Ets2^{A72/A72}$ versus WT mice. A) Representative photographs of distal colon following treatment with 3.5% DSS. B) Measurement of body weight as a percentage based on the weight before the start of DSS treatment. Arrow represents the time point at which DSS is replaced with normal drinking water. C) Measurement of colon length divided by the weight of the animal. D) Colitis score based on the colitis scoring system described in the Materials and Methods section.

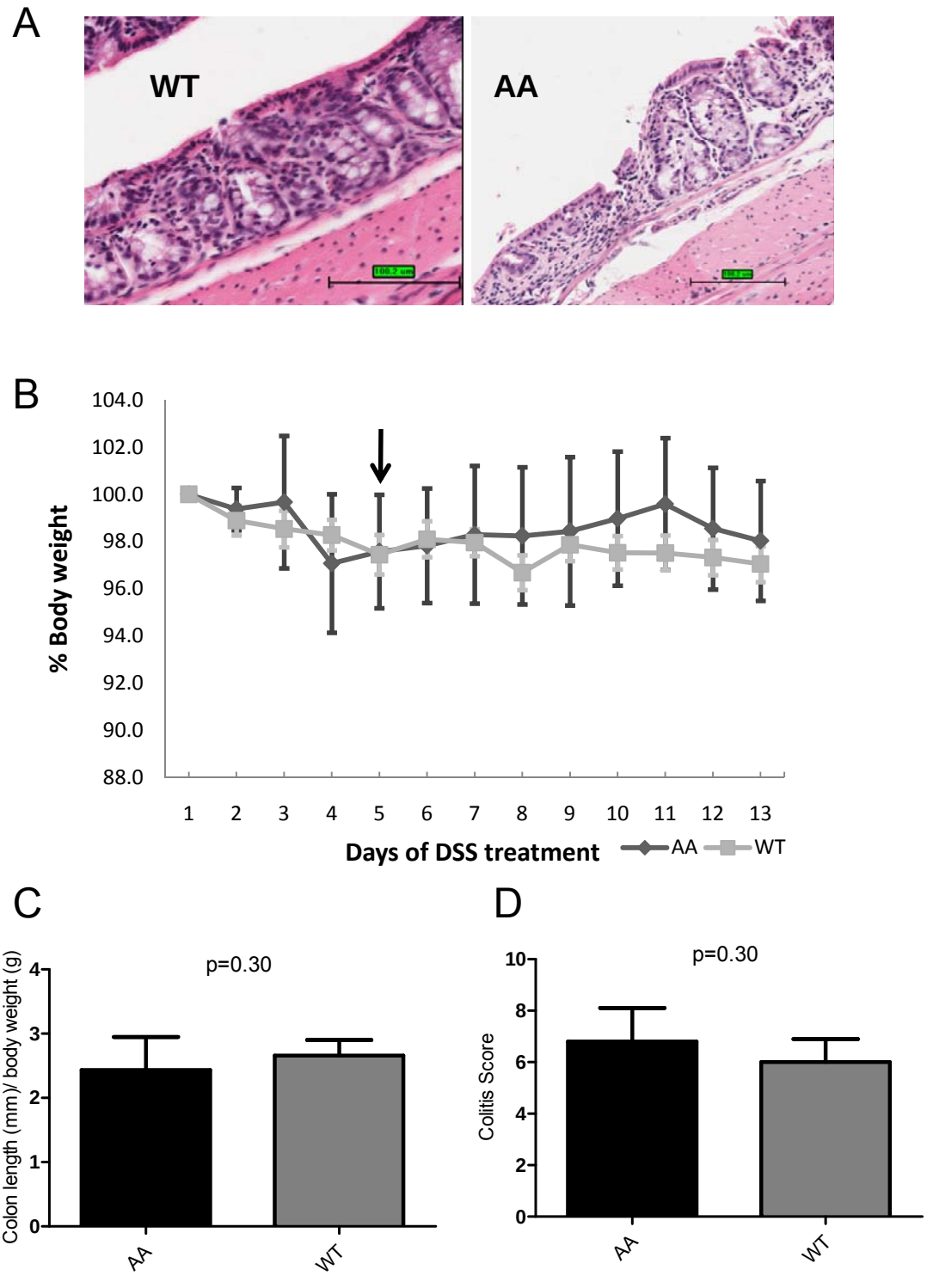
A
WT
AA
B
% Body weight
104.0
102.0
100.0
98.0
96.0
94.0
92.0
90.0
88.0
1 2 3 4 5 6 7 8 9 10 11 12 13
Days of DSS treatment
AA
WT
C
p=0.30
Colon length (mm)/ body weight (g)
4
3
2
1
0
AA
WT
D
p=0.30
Colitis Score
10
8
6
4
2
0
AA
WT

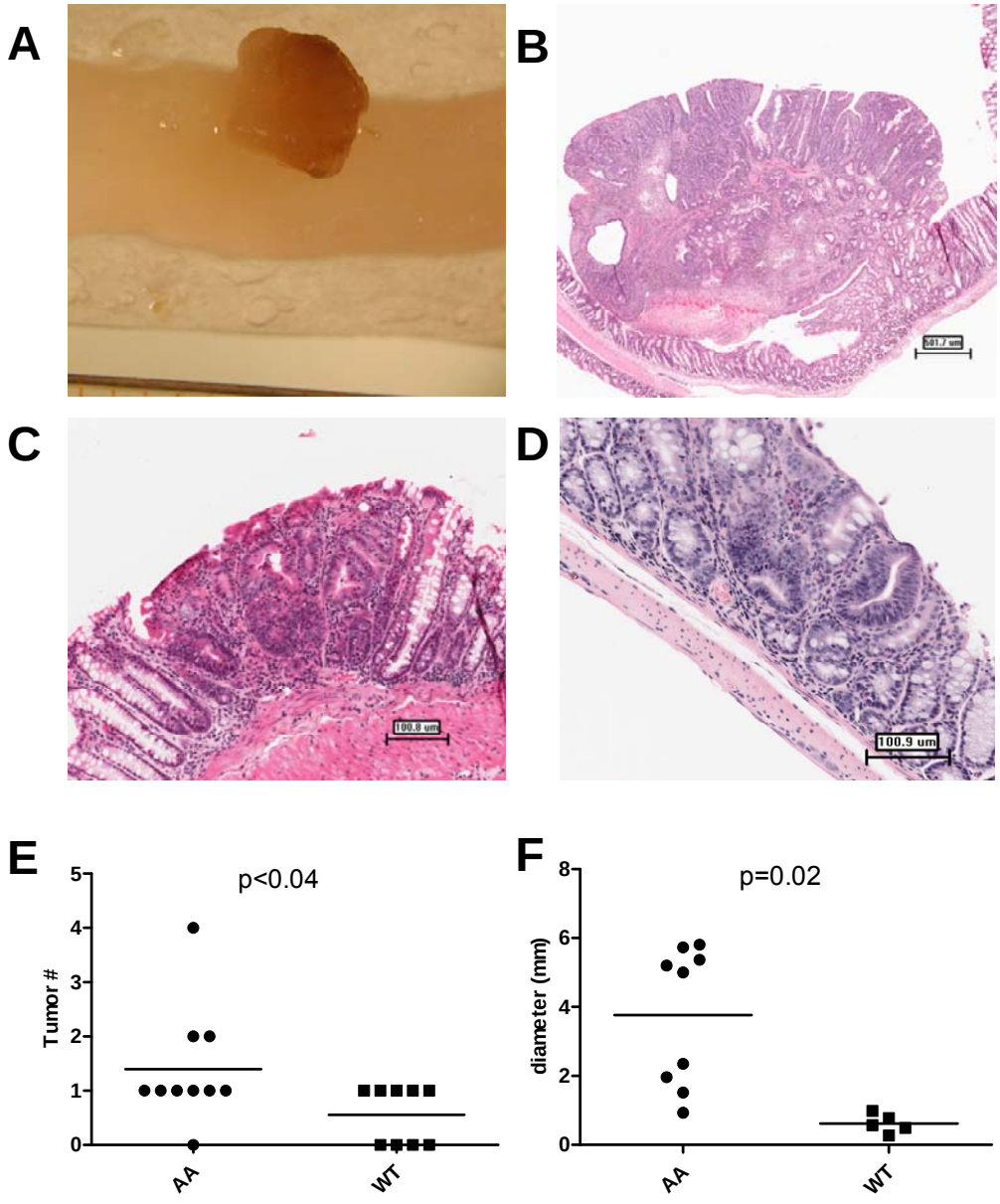

Figure 26. Tumor multiplicity and size are increased in Ets2$^{A72/A72}$ following multiple AOM injections. A) Example of Ets2$^{A72/A72}$ tumor from a colon whole mount. B) Histology of tumor shown in panel A (Scale bar = 500 microns). C and D) Examples of microscopic adenomas seen in WT mice (Scale bar = 100 microns). E) Comparison of tumor numbers between Ets2$^{A72/A72}$ and Ets2$^{+/+}$ tumor numbers. F) Comparison of tumor sizes between Ets2$^{A72/A72}$ and Ets2$^{+/+}$ tumors.

V. ETS2 IS ASSOCIATED WITH CDX2 EXPRESSION AND DIFFERENTIATION OF A HUMAN COLON CANCER CELL LINE.

1. Ets2 regulates Cdx2 transcription through a conserved 242bp region in the distal promoter.

A 242bp region of the distal Cdx2 promoter was found to be bound by Ets2 in trophoblast stem cells (Wen et al., 2007). In order to determine if Ets2 could activate transcription of Cdx2 through this distal enhance in Caco2 cells, an analysis of the promoter was performed. The conserved 242 distal region of the promoter was found to contain 3 Ets sites which matched 8-10 bases of the 13bp consensus Ets2 binding site (Umezawa et al., 1997). This conserved region was fused with the minimal Cdx2 promoter (-51 to +73). A series of mutations was made to each of the Ets sites within this region. The effect of each of these mutations on Ets2 activation of the distal Cdx2 region was determined by luciferase assay. Although mutations in the first two Ets sites were able to diminish activation by Ets2 (data not shown), mutation in the third site leads to an increase in activation by Ets2. Similar results were obtained after transfecting a human ES cell line which was differentiated into a trophoblast stem cell like lineage (data not shown). This suggests that this 3rd Ets site could bind another Ets factor which acts as a transcriptional repressor of Cdx2.

2. ETS2 is associated with differentiation of the Caco2 cell line.

A previous study in the Oshima lab has identified Cdx2 as a transcriptional target of Ets2 in mouse trophoblast stem cells and in the colon (Wen et al., 2007). In order to examine the role of Ets2 during intestinal epithelial cell differentiation, the Caco2

differentiation model was used. Caco2 cells plated at low density mimic the molecular and phenotypic changes which occur during maturation of intestinal epithelial cells from the crypt base to the top of the crypt (Sambuy et al., 2005). Upon reaching confluence, Caco2 cells undergo spontaneous differentiation characterized by upregulation of differentiation markers alkaline-phosphatase, sucrose isomaltase and CDX2. This Caco2 model was used to examine how ETS2 changes during cell culture based IEC differentiation.

Gene expression changes during Caco2 differentiation where examined in order to determine the how reliably the differentiation method mimicked in vivo differentiation. To validate the microarray of Day2 vs Day9 Caco2 cells several steps were taken. First, a dendogram to examine the relationship of gene expression pattern between the various replicates. Not surprisingly Day2 samples cluster together and Day9 samples also cluster together (Figure 28). Using Beadstudio, genes which were upregulated in Day2 Caco2 cells versus Day9 Caco2 cells were examined. Table 4 lists the top 21 genes upregulated at day2. The set of genes which were most upregulated at Day9 versus Day2 are shown in table 5 along with CDX2 expression change.

To validate the gene expression changes during the Caco2 differentiation time course, the top 20 genes from day2 and the top 20 genes from day9 were compared to a publicly available study on Caco2 polarization (Geo accession: GSE7442). For Day2 Caco2 cells, 14 of the top 20 upregulated genes were significantly downregulated during polarization of Caco2 cells. In contrast, 15 of the top 20 upregulated genes from Day9 Caco2 cells were also upregulated during Caco2

polarization. In aggregate these data suggests that the Caco2 differentiation time course used in this study is valid.

3. Ets2 is regulated post-transcriptionally during Caco2 differentiation

Examination of Ets2 protein levels during differentiation revealed that ETS2 protein was absent during the proliferative phase of differentiation cycle but ETS2 protein levels increased drastically and maintained a high level of expression during the differentiating non-proliferative phase and the fully differentiatited phase. During the same time period CDX2 protein levels were mimicked by ETS2 protein levels suggesting that Ets2 may be involved in differentiation. RNA samples from the same clones were used to examine differential gene expression between proliferating (Day2) and differentiating non-proliferative (Day9) Caco2 cells. ETS2 mRNA levels did not vary significantly between Day2 and Day9 (Figure 29). This suggested that ETS2 may be regulated at the protein level in these cells. Contrary to one published report using the Caco2/15 cell line the increase in CDX2 expression was not correlated with protein stabilization but rather with an increase in the mRNA (Boulanger et al., 2005).

Figure 27. Ets2 regulation of Cdx2 transcription. A) Schematic of luciferase reporter constructs. Cdx2_56 indicates the minimal Cdx2 promoter from −56 to +73. Cdx2_56DE1 represents the minimal promoter with the additional distal element of 242 bp. The sequence of the DE1 is shown with three potential Ets binding elements I red. Above each potential binding site is the site directed sequence change in the corresponding mutant. (B) Activation of reporters by co-expressed Ets2. Caco-2 cells were transfected with indicated reporter gene and an Ets2 expression vector or a control plasmid (pcDNA3) and the Renilla luciferase transfection control plasmid. E18, a synthetic Ets responsive reporter (Galang et al., 1994) and pGL3B, a control reporter plasmid without a promoter represent positive and negative controls. Values are representative of multiple experiments. Values represent the ratio of firefly luciferase activity to the control Renilla luciferase activity.

A

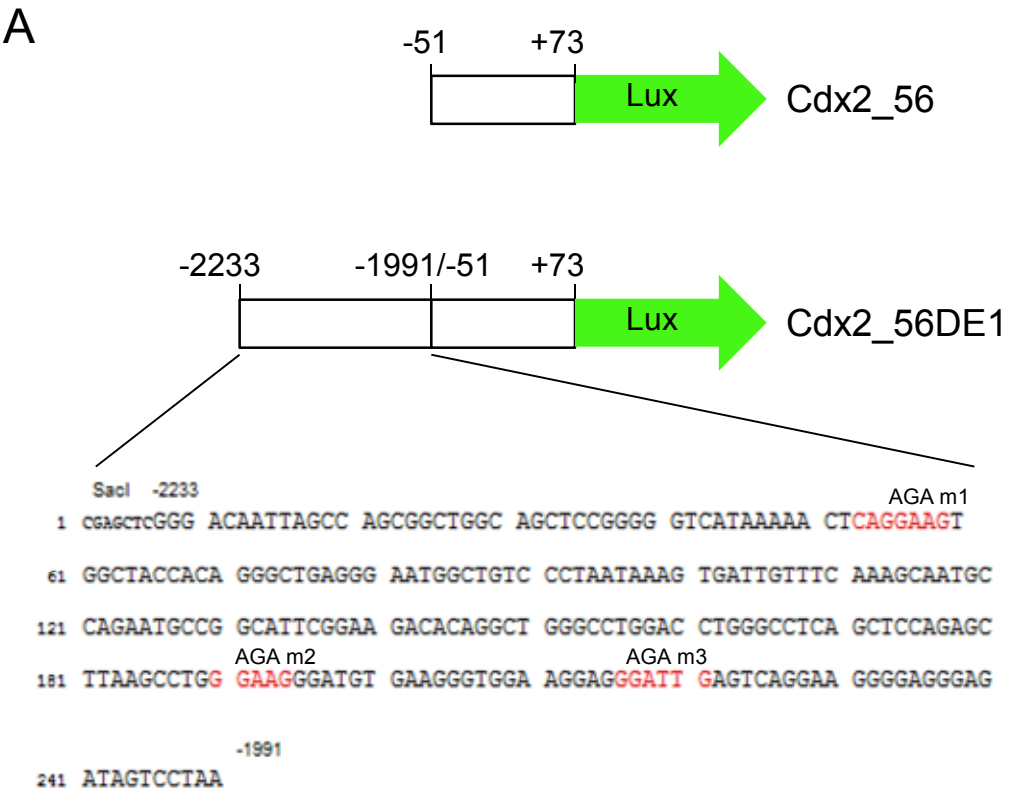
-51
+73
Lux
Cdx2_56
-2233
-1991/-51
+73
Lux
Cdx2_56DE1
SacI -2233
AGA m1
1 CGAGCTCGGG ACAATTAGCC AGCGGCTGGC AGCTCCGGGG GTCATAAAAA CTCAGGAAGT
61 GGCTACCACA GGGCTGAGGG AATGGCTGTC CCTAATAAAG TGATTGTTTC AAAGCAATGC
121 CAGAATGCCG GCATTCGGAA GACACAGGCT GGGCCTGGAC CTGGGCCTCA GCTCCAGAGC
AGA m2
AGA m3
181 TTAAGCCTGG GAAGGGATGT GAAGGGTGGA AGGAGGGATT GAGTCAGGAA GGGGAGGGAG
-1991
241 ATAGTCCTAA

B

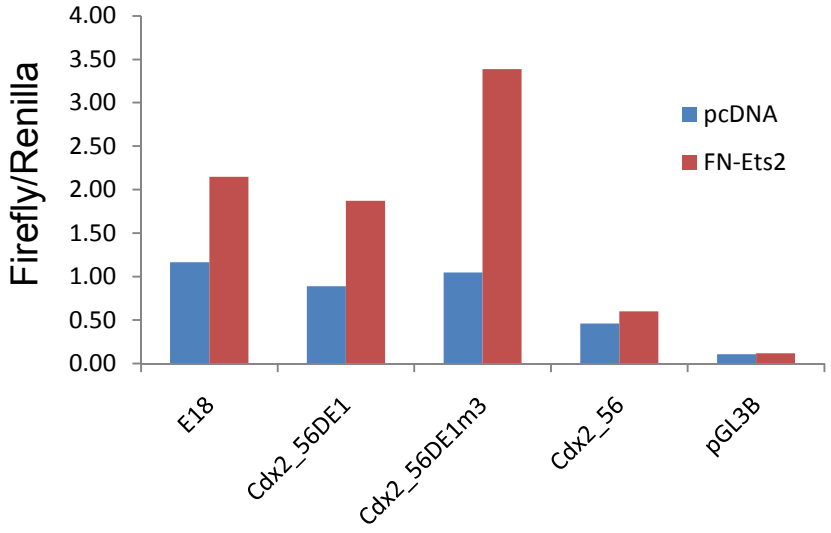
Firefly/Renilla
4.00
3.50
3.00
2.50
2.00
1.50
1.00
0.50
0.00
pcDNA
FN-Ets2
E18
Cdx2_56DE1
Cdx2_56DE1m3
Cdx2_56
pGL3B

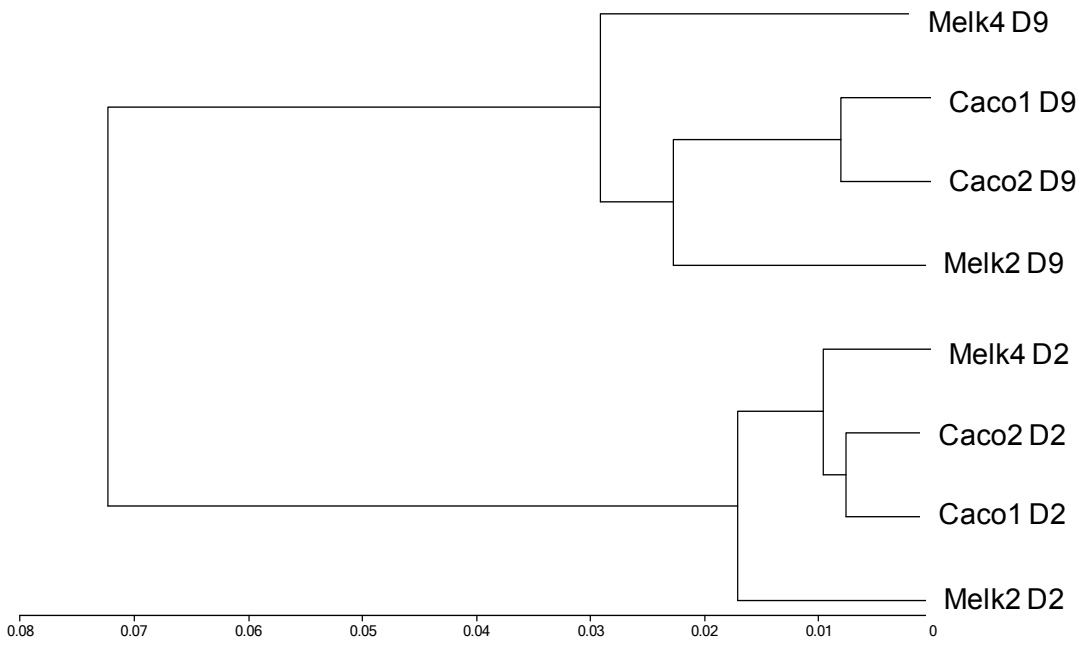

Figure 28. Dendogram of Caco2 cells grown for 2 days and 9 days. Caco1 and Caco2 represent 2 separate splits of Caco2 cells. Melk2 and Melk4 represent 2 different clones of Caco2 cells.

Table 2. List of genes upregulated in day2 Caco2 cells.

Gene	Fold Change	Accession No
NPPB	97.90	NM_002521.1
TAGLN	40.51	NM_003186.3
MYL7	16.96	NM_021223.2
STS-1	15.41	NM_032873.3
RAFTLIN	13.19	NM_015150.1
SOCS2	11.58	NM_003877.3
CYR61	11.10	NM_001554.3
EDN1	9.90	NM_001955.2
FABP5	9.35	NM_001444.1
RGC32	9.09	NM_014059.1
HSPB8	8.44	NM_014365.2
C20orf75	8.18	NM_152611.2
DPYSL3	7.71	NM_001387.2
ANKRD1	7.65	NM_014391.2
AP1S3	6.72	NM_178814.2
MAP6	6.67	NM_033063.1
OLR1	6.52	NM_002543.2
MYBPH	6.40	NM_004997.2
DKFZP586H2123	5.78	NM_001001991.1
LRP8	5.51	NM_033300.2
CCND2	5.36	NM_001759.2

Table 3. List of genes upregulated in day9 Caco2 cells

Gene	Fold Change	Accession No
APOA4	30.42	NM_000482.3
SLC26A3	26.97	NM_000111.1
HPN	23.96	NM_002151.1
ATAD4	23.70	NM_024320.2
MST1	22.17	NM_020998.2
NDRG1	22.07	NM_006096.2
PRODH	17.95	NM_016335.2
SDCBP2	17.20	NM_080489.2
SERPINC1	17.18	NM_000488.2
CRYL1	15.62	NM_015974.1
SLC23A3	14.87	NM_144712.2
GUCY2C	14.46	NM_004963.1
APOC3	12.75	NM_000040.1
CAPN12	12.25	NM_144691.3
APOM	11.55	NM_019101.2
PFKFB4	11.35	NM_004567.2
CFB	11.27	NM_001710.4
MEP1A	11.18	NM_005588.1
ANKRD37	11.17	NM_181726.1
MSMB	11.09	NM_002443.2
CDX2	2.71	NM_001265.2

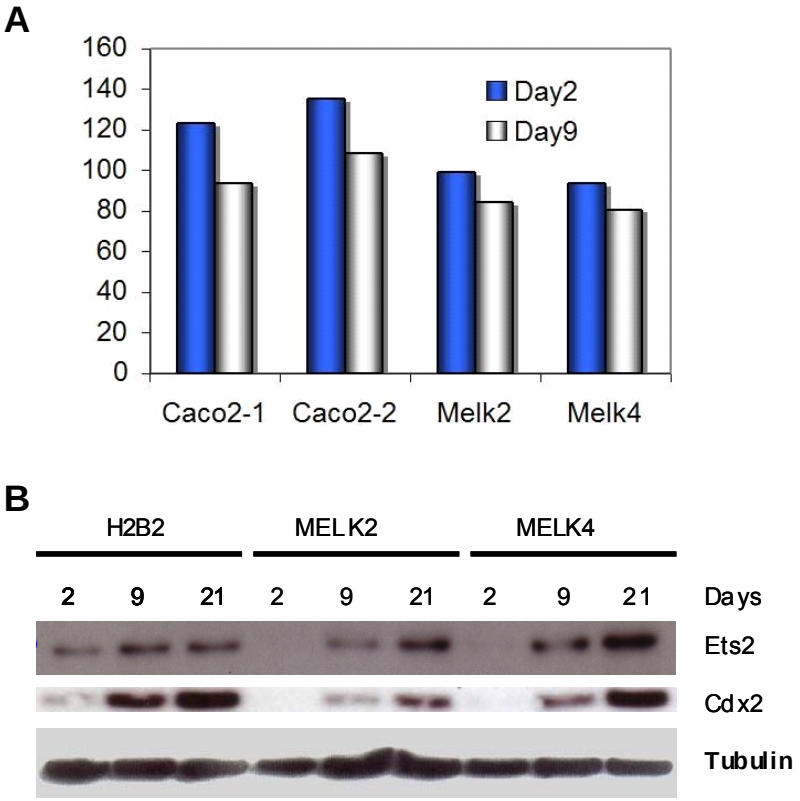

Figure 29. Ets2 mRNA and protein expression in differentiating Caco2 cells. A) Normalized Ets2 mRNA levels in 4 different samples at day 2 and day 9. Each bar represents the mRNA level for a single biological sample. B) Changes in Ets2 and Cdx2 protein levels during a 21 differentiation time course in Caco2 cells. Caco2 cells were cultured for 21 days and protein was extracted at 2, 9 and 21 days. Lysates were run SDS-Page gels, transferred and blotted with antibodies against ETS2, CDX2 and tubulin.

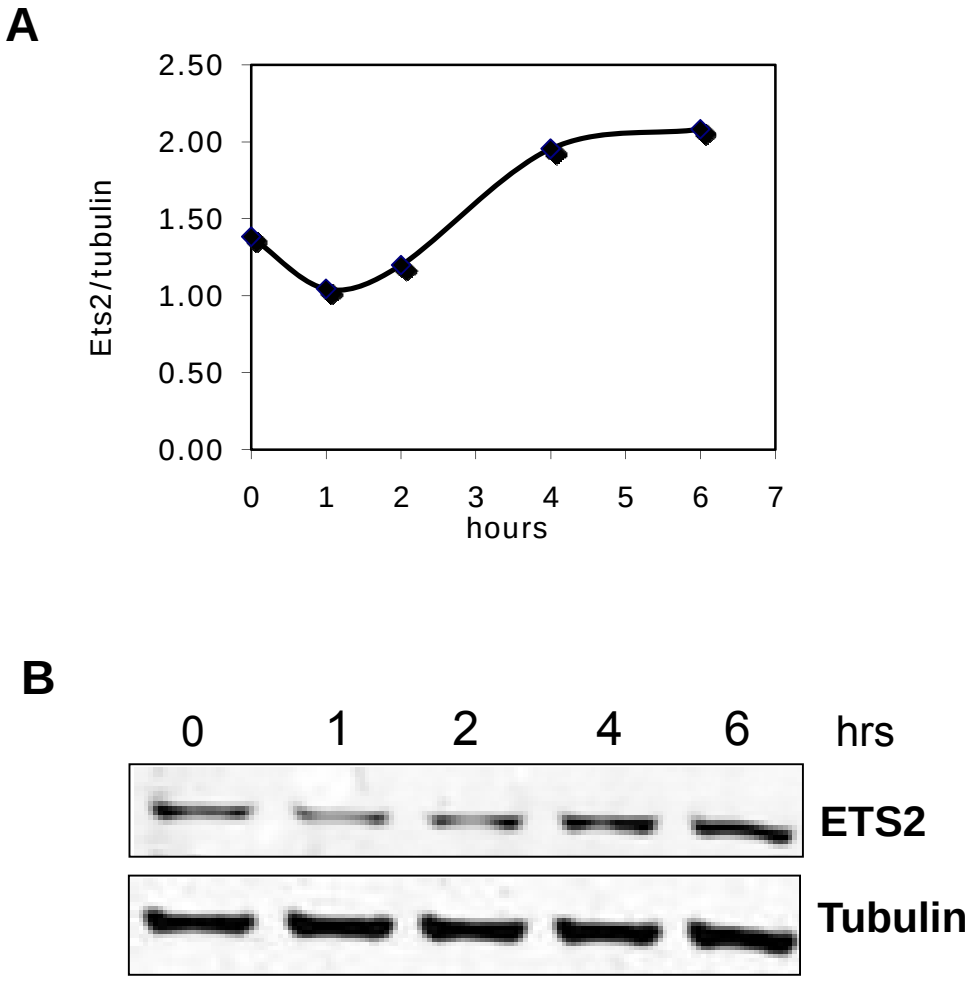

Figure 30. MG132 treatment stabilizes ETS2 protein levels in proliferative Caco2 cells. Caco2 cells were treated with 25μM MG132 for 0, 1, 2, 4 and 6 hrs. Protein was isolated at each timepoint. A) Graph presenting ETS2 protein levels following treatment of Caco2 cells with the proteasome inhibitor MG132. An increase in ETS2 protein levels is apparent at 4 and 6 hours. B) Western blot used to quantitate levels of Ets2 protein with tubulin as a control.

VI. DISCUSSION

1. Ets2 deficient stem cells have a selective advantage.

It was very surprising to find that Ets2 deficiency leads to a selective advantage for stem cells in the distal colon. This observation was even more surprising considering that Ets2 has been identified as a target of Wnt. Unlike the phenotype seen in Ets2 deficient mice, intestinal specific knockout of other Wnt targets generally leads to a decrease in proliferation in the stem cell compartment and loss of deficient crypts due to replacement by crypts containing the wild-type allele (Muncan et al., 2006; van der Flier et al., 2009b). Furthermore the effect of Ets2 deficiency is even more striking considering that the strain used (FVB) is resistant to *Min*-induced tumors in the intestine and mammary gland (Moser et al., 2001).

In contrast to the phenotype observed in knockouts of other TCF target genes, an intestinal epithelial cell specific knockout of Ets2 led to an increase in crypt fission of deficient crypts. Based on the current understanding of crypt fission, this phenomenon is likely due to an increase in stem cell number or in stem cell proliferation (He et al., 2007; Loeffler et al., 1997). Proving that there is an increase in stem cell number is difficult due to the unavailability of a reliable Lgr5 antibody and relatively low abundance of Lgr5 protein (van der Flier et al., 2009a). In addition, its likely that crypts with excessive numbers of stem cells likely undergo crypt fission and thus the increase in stem cell number may be very transient. To test this hypothesis, the Lgr5 knockin mouse could be used not only to track the stem cells but also to isolate Ets2 deficient stem cells for use in a tissue culture system (Sato et al., 2009).

Crypt fission has been implicated as a mechanism for spread of mutations in the intestine of both mice and humans (Greaves et al., 2006; Park et al., 1995). It should be noted however the mouse study, the mutagen Ethyl nitrosourea (ENU) was used. This chemical causes extensive damage to the intestinal epithelium. Thus the spread of these mutations may be due to hitchhiking of mutations and normal expansion of crypts through crypt fission during healing. The spread of Ets2 deficiency is independent of any treatment which makes it an attractive system for investigating the control of crypts fission.

Previous studies have reported that Ets2 mRNA is upregulated in several intestinal disease states including UC, Crohn's and colorectal cancer (Horiuchi et al., 2003; Notterman et al., 2001; van der Pouw Kraan et al., 2009). Interestingly these disease states display increased fission (Cheng et al., 1986). This is in contrast to my findings in which Ets2 deficiency leads to an increase in crypt fission. It should be noted however, that these studies only examined Ets2 mRNA levels and not protein levels and that the increase in mRNA levels could be due to stromal contributions. However, the lack of evidence for upregulation of Ets2 protein levels along with the results of the Caco2 studies suggests that and increase in Ets2 protein levels is associated with a decrease in proliferation.

2. Ets2 represses colon tumorigenesis

Ets2 was independently found to be a tumor repressor of APC/Min intestinal tumorigenesis in a mouse model of Down's syndrome (Sussan et al., 2008). Tumor multiplicity was reduced in gene dosage dependent manner. The results of this study are in accordance with these studies. However, it should be noted that there are

several differences between the two studies. First, instead of APC/min the colitis associated cancer model was used. APC/min tumors appear primarily in the small intestine with very few tumors appearing in the colon. Second, in the Sussan study Ets2 overexpression and Wnt activation (due to APC/Min) occur throughtout embryogenesis. In contrast, in this study the deletion of Ets2 at the site of tumorigenesis occurs mostly between days 15 and 30. In addition, intestinal tumorigenesis is induced at 8 weeks of age. Finally, in the Down syndrome model Ets2 is expressed within all cell types whereas in the Ets2 Villin-Cre model Ets2 is only deleted within the intestinal epithelium.

Despite the differences in the mouse models of tumorigenesis and Ets2 deficiency used, the same conclusion can be drawn: Ets2 represses intestinal tumorigenesis. However, this study advances the understanding of Ets2 tumor repression by demonstrating that Ets2 repressed tumorigenesis in a cell autonomous fashion. This cell autonomous role of Ets2 in suppression of intestinal tumorigenesis has been previously suggested but not demonstrated experimentally (Baek et al., 2009).

The exact mechanism by which Ets2 represses tumorigenesis remains unclear. The increase of crypt fission in Ets2 deficient colons suggests that there is an increase in stem cell number or proliferation. An increase in intestinal stem cell number would lead to an increase in cells targeted by AOM since stem cells have been identified as the cell of origin of intestinal tumorigenesis in mice (Barker et al., 2009). In addition monocryptal adenomas, the earliest detectable lesion in intestinal tumorigenesis have been shown to spread by crypt fission (Preston et al., 2003). Thus Ets2 may inhibit intestinal tumorigenesis by controlling stem cell numbers and/or by inhibiting the expansion of monocryptal adenomas by crypt fission.

Another possible mechanism for tumor repression by Ets2 may be through transcriptional activation of 2 of its target genes: Cdx2 and MMP9. Cdx2 is also involved in differentiation toward the absorptive lineage in the intestine (Tamai et al., 1999). Like Ets2 deficient mice, Cdx2 heterozygous mice have increased tumorigenesis in the distal colon in response to multiple AOM injections (Bonhomme et al., 2003). In addition, MMP9 has been shown to be involved in differentiation towards the absorptive lineage by its ability to cleave Notch-1. Previous studies have shown that inhibition of Notch-1 cleavage, either through treatment of mice with a gamma secretase inhibitor or by knocking out MMP9, leads to an accumulation of goblet cells (Garg et al., 2007; van Es et al., 2005). MMP9 has also been shown to function as a tumor repressor in colitis associated cancer.

3. Phosphorylation of threonine 72 is required for tumor repressive activity of Ets2.

Phosphorylation of Ets2 at the MAPK phosphorylation site found at threonine 72 leads to upregulated transcription from Ets2 target promoters (Yang et al., 1996). $Ets2A^{72/A72}$ have increased sensitivity to colon tumorigenesis induced by AOM injection alone or in tandem with DSS treatment. These observations suggest activation of Ets2 through the Ras pathway is required for optimal Ets2 tumor repressive activity. K-ras mutations are found in nearly 50% of colorectal cancers in humans (Bos et al., 1987; Forrester et al., 1987). These mutations are usually associated with malignant progression of tumors. Several studies have attempted to examine the role of constitutively active K-ras ($K\text{-}ras^{V12G}$) in the mouse intestine. Results of these studies vary from not tumors to a few tumors as a result of

expression of K-ras^{V12G} (Coopersmith et al., 1997; Janssen et al., 2002). Recently Haigis and co-workers examined K-ras expression in the colon (Haigis et al., 2008). K-ras is expressed throughout the crypt but increases from the bottom to the top of the crypt in both mice and humans. Phospho-Erk levels were undetectable in wild-type colons and expressed only in the colon tops in K-Ras^{G12D} expressing mice. Expression of K-Ras^{G12D} has been shown to induce senescence of human diploid fibroblast by induction of p16INK^{4a} via Ets2 (Ohtani et al., 2001). It is possible that K-Ras^{G12D} may also cause senescence in colon epithelial cells and thus its tumorigenic potential is limited by Ets2.

In one report, MAP Kinase activity was necessary for proliferation and differentiation in the Caco2 cells line (Aliaga et al., 1999). MAP kinase was found to be expressed at high levels in proliferating Caco2 cells and decreases in differentiating Caco2 cells. However, inhibition of MAPK with the inhibitor PD-98059 led to decreased transcription of the differentiation associated sucrose-isomaltase reporter.

4. Tumor promoting versus tumor repressive functions of Ets2.

Previous studies of Ets2 function have shown that Ets2 is required for stromal support of mammary tumors (Man et al., 2003a; Neznanov et al., 1999; Trimboli et al., 2009; Tynan et al., 2005). In contrast, this work and work by Sussan and co-workers has shown that Ets2 has a tumor repressive activity in the intestine (Sussan et al., 2008). This opposite effect of Ets2 raises the question: Is the repressive activity of Ets2 due to a tissue specific context or due to a oncogene specific effect? The effect of Ets2 in mammary tumorigenesis has been studied in neu/ErbB2 tumors and

Polyoma virus middle T antigen (PyMT) tumors. Neu/ErbB2 is one member of the ErbB family that includes EGFR, ErbB2 and ErbB3 (Schechter et al., 1985) while PyMT activates the src (Courtneidge, 1985) and PI3K (Courtneidge and Heber, 1987) pathways by after its localization to the plasma membrane leading to tumor formation. In contrast, APC^{Min} and AOM induced tumors activate the Wnt pathway. It would be interesting to examine the role of epithelial Ets2 in Wnt1 mammary tumors (Rijsewijk et al., 1987). This would clarify if Ets2 represses tumorigenesis in a tissue specific or oncogene specific context.

5. Ets2 protein is degraded by the proteasome in subconfluent Caco2 cells.

The expression of Ets2 message and protein was examined in Caco2 cells during differentiation. Ets2 protein was found to be upregulated during the differentiation despite the fact that Ets2 messenger RNA levels remain constant. Treatment of proliferative Caco2 cells with the proteasome inhibitor MG132 led to stabilization of Ets2 protein levels. Recently Ets2 has been implicated as a potential substrate for APC-Cdh1 complex which acts as a ubiquitin ligase. Interestingly Cdc20, a factor which complexes with Cdh1 to activate the APC (Anaphase promoting complex) is hightly upregulated in proliferative Caco2 cells and in human intestinal crypts (Kosinski et al., 2007). These data suggest accumulation of Ets2 protein following mitosis induces cell cycle arrest and differentiation. Loss of Ets2 may mediate mis-regulation of the colonic stem cells' cell cycle progression leading to an increased number of stem cells or increased proliferation of the stem cells. This could result in a proliferative advantage for Ets2 deficient stem cells increasing their ability to colonize crypts and increasing their sensitivity to adenoma formation.

5. Future directions

The results of this thesis suggest that Ets2 deficiency results in a selective advantage of intestinal stem cells. Increases in crypt fission and tumor multiplicity suggest that there is an increase in colon stem cell number or proliferation. These conclusions could be directly tested by the crossing EtsFlox/Flox R26R and Ets2Flox/+ R26R mice with the Lgr5-eGFP-IRES-creERT2 knockin mouse. This would allow deletion of Ets2 directly within the stem cells and would allow determination of colon stem cell numbers using the GFP marker. In addition the fate of Ets2 deficient stem cells could be examined following a single pulse (injection with tamoxifen). Unlike our current system this would allow tracing of Ets2 deficient cells following a one time activation of Cre within the intestinal stem cells.

In addition to the in vivo work, the Lgr5-eGFP-IRES-creERT2 knockin mouse could be used to isolate $Ets2^{db2/db2}$ and $Ets2^{db2/+}$ colon stem cells. These cells could then be grown in vitro using the recently described intestinal organoid system (Sato et al., 2009). This would allow examination of the properties of Ets2 deficient stem cells including cloning efficiency, proliferation and differentiation capacity. Furthermore, since intestinal organoids grow by a crypt fission like process, gene expression changes in Ets2 deficient organoids could be examined. These studies could identify genes involved in crypt fission and would be beneficial not only for the understanding of this process, but also could provide molecular targets for improving recovery after bowel resection, treating inflammatory bowel disease and preventing the growth of adenomas form aberrant crypt foci.

References

Aliaga, J. C., et al., 1999. Requirement of the MAP kinase cascade for cell cycle progression and differentiation of human intestinal cells. Am J Physiol. 277**,** G631-41.

Aoki, K., et al., 2003. Colonic polyposis caused by mTOR-mediated chromosomal instability in Apc+/Delta716 Cdx2+/- compound mutant mice. Nat Genet. 35**,** 323-30.

Baek, K. H., et al., 2009. Down's syndrome suppression of tumour growth and the role of the calcineurin inhibitor DSCR1. Nature. 459**,** 1126-30.

Barker, N., et al., 2009. Crypt stem cells as the cells-of-origin of intestinal cancer. Nature. 457**,** 608-11.

Barker, N., et al., 2007. Identification of stem cells in small intestine and colon by marker gene Lgr5. Nature. 449**,** 1003-7.

Bienz, M., Clevers, H., 2000. Linking colorectal cancer to Wnt signaling. Cell. 103**,** 311-20.

Biswas, S., et al., 2004. Transforming growth factor beta receptor type II inactivation promotes the establishment and progression of colon cancer. Cancer Res. 64**,** 4687-92.

Bjerknes, M., et al., 1997. APC mutation and the crypt cycle in murine and human intestine. Am J Pathol. 150**,** 833-9.

Bonhomme, C., et al., 2003. The Cdx2 homeobox gene has a tumour suppressor function in the distal colon in addition to a homeotic role during gut development. Gut. 52**,** 1465-71.

Bos, J. L., et al., 1987. Prevalence of ras gene mutations in human colorectal cancers. Nature. 327**,** 293-7.

Boulanger, J., et al., 2005. Cdk2-dependent phosphorylation of homeobox transcription factor CDX2 regulates its nuclear translocation and proteasome-mediated degradation in human intestinal epithelial cells. J Biol Chem. 280**,** 18095-107.

Brunner, D., et al., 1994. The ETS domain protein pointed-P2 is a target of MAP kinase in the sevenless signal transduction pathway. Nature. 370**,** 386-9.

Cairnie, A. B., Millen, B. H., 1975. Fission of crypts in the small intestine of the irradiated mouse. Cell Tissue Kinet. 8**,** 189-96.

Cheng, H., Bjerknes, M., 1985. Whole population cell kinetics and postnatal development of the mouse intestinal epithelium. Anat Rec. 211**,** 420-6.

Cheng, H., et al., 1986. Crypt production in normal and diseased human colonic epithelium. Anat Rec. 216**,** 44-8.

Cooper, H. S., et al., 1993. Clinicopathologic study of dextran sulfate sodium experimental murine colitis. Lab Invest. 69**,** 238-49.

Coopersmith, C. M., et al., 1997. Bi-transgenic mice reveal that K-rasVal12 augments a p53-independent apoptosis when small intestinal villus enterocytes reenter the cell cycle. J Cell Biol. 138**,** 167-79.

Courtneidge, S. A., 1985. Activation of the pp60c-src kinase by middle T antigen binding or by dephosphorylation. EMBO J. 4**,** 1471-7.

Courtneidge, S. A., Heber, A., 1987. An 81 kd protein complexed with middle T antigen and pp60c-src: a possible phosphatidylinositol kinase. Cell. 50**,** 1031-7.

Dai, C. Y., et al., 2000. p16(INK4a) expression begins early in human colon neoplasia and correlates inversely with markers of cell proliferation. Gastroenterology. 119**,** 929-42.

Domon-Dell, C., et al., 2002. Stimulation of the intestinal Cdx2 homeobox gene by butyrate in colon cancer cells. Gut. 50**,** 525-9.

el Marjou, F., et al., 2004. Tissue-specific and inducible Cre-mediated recombination in the gut epithelium. Genesis. 39**,** 186-93.

Esteller, M., et al., 2001. A gene hypermethylation profile of human cancer. Cancer Res. 61**,** 3225-9.

Flentjar, N., et al., 2007. TGF-betaRII rescues development of small intestinal epithelial cells in Elf3-deficient mice. Gastroenterology. 132**,** 1410-9.

Forrester, K., et al., 1987. Detection of high incidence of K-ras oncogenes during human colon tumorigenesis. Nature. 327**,** 298-303.

Furth, E. E., et al., 2006. Induction of the tumor-suppressor p16(INK4a) within regenerative epithelial crypts in ulcerative colitis. Neoplasia. 8**,** 429-36.

Galang, C. K., et al., 1994. Oncogenic Ras can induce transcriptional activation through a variety of promoter elements, including tandem c-Ets-2 binding sites. Oncogene. 9**,** 2913-21.

Galang, C. K., et al., 1996. Oncogenic Neu/ErbB-2 increases ets, AP-1, and NF-kappaB-dependent gene expression, and inhibiting ets activation blocks Neu-mediated cellular transformation. J Biol Chem. 271**,** 7992-8.

Garg, P., et al., 2007. Matrix metalloproteinase-9 regulates MUC-2 expression through its effect on goblet cell differentiation. Gastroenterology. 132**,** 1877-89.

Gordon, J. I., Hermiston, M. L., 1994. Differentiation and self-renewal in the mouse gastrointestinal epithelium. Curr Opin Cell Biol. 6**,** 795-803.

Greaves, L. C., et al., 2006. Mitochondrial DNA mutations are established in human colonic stem cells, and mutated clones expand by crypt fission. Proc Natl Acad Sci U S A. 103**,** 714-9.

Gregorieff, A., Clevers, H., 2005. Wnt signaling in the intestinal epithelium: from endoderm to cancer. Genes Dev. 19**,** 877-90.

Gregorieff, A., et al., 2009. The ets-domain transcription factor Spdef promotes maturation of goblet and paneth cells in the intestinal epithelium. Gastroenterology. 137**,** 1333-45 e1-3.

Greten, F. R., et al., 2004. IKKbeta links inflammation and tumorigenesis in a mouse model of colitis-associated cancer. Cell. 118**,** 285-96.

Haigis, K. M., et al., 2008. Differential effects of oncogenic K-Ras and N-Ras on proliferation, differentiation and tumor progression in the colon. Nat Genet. 40**,** 600-8.

Hatzis, P., et al., 2008. Genome-wide pattern of TCF7L2/TCF4 chromatin occupancy in colorectal cancer cells. Mol Cell Biol. 28**,** 2732-44.

He, X. C., et al., 2007. PTEN-deficient intestinal stem cells initiate intestinal polyposis. Nat Genet. 39**,** 189-98.

Horiuchi, S., et al., 2003. Association of ets-related transcriptional factor E1AF expression with tumour progression and overexpression of MMP-1 and matrilysin in human colorectal cancer. J Pathol. 200**,** 568-76.

Jaksch, M., et al., 2008. Cell cycle-dependent variation of a CD133 epitope in human embryonic stem cell, colon cancer, and melanoma cell lines. Cancer Res. 68**,** 7882-6.

Janssen, K. P., et al., 2002. Targeted expression of oncogenic K-ras in intestinal epithelium causes spontaneous tumorigenesis in mice. Gastroenterology. 123**,** 492-504.

Korinek, V., et al., 1998. Depletion of epithelial stem-cell compartments in the small intestine of mice lacking Tcf-4. Nat Genet. 19**,** 379-83.

Korinek, V., et al., 1997. Constitutive transcriptional activation by a beta-catenin-Tcf complex in APC-/- colon carcinoma. Science. 275**,** 1784-7.

Kosinski, C., et al., 2007. Gene expression patterns of human colon tops and basal crypts and BMP antagonists as intestinal stem cell niche factors. Proc Natl Acad Sci U S A. 104**,** 15418-23.

Leprince, D., et al., 1983. A putative second cell-derived oncogene of the avian leukaemia retrovirus E26. Nature. 306**,** 395-7.

Li, M., et al., 2008. The adaptor protein of the anaphase promoting complex Cdh1 is essential in maintaining replicative lifespan and in learning and memory. Nat Cell Biol.

Li, Y. Q., et al., 1994. The crypt cycle in mouse small intestinal epithelium. J Cell Sci. 107 (Pt 12)**,** 3271-9.

Lickert, H., et al., 2002. Formation of multiple hearts in mice following deletion of beta-catenin in the embryonic endoderm. Dev Cell. 3**,** 171-81.

Lin, E. Y., et al., 2001. Colony-stimulating factor 1 promotes progression of mammary tumors to malignancy. J Exp Med. 193**,** 727-40.

Loeffler, M., et al., 1997. Clonality and life cycles of intestinal crypts explained by a state dependent stochastic model of epithelial stem cell organization. J Theor Biol. 186**,** 41-54.

Lorentz, O., et al., 1999. Downregulation of the colon tumour-suppressor homeobox gene Cdx-2 by oncogenic ras. Oncogene. 18**,** 87-92.

Madison, B. B., et al., 2002. Cis elements of the villin gene control expression in restricted domains of the vertical (crypt) and horizontal (duodenum, cecum) axes of the intestine. J Biol Chem. 277**,** 33275-83.

Man, A. K., et al., 2003b. Ets2-dependent stromal regulation of mouse mammary tumors. Mol. Cell Biol. 23**,** 8614-8625.

Menard, D., et al., 1994. Morphological changes and cellular proliferation in mouse colon during fetal and postnatal development. Anat Rec. 238**,** 349-59.

Moser, A. R., et al., 2001. Genetic background affects susceptibility to mammary hyperplasias and carcinomas in Apc(min)/+ mice. Cancer Res. 61**,** 3480-5.

Muncan, V., et al., 2006. Rapid loss of intestinal crypts upon conditional deletion of the Wnt/Tcf-4 target gene c-Myc. Mol Cell Biol. 26**,** 8418-26.

Neufert, C., et al., 2007. An inducible mouse model of colon carcinogenesis for the analysis of sporadic and inflammation-driven tumor progression. Nat Protoc. 2**,** 1998-2004.

Neznanov, N., et al., 1999. A single targeted Ets2 allele restricts development of mammary tumors in transgenic mice. Cancer Res. 59**,** 4242-6.

Notterman, D. A., et al., 2001. Transcriptional gene expression profiles of colorectal adenoma, adenocarcinoma, and normal tissue examined by oligonucleotide arrays. Cancer Res. 61**,** 3124-30.

Nusse, R., Varmus, H. E., 1982. Many tumors induced by the mouse mammary tumor virus contain a provirus integrated in the same region of the host genome. Cell. 31, 99-109.

O'Brien, C. A., et al., 2007. A human colon cancer cell capable of initiating tumour growth in immunodeficient mice. Nature. 445, 106-10.

Ohtani, N., et al., 2001. Opposing effects of Ets and Id proteins on p16INK4a expression during cellular senescence. Nature. 409, 1067-70.

Oikawa, T., Yamada, T., 2003. Molecular biology of the Ets family of transcription factors. Gene. 303, 11-34.

Okayasu, I., et al., 1990. A novel method in the induction of reliable experimental acute and chronic ulcerative colitis in mice. Gastroenterology. 98, 694-702.

Okayasu, I., et al., 1996. Promotion of colorectal neoplasia in experimental murine ulcerative colitis. Gut. 39, 87-92.

Park, H. S., et al., 1995. Crypt fission in the small intestine and colon. A mechanism for the emergence of G6PD locus-mutated crypts after treatment with mutagens. Am J Pathol. 147, 1416-27.

Pinto, D., et al., 1999. Regulatory sequences of the mouse villin gene that efficiently drive transgenic expression in immature and differentiated epithelial cells of small and large intestines. J Biol Chem. 274, 6476-82.

Ponder, B. A., et al., 1985. Derivation of mouse intestinal crypts from single progenitor cells. Nature. 313, 689-91.

Preston, S. L., et al., 2003. Bottom-up histogenesis of colorectal adenomas: origin in the monocryptal adenoma and initial expansion by crypt fission. Cancer Res. 63, 3819-25.

Ramsay, R. G., et al., 2004. c-myb Heterozygous mice are hypersensitive to 5-fluorouracil and ionizing radiation. Mol Cancer Res. 2, 354-61.

Ricci-Vitiani, L., et al., 2007. Identification and expansion of human colon-cancer-initiating cells. Nature. 445, 111-5.

Rijsewijk, F., et al., 1987. The Drosophila homolog of the mouse mammary oncogene int-1 is identical to the segment polarity gene wingless. Cell. 50, 649-57.

Sambuy, Y., et al., 2005. The Caco-2 cell line as a model of the intestinal barrier: influence of cell and culture-related factors on Caco-2 cell functional characteristics. Cell Biol Toxicol. 21, 1-26.

Sato, T., et al., 2009. Single Lgr5 stem cells build crypt-villus structures in vitro without a mesenchymal niche. Nature. 459, 262-5.

Schechter, A. L., et al., 1985. The neu gene: an erbB-homologous gene distinct from and unlinked to the gene encoding the EGF receptor. Science. 229, 976-8.
Schmidt, G. H., et al., 1988. Development of the pattern of cell renewal in the crypt-villus unit of chimaeric mouse small intestine. Development. 103, 785-90.

Segditsas, S., et al., 2008. Putative direct and indirect Wnt targets identified through consistent gene expression changes in APC-mutant intestinal adenomas from humans and mice. Hum Mol Genet. 17, 3864-75.

Snippert, H. J., et al., 2009. Prominin-1/CD133 marks stem cells and early progenitors in mouse small intestine. Gastroenterology. 136, 2187-2194 e1.

Sparks, A. B., et al., 1998. Mutational analysis of the APC/beta-catenin/Tcf pathway in colorectal cancer. Cancer Res. 58, 1130-4.

Sussan, T. E., et al., 2008. Trisomy represses Apc(Min)-mediated tumours in mouse models of Down's syndrome. Nature. 451, 73-5.

Tamai, Y., et al., 1999. Colonic hamartoma development by anomalous duplication in Cdx2 knockout mice. Cancer Res. 59, 2965-70.

Threadgill, D. W., 2008. Down's syndrome: paradox of a tumour repressor. Nature. 451, 21-2.

Trimboli, A. J., et al., 2009. Pten in stromal fibroblasts suppresses mammary epithelial tumours. Nature. 461, 1084-91.

Tymms, M. J., et al., 1997. A novel epithelial-expressed ETS gene, ELF3: human and murine cDNA sequences, murine genomic organization, human mapping to 1q32.2 and expression in tissues and cancer. Oncogene. 15, 2449-62.

Tynan, J., 2005. Ets2 dependent microenvironmental regulation of mouse mammary tumor development and Ets2 regulation of Cdx2 promoter activity. PhD Thesis University of California,San Diego.

Tynan, J. A., et al., 2005. Ets2-dependent microenvironmental support of mouse mammary tumors. Oncogene.

Umezawa, A., et al., 1997. Methylation of an ETS site in the intron enhancer of the keratin 18 gene participates in tissue-specific repression. Mol Cell Biol. 17, 4885-94.

van de Wetering, M., et al., 2002. The beta-catenin/TCF-4 complex imposes a crypt progenitor phenotype on colorectal cancer cells. Cell. 111, 241-50.

van der Flier, L. G., Clevers, H., 2009. Stem cells, self-renewal, and differentiation in the intestinal epithelium. Annu Rev Physiol. 71**,** 241-60.

van der Flier, L. G., et al., 2009a. OLFM4 is a robust marker for stem cells in human intestine and marks a subset of colorectal cancer cells. Gastroenterology. 137**,** 15-7.
Van der Flier, L. G., et al., 2007. The Intestinal Wnt/TCF Signature. Gastroenterology. 132**,** 628-32.

van der Flier, L. G., et al., 2009b. Transcription factor achaete scute-like 2 controls intestinal stem cell fate. Cell. 136**,** 903-12.

van der Pouw Kraan, T. C., et al., 2009. Acute experimental colitis and human chronic inflammatory diseases share expression of inflammation-related genes with conserved Ets2 binding sites. Inflamm Bowel Dis. 15**,** 224-35.

van Es, J. H., et al., 2005. Notch/gamma-secretase inhibition turns proliferative cells in intestinal crypts and adenomas into goblet cells. Nature. 435**,** 959-63.

van Staa, T. P., et al., 2005. 5-Aminosalicylate use and colorectal cancer risk in inflammatory bowel disease: a large epidemiological study. Gut. 54**,** 1573-8.

Wang, Y., et al., 2006. Epimorphin(-/-) mice have increased intestinal growth, decreased susceptibility to dextran sodium sulfate colitis, and impaired spermatogenesis. J Clin Invest. 116**,** 1535-46.

Wasylyk, B., et al., 1993. The Ets family of transcription factors. Eur J Biochem. 211**,** 7-18.

Wasylyk, C., et al., 1997. Conserved mechanisms of Ras regulation of evolutionary related transcription factors, Ets1 and Pointed P2. Oncogene. 14**,** 899-913.
Wei, G., et al., 2004. Activated Ets2 is required for persistent inflammatory responses in the motheaten viable model. J. Immun. 173**,** 137-9.

Wen, F., et al., 2007. Ets2 is required for trophoblast stem cell self-renewal. Dev Biol. 312**,** 284-99.

Williams, K. L., et al., 2001. Enhanced survival and mucosal repair after dextran sodium sulfate-induced colitis in transgenic mice that overexpress growth hormone. Gastroenterology. 120**,** 925-37.

Yamamoto, H., et al., 1998. Defective trophoblast function in mice with a targeted mutation of Ets2. Genes Dev. 12**,** 1315-26.

Yang, B. S., et al., 1996. Ras-mediated phosphorylation of a conserved threonine residue enhances the transactivation activities of c-Ets1 and c-Ets2. Mol Cell Biol. 16**,** 538-47.

Zabuawala, T., et al., An ets2-driven transcriptional program in tumor-associated macrophages promotes tumor metastasis. Cancer Res. 70**,** 1323-33.

Zhu, L., et al., 2009. Prominin 1 marks intestinal stem cells that are susceptible to neoplastic transformation. Nature. 457**,** 603-7.